博士論文

Development and applications of a bio-hybrid platform for myocyte investigation using Thin-Film Transistor technology

(薄膜トランジスタ回路による筋細胞の培養・計測・スクリーニング技術の構築)

Anne-Claire Madeleine Eiler

アイラー　アンクレア　マドレーヌ

博士論文

Doctoral Dissertation

Development and applications of a bio-hybrid platform for myocyte investigation using Thin-Film Transistor technology

(薄膜トランジスタ回路による筋細胞の培養・計測・スクリーニング技術の構築)

Supervisor: Associate Professor Agnès Tixier-Mita

The Institute of Industrial Science

The University of Tokyo

Department of Advanced Interdisciplinary Studies

Graduate School of Engineering

The University of Tokyo

37-187276

Anne-Claire Madeleine Eiler

アイラー　アンクレア　マドレーヌ


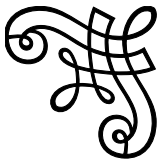

To the memory of

my beloved grandparents,

Madeleine and Jean Gomez, and

Caroline and Heinrich Eiler,

who taught me courage and resilience.

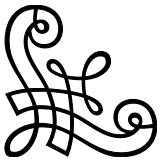
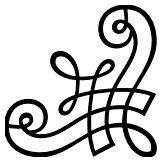

Acknowledgments

I would like to express my deepest thankfulness to my advisor Prof. Agnès Tixier-Mita for her unconditional support of my Ph.D. study and research, for her patience, motivation, enthusiasm, and immense knowledge. Her guidance and kindness helped me in all the time professionally and personally. I could not have imagined having a better mentor for my Ph.D study. I will forever be grateful.

Besides my advisor, I would like to extend my gratefulness towards Prof. Hiroshi Toshiyoshi for his continuous support and insightful comments that pushed me to sharpen my thinking and brought my work to a higher level.

I would also like to thank the other members of my thesis committee: Prof. Katsuhito Fujiu, Prof. Yoshiho Ikeuchi, Prof. Yoshio Mita, and Prof. Yasuyuki Sakai for their encouragement, insightful comments, and judicious questions.

My sincere thanks also go to Mr. Satoshi Ihida for his invaluable support and all of the help he provided on my research. His ideas and insights made it much easier to proceed in the right direction and complete the research successfully. I really enjoyed working with him and I consider myself really lucky to have got the opportunity to have him as a teammate.

I would also like to thank all team members from Toshiyosi laboratory. Special thanks go to Ms. Hiroko Koizumi for her kindness and assistance with the university bureaucracy, Dr. Hiroaki Honma for his help and constant cheerfulness, and Mr. Takuya Takahashi for taking care of the orders of the materials needed for my experiments.

I also would like to thank all members from the Laboratory for Integrated Micro Mechatronic Systems (LIMMS) and other laboratories I had the chance to work with during my Ph.D. study. Thanks to all members who have provided me extensive professional guidance and taught me a great deal about scientific research. I am grateful to all of those with whom I have had the pleasure to work during this research and other related projects.

My sincere gratitude also go to Kerstin Kentsch and Jean-Marie Jaeger for believing in me and encouraging me to pursue a Ph.D. This incredible journey would not have been possible without their kind support.

My special thanks to all my friends who were always here to cheer me on, relax my mind and entertain me outside of my research. Thank you for being by my side and helping me in times of need. My deepest appreciation goes to my cousin and best friend Leïla Zagrabski for her unconditional love, care, support, kindness, and generosity. My heartfelt gratitude also goes to the person who has filled my life with joy and laughter, and spread so many colors around it.

Most importantly, I want to express my sincere appreciation to my family for all the support they have shown me throughout my life. My deepest gratitude to my parents, Henri Eiler and Danièle Eiler, for their wise counsel and sympathetic ear. Thank you for helping me to shape my life with integrity and courage.

Abstract

In the past several decades, the wealth of recent research on applications of microelectromechanical systems (MEMS) in the biomedical field have played an important role in the generation of new microsystems that can enhance bioanalysis. Multielectrode arrays (MEAs) are part of these new instruments that contain multiple microelectrodes through which electrical signals from excitable cells are obtained or delivered. *Excitable* cells, also known as *electrogenic* cells, have the specificity and ability to be electrically excited resulting in the generation of action potentials. They include cells such as neurons, muscle cells (skeletal, smooth, cardiac), and also pancreatic cells. Their electrical properties are fundamental for propagating electrical signals through our body and maintaining the well-functioning of vital organs, such as the rhythm of our heartbeat. The heart conduction system is indeed based on the electrical specificity of cardiac muscle cells, also called *cardiomyocytes*. As a result, understanding the relationships between the electrical connectivity of cardiomyocytes and their physiopathological functions became one of the central goals of contemporary electrocardiology.

Novel MEA devices providing a non-invasive electrophysiology technique have been designed and developed for recordings of the extracellular potential of excitable cells. These devices eventually became more efficient than previous methods for single cell analysis such as the patch-clamp method. However, a challenging problem which arises in this domain is the difficulty to combine transparency, large number and high density of µm-sized electrodes on a large surface of study, with multiple measurement techniques.

Transparency is a fundamental parameter for assessing the cell viability and combining optical and electrical analysis of cell cultures simultaneously. Additionally, a high density of small electrodes allows the acquisition of the electrical conduction in a whole cell network with high spatial resolution without losing information. Then, a large surface of study fully covered with electrodes allows the possibility to integrate microfluidic systems and divide the surface into connected culture chambers for analysis of co-cultures and organoids. Finally, a multiple measurement array would offer a better characterization of cell cultures and tissues by providing more flexibility of the cell culture conditions, and by measuring optical, electrical, and chemical properties of cells on the same platform. A microsystem possessing these valuable characteristics is thus clearly needed to fulfill the requirements for a more accurate and sensitive recording of the extracellular potential of excitable cells and therefore perform better analyses of their electrical connectivity.

To overcome this problem, this research proposes the development and applications of a novel *in vitro* MEA using the thin-film transistor (TFT) technology. TFT technology is mainly used in the field of display technology with a wide range of applications including liquid crystal display televisions. In this work, integrated TFTs are used for controlling a large, dense array of 150 × 150 indium tin oxide (ITO) microelectrodes. The surface of the TFT platform is made of square-shaped transparent microelectrodes of 100 µm fabricated on top of a glass substrate. Each electrode is independently connected to an integrated TFT, which is used for switching ON/OFF the corresponding electrode that can be used for sensing or applying electrical signals.

Fundamentally, this research aims to develop a bio-hybrid platform using the TFT technology for investigations of myocytes. The platform is used as an *in vitro* MEA to perform electrical measurements with cultures of excitable cells and assess their biological meanings. In order to complete this research, it was of interest to focus on three main electrical techniques: (1) electrophysiology, (2) electrochemistry, and (3) dielectrophoresis. These techniques are essential in research with the physiology, pharmacology, and biophysics of cell membranes in cell and tissue cultures. Indeed, the characterization of excitable cells requires to precisely evaluate both their electrical and chemical properties to understand the mechanisms behind them.

Combining different techniques on one platform is still hard to develop and remains a challenge. With this aim in mind, the research mainly focused on the use of the TFT platform for measurement of extracellular potentials of cardiomyocytes and the data interpretation from the cell electrical signals. Then, the possibility to perform electrochemical measurements was considered by performing voltammetric and amperometric measurements with the TFT platform. Lastly, dielectrophoresis of skeletal muscle cells was explored for patterning and displacement of cells on specific areas of the TFT-MEA.

As a result, a TFT-MEA has been developed and evaluated for the study of myocytes by combining multiple electrical techniques for the first time in the world. ITO microelectrodes can be used not only for electrophysiological measurements but also for electrochemistry and dielectrophoresis through appropriate functionalization. Moreover, electrophysiological measurements are repeatable under the same conditions, and experiments can be reproduced in their entirety. On this basis, future research involving co-cultures and stimulation of excitable cells is considered. Finally, we hope that the use of MEMS and TFT technology can lead to the development of unique and valuable *in vitro* MEAs that combine different types of electrical measurements for novel lab on a chip systems.

Contents

Acknowledgments **i**

Abstract **iv**

List of Figures **xv**

List of Tables **xxi**

List of Abbreviations **xxiii**

CHAPTER 1 Introduction **1**

1.1 Purpose of the Thesis 2

1.2 Background 3

1.2.1 Heart Diseases 3

1.2.2 *In vitro* Study of Cells 5

1.3 Research Motivation 8

1.4 Research Proposal 9

1.5 Research Challenges 16

1.6 Significance and Originality 17

1.7 Present Ongoing Research 18

1.7.1 Microelectrode Array 18
1.7.2 Complementary Metal-Oxide-Semiconductor . . 20
1.7.3 Thin-Film Transistor 21
1.8 Thesis Structure 23
1.9 Chapter Summary 25

CHAPTER 2 Theory **27**
2.1 Cardiac Muscle 28
2.1.1 Muscle Cells 28
2.1.2 Cellular Organization in the Cardiac Muscle . . . 29
2.1.3 Function of the Cardiac Muscle 32
2.2 Electrical Properties of Cardiomyocytes 35
2.2.1 Membrane Potential 35
2.2.2 Action Potential 37
2.2.3 Electrical Model 39
2.3 Recording Techniques 41
2.3.1 Electrocardiogram 41
2.3.2 Fluorescence Microscope 44
2.3.3 Patch-clamp Technique 46
2.3.4 Microelectrode Arrays 48
2.3.5 Electrochemical Sensors 51
2.3.6 Impedance-based Techniques 53
2.3.7 Dielectrophoresis 55
2.4 Thin-Film Transistor Technology 58
2.4.1 Basic Structure 58

2.4.2 Types of Thin-Film Transistors 59
2.5 Chapter Summary 61

CHAPTER 3 Methodology **63**
3.1 Thin-Film Transistor based MEAs 64
3.1.1 Structure 64
3.1.2 Working Principle 65
3.1.3 Fabrication 66
3.1.4 Characterization 68
3.2 Experiments for Electrophysiology 71
3.2.1 Preparation of the Device 71
3.2.2 Preparation of Cardiac Muscle Cells 73
3.2.3 Experimental Setup 75
3.3 Experiments for Electrochemistry 79
3.3.1 Preparation of the Device 79
3.3.2 Preparation of Tyramine 79
3.3.3 Experimental Setup 80
3.4 Experiments for Dielectrophoresis 82
3.4.1 Preparation of the Device 82
3.4.2 Preparation of Liver and Skeletal Muscle Cells . 83
3.4.3 Experimental Setup 86
3.5 Data Analysis for Electrophysiology 87
3.5.1 Wave Propagation 87
3.5.2 Spike Sorting Algorithm 89
3.6 Chapter Summary 90

CHAPTER 4 Results **91**

4.1 Electrophysiology 92

4.1.1 Extracellular Potentials of Cardiomyocytes . . . 92

4.1.2 Scanning of Gate Lines 96

4.1.3 2D Mappings 99

4.1.4 Signal Propagation 102

4.1.5 Regions of Active Cardiomyocytes 104

4.1.6 Evolution of Cell Culture 105

4.1.7 Effect of Temperature 107

4.2 Electrochemistry 109

4.2.1 Cyclic Voltammetry 109

4.2.2 Amperometry 111

4.3 Dielectrophoresis 113

4.3.1 Preliminary Tests 113

4.3.2 Skeletal Muscle Cells 116

4.4 Chapter Summary 117

CHAPTER 5 Discussion **119**

5.1 Electrophysiology 120

5.1.1 Analysis Conditions 120

5.1.2 Properties of Extracellular Data 124

5.1.3 Correlation between Optical and Electrical Data 126

5.1.4 Evolution of Cell Culture 127

5.1.5 Cell Stimulation 128

5.1.6 Scanning Rate 136

5.1.7 Drug Testing 144
5.2 Electrochemistry 145
5.2.1 Significance 145
5.2.2 ITO Working Electrode 146
5.2.3 Integrated Reference Electrode 148
5.2.4 Electrode Polarization 149
5.2.5 Conductive Lines 150
5.2.6 Unspecific and Specific Detection 150
5.3 Dielectrophoresis 153
5.3.1 Cell Mobility and Patterning 153
5.3.2 Insulation layer 154
5.4 Cell Viability and Activity 156
5.4.1 Cell Viability 156
5.4.2 Cell Electrical Activity 158
5.5 Cleaning and Reuse of Device 160
5.6 Electromagnetic Point of View 162
5.7 Chapter Summary 167

CHAPTER 6 Conclusion **169**
6.1 Research Summary 170
6.2 Conclusion of this Work 184
6.3 Future Research Outlook 186

Bibliography **191**

Publications **219**

List of Figures

1.1 Heartbeat coordination 4
1.2 Overview of the research proposal 10
1.3 Importance of transparency of the substrate for analysis of cell cultures 12
1.4 Comparison between 1D and 2D addressing 13
1.5 Example of commercially available standard MEA from Multi Channel Systems MCS GmbH 19
1.6 Example of commercially available CMOS-MEA chip from Multi Channel Systems MCS GmbH 21
1.7 TFT structure 22
1.8 Chapter structure schematic 24

2.1 Multi-scale structure of the heart 29
2.2 Conduction system of the heart 33
2.3 Schematic view of resting membrane potential and ion movement in cardiomyocytes 35
2.4 Various action potentials recorded in cardiac tissues . . 38
2.5 Electrical model of cardiomyocytes 39
2.6 Pattern recognition in ECG 43

2.7 Principle of patch-clamp technique 47
2.8 Electrical equivalent circuit of a FET-based MEA 49
2.9 Electrodes for amperometric electrochemical sensor . . . 52
2.10 Schematic of electrical cell-substrate impedance-based sensing 55
2.11 Dielectric properties of cells 56
2.12 General TFT configurations 58
2.13 Structure of a TFT LCD 60

3.1 Structure of transistor in a TFT-MEA 65
3.2 Working Principle of TFT-MEAs 66
3.3 Photo of the TFT-MEA platform after post-processing . 67
3.4 TFT array characterization 69
3.5 Bode diagram for one transistor 70
3.6 Flowchart for neonatal heart dissociation 73
3.7 General experimental setup scheme for electrophysiological and electrochemical measurements with a TFT-MEA 76
3.8 Schematic view of 6 × 6 connected electrodes for electrophysiological measurements 77
3.9 Photos of equipment used for electrophysiological measurements with cardiomyocytes 78
3.10 Schematic view of 6 × 6 connected electrodes for electrochemical measurements and photo of standard electrochemistry cell 80
3.11 Experimental setup for DEP 86

3.12 Calculation of signal propagation 88
3.13 Biosignal processing with Matlab program 89

4.1 Extracellular potential of cardiomyocytes recorded on one microelectrode of a TFT-MEA 92
4.2 Gate scanning for extracellular recordings of cardiomyocytes with TFT-MEAs 93
4.3 Extracellular potential of cardiomyocytes 95
4.4 Gate scanning for extracellular recordings of cardiomyocytes with TFT-MEAs after filtering 96
4.5 Calculation of signal velocity with Excel and MC Rack software analysis from Multi Channel System MCS GmbH 98
4.6 2D mapping of cardiomyocyte electrical activity built with Excel calculation 100
4.7 Microscopic observation of cell contraction compared with extracellular recordings of cardiomyocytes 100
4.8 Electrical 2D mappings and optical evolution of cardiomyocytes cultured on TFT-MEAs 101
4.9 Excel calculation of delay and velocity of cell electrical signal 102
4.10 Calculation of delay and velocity of cell electrical signal using MC Rack software analysis from Multi Channel System MCS GmbH 103
4.11 Culture of heart cells (cardiomyocytes and fibroblasts) and the corresponding electrical signals measured 104

4.12 Electrical evolution of a culture of cardiomyocytes over several days 106
4.13 Effect of the temperature on the frequency of cardiomyocyte electrical signals 107
4.14 2D mappings of the average pk-pk amplitude and period of cardiomyocyte signals at +37°C and room temperature 108
4.15 Results of cyclic voltammetric experiments 109
4.16 Results of amperometric experiments 111
4.17 Scheme of expected DEP patterning with mammalian cells and microbeads 114
4.18 Results of DEP patterning with liver HepG2 cells and microbeads on TFT-MEA 115
4.19 Displacement of liver HepG2 cells by DEP on TFT-MEA 115
4.20 Displacement of skeletal muscle cells (C2C12) with DEP 116

5.1 Motion analysis of neonatal heart cells with microscope . 126
5.2 Effect of bipolar pulse on the electrode voltage 130
5.3 Three ways to deliver electrical stimulation to myocytes 133
5.4 Structural formula of isoproterenol hydrochloride 135
5.5 Working principle of high resolution CMOS-MEA 137
5.6 First attempt to build a mapping of signal propagation of cardiomyocyte electrical activity measured on TFT-MEA 139
5.7 Fast scanning: measurement of the control card (JAPASTIM) output with an oscilloscope 140

5.8 Commutation spikes when duration between closing/opening gates is 1000 ms 142
5.9 Commutation spikes when duration between closing/opening gates is 1 ms 143
5.10 Integrated reference electrode on TFT substrate 149
5.11 Cardiovascular effects of tyramine 151
5.12 Damaged vs undamaged TFT array substrate after DEP experiments 155
5.13 Temporal and spatial resolution with differential measurements on TFT-MEAs 163
5.14 Interconnection pairs for enhanced SNR 164
5.15 Illustration of TFT-MEA for differential measurements . 166

6.1 Prospective lab on chip biohybrid system for investigation of brain-heart cell co-cultures/organoids 187

List of Tables

1.1 Methodology comparison 6

1.2 Comparison of state of the art devices: standard MEAs, CMOS-MEAs, TFT-MEAs 23

3.1 Reagents for cell culture of cardiomyocytes 75

3.2 Reagents for cell culture of HepG2 liver cells and C2C12 skeletal muscle cells 84

5.1 Proliferation of C2C12 cells on different substrates: glass, ITO, and flat-bottomed 96-well plate (polystyrene) . . . 156

List of Abbreviations

I_d drain current

I_{dsat} saturation current

V_{TH} threshold voltage

V_d drain voltage

V_{ds} drain-source voltage

V_g gate voltage

V_{gs} gate-source voltage

ACEO AC electro-osmosis

AD analog-to-digital

ADCs analog-to-digital converters

APS active pixel sensor

ATE automated testing equipment

AV atrioventricular

CDC Centers for Disease Control

CE counter electrode

CM Clausius-Mossotti

CMOS complementary metal-oxide semiconductors

CMRR common mode rejection ratio

DEP dielectrophoresis

ECARs extracellular acidification rates

ECG electrocardiogram

FET field effect transistor

FF fill factor

FIR finite impulse response

FP field potential

FPGA field-programmable gate array

gm transconductance

IGZO indium gallium zinc oxide

iPS induced pluripotent stem

IrOx iridium oxide

ISFETs ion sensitive field effect transistors

ITO indium tin oxyde

IV current-voltage

LCD liquid crystal display

LOC lab on a chip

MAOA monoamine oxidase A

MAOB monoamine oxidase B

MEAs microelectrode arrays

MEMS microelectromechanical systems

MOSFET metal-oxide-semiconductor field-effect transistor

OCRs oxygen consumption rates

OFETs organic field-effect transistors

PBS phosphate buffered saline

PCB printed circuit board

PEMF electromagnetic field stimulation

PI propidium iodide

pk-pk peak-to-peak

RE reference electrode

RT room temperature

RuOx ruthenium oxide

SA sinoatrial

SNN spiking neuronal network

SNR signal to noise ratio

TFT thin-film transistor

TiN titanium nitride

WE working electrode

Chapter 1

Introduction

This chapter starts by introducing the purpose of the thesis. We then explore the electrical conduction system of the heart and the recent research trends to study heart cells. Then we describe the motivation for undertaking this research, the proposal, and the challenges it is implying. Finally, this chapter ends with the significance and originality of this work, and concludes with a presentation of the ongoing research in that field.

1.1 Purpose of the Thesis

As early as six weeks of pregnancy, a flutter can be detected in the embryo. This flutter happens because the group of cells that will become the future "pacemaker" cells of the heart gain the capacity to fire electrical signals. This electrical communication will eventually mature and generate the first heartbeats of the approximately three billion that will sustain a human being over a lifetime. Heartbeats are generated by specialized cardiac muscle cells located in specific regions of the cardiac muscle. Cardiac muscle cells, also known as *cardiomyocytes*, are called *excitable* or *electrogenic* cells due to their ability to be electrically excited resulting in the generation of action potentials. Heartbeats are triggered by these electrical impulses that travel down a special pathway through the cardiac muscle. Many heart diseases are thus closely related to a dysfunction of the electrical communication of cardiomyocytes. As a result, one of the central goals of contemporary electrocardiology is to understand the relationships between the electrical connectivity of cardiomyocytes and their physiological and pathological functions. To accomplish this, specific instruments that involve multidisciplinary approaches need to be developed.

The purpose of this thesis is to discuss the current research performed for the study of electrically excitable cells and to propose a novel technology for *in vitro* measurements that can overcome the drawbacks of current technologies.

The device has been successfully designed, fabricated, characterized and applied to diverse electrical measurements. The extracellular potential of cultures of cardiac muscle cells was successfully measured for the *in vitro* study of the electrical signals that underpin the communication networks of heart cells. Additional techniques, such as electrochemical measurements and mobility of cells on the surface of the device were also demonstrated. As a result, the device involves multidisciplinary approaches for various bioelectrochemical applications; electrophysiology, electrochemistry, dielectrophoresis.

1.2 Background

1.2.1 Heart Diseases

In 2017, approximately 2.8 million resident deaths were registered in the United States. Ten leading factors were at the origin of among 74% of all registered deaths. Among these 10 factors, heart disease was the leading cause registered [1]. Heart disease is a term covering any disorder of the heart and refers to issues and deformities in the heart itself. About 655,000 people die from heart disease in the United States every year, which is almost 1 in every 4 deaths as reported in the Centers for Disease Control (CDC), Cleveland Clinic Reports, OH, USA [2]. There are many types of heart diseases and some of which are preventable.

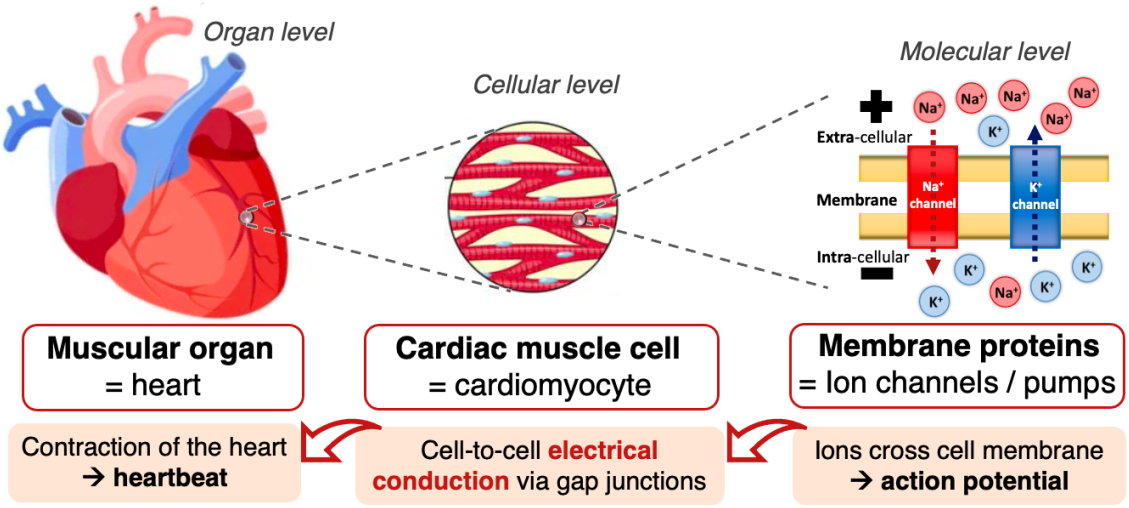

Figure 1.1: Heartbeat coordination

Arrhythmia is one example of heart disease, which is characterized by an irregular heartbeat. Arrhythmia occurs when the electrical impulses in the heart that coordinate the heartbeats do not work properly, whether that be too fast (tachycardia), too slow (bradycardia), or too erratic (premature ventricular contractions, fibrillation). About 50% of heart patients die of sudden death due to cardiac arrhythmias [3]. Additionally, heart failure increases the risk of sudden death by 6-9 times and most cases are the result of ventricular arrhythmias [4].

As a result, a deeper understanding of the relationships between the electrical connectivity of cardiomyocytes and their physiopathological functions is truly needed. However, maintenance of the normal functions of the cardiac conduction system depends on the electrical properties generated by ion movements between cardiomyocytes through their cell membrane. It is thus essential not only to study the heart as a whole, but also to look at the molecular and cellular levels (**Figure 1.1**).

1.2.2 *In vitro* Study of Cells

The study of cardiac muscle cells can be performed *in vivo* at the level of the organ, but also *in vitro* at the cellular and molecular levels. Medical studies are often first performed *in vitro*. An example would be looking at the ability of a drug to treat arrythmia on growing cardiomyocytes in a dish outside of the body. *In vitro* studies allow a substance to be studied safely, without subjecting humans or animals to the possible side effects or toxicity of a new drug. They also allow more rapid development of new treatments. Indeed, many drugs can be studied at one time in a large number of samples, and only those that appear to be efficacious go on to human studies. *In vitro* study of excitable cells can be roughly divided in two methods: optical and electrical. A comparison of the methodologies can be seen in **Table 1.1**.

Optical

Fluorescence imaging is the main technique used among optical methods for *in vitro* research today. Since its discovery in 1967 [5], this technique has become a standard method for observing and analyzing biological samples. It allows a clear 2D observation of the studied area with a high spatial resolution. However, fluorescent microscopy requires the use of fluorescent dyes, does not allow electrical stimulation, and the area of study is quite small. As a result, it is difficult to perform long-term analysis, interact with the cells, or study large regions of cell cultures.

	Fluorescence	**Voltage**	**Impedance**
Equipment	Microscope	Circuitry	Circuitry
Substrate	Any transparent substrate	Electrodes	Electrodes
Measurable Properties	All	Membrane potential	Ionic transfer, Conductivity
Surface of Study	Small	Large	Small
Cytotoxicity	High	Low	Low
Long-term Analysis	No	Yes	Yes
Cell Stimulation	No	Yes	Yes

Table 1.1: Methodology comparison

Electrical

Electrical techniques are dye free techniques that allow electrical stimulation and multilevel of analysis, which is suitable for long-term analysis, interaction with cells, and study of single cell or tissues. However, these techniques obviously require dedicated substrates and specific electrical instrumentation. Among electrical techniques, two main methods are usually applied: voltage sensing and impedance spectroscopy.

- **Voltage Sensing**: When electrically analyzing cells, voltage sensing is one of the principal area of study. Among these techniques, the most commonly used is the patch-clamp technique for intracellular recordings and stimulation of single cell by sharp or patch electrodes. Microsystems such as microelectrode arrays (MEAs) are then used

for extracellular recordings and stimulation of cell cultures, tissues or organoids [6]. Direct voltage sensing with MEAs has mainly been performed with neurons [7] and cardiomyocytes [8]. Another technique for extracellular recordings is indirect voltage sensing, which is the detection of signals modulated by the ionic activity of excitable cells with ion sensitive field effect transistors (ISFETs). For this method, the current between the source and the drain of the transistor changes accordingly to the ion accumulation above the gate of the transistor [9].

- **Impedance Spectroscopy**: Among electrical techniques, impedance measurement between two electrodes can also be performed for differentiation between diverse elements on the electrode surface. When evaluating the impedance through a large spectrum of AC frequencies, characterizations of a wide variety of objects can be performed. Impedance measurement of live cells is now widely accepted as a label-free, non-invasive and quantitative analytical method to assess cell functions involving ion transfers or a change in membrane capacity [10]. Diverse applications have already been possible with impedance spectroscopy, which include cell counting and cell state differentiation [11] [12].

1.3 Research Motivation

The wealth of recent research on applications of microelectromechanical systems (MEMS) in the biomedical field is leading to a new generation of microsystems for bioanalysis [13]. MEMS have enabled the study of biological cells from the single unit to the large scale, which provided access to a huge amount of information not otherwise accessible. A variety of materials and methods have particularly been explored for study of the electrical properties of excitable cells, such as neurons and cardiomyocytes, at a resolution never achieved before [14].

Recently, microfabricated MEAs are the main devices used for *in vitro* extracellular recordings of excitable cells. Other types of techniques continue to be developed and tested to also improve electrochemical detection of biochemical compounds, especially neuromodulators. Associated with nanotechnology, current electrochemical sensors are now becoming increasingly precise, selective, specific, and highly sensitive [15]. Even though MEAs have been widely used in electrophysiology, these *in vitro* arrays are less suited for recording and stimulation of single cells due to their low spatial resolution compared to patch-clamp technique that remains the standard approach for studying ionic currents in single cell membrane. The intracellular electrode has been fundamental to understanding the action potential of excitable cells; nonetheless, parallelization is difficult with this technique and it is damaging to the cells [16] [17].

Active arrays such as complementary metal-oxide semiconductors (CMOS) also give access to some major benefits over standard MEAs such as high density of microelectrodes, and robustness [18]. However, none of these techniques combine the requirements for flexible, efficient, and sensitive analysis of cell cultures, which include: transparency of the substrate, large number of electrodes, and high density of µm-sized electrodes on a large surface.

In this study, we thus focus on the development of a device possessing those valuable characteristics for more accurate and sensitive recordings of the extracellular potential of excitable cells. The possibility to perform additional electrical techniques with this device is also evaluated as it can provide more biological information and control of the cell culture.

1.4 Research Proposal

A constant cell-to-cell communication among biological entities occurs in the human body, which makes the analysis of excitable cells with a sparse disposition of electrodes not sufficient for understanding such biological processes. It is thus of special interest to develop and implement novel MEAs with high density of transparent electrodes as it can allow scientists to obtain more information about the biophysical mechanism behind the communication within a network of neural or cardiac cells.

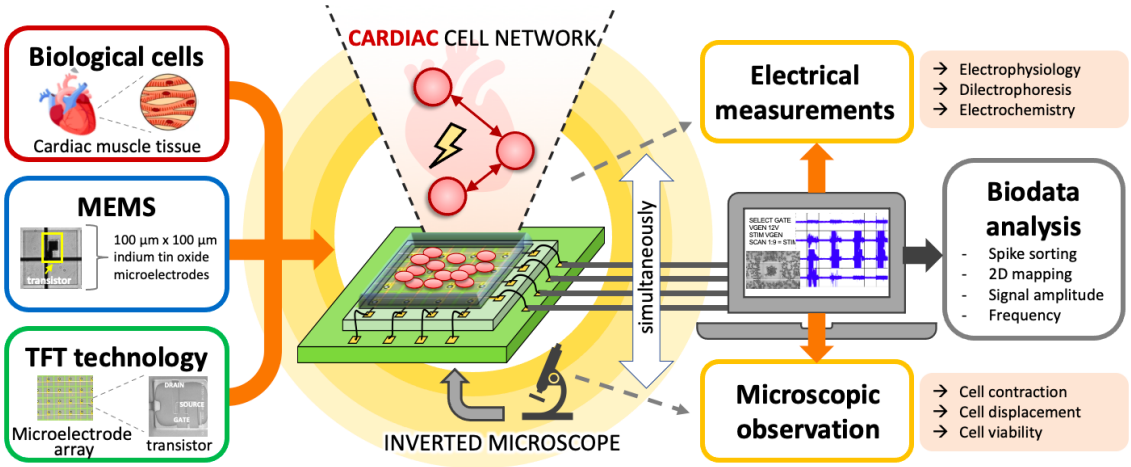

Figure 1.2: Overview of the research proposal

With this aim in mind, this research explores a novel technique for *in vitro* recordings of the extracellular potential of cardiomyocytes using the thin-film transistor (TFT) technology. The combination of MEMS with the TFT technology makes it very attractive for the development of novel transparent MEAs that can combine multiple electrical techniques on one platform. The purpose of this research is thus the establishment of a fundamental technology to perform *in vitro* analyses of excitable cells for a better understanding of their bioelectrochemical behaviors. This includes the development of a sensitive biocompatible MEA with a high density of µm-size electrodes on a transparent glass substrate. The key contribution of this work is thus the novel use of TFT technology as a base for integrated MEMS to overcome the common difficulties faced with current *in vitro* MEAs for the study of excitable cells such as cardiomyocytes.

In order to complete this research, it was of interest to focus on three main electrical techniques: (1) electrophysiology, (2) electrochemistry, and (3) dielectrophoresis, with an emphasis on the electrophysiological part. Combining different techniques on one platform is still hard to develop and remains a challenge. Moreover, techniques and applications that are not yet fully developed for widespread use necessitate validations before practical employment. This means that this research involves an evaluation of the potentials and limits of the TFT platform for each electrical technique. An overview of the research proposal can be seen in **Figure 1.2**.

Additionally, in order to develop an optimal measurement system for biological applications the following features and properties need to be carefully considered.

- **Biocompatibility**: The most fundamental property needed for any device used for bioanalysis is the biocompatibility of the substrate with biological materials. This property is vital as systemic toxicity can impair an entire biological system of study. In the case of cells, it is referred to as cytotoxicity; whether the device can cause cell death due to leaching of toxic substances or from direct contact. It is thus essential to ensure that the substrate in contact with the cells does not interfere with the viability and proliferation of the cell culture.

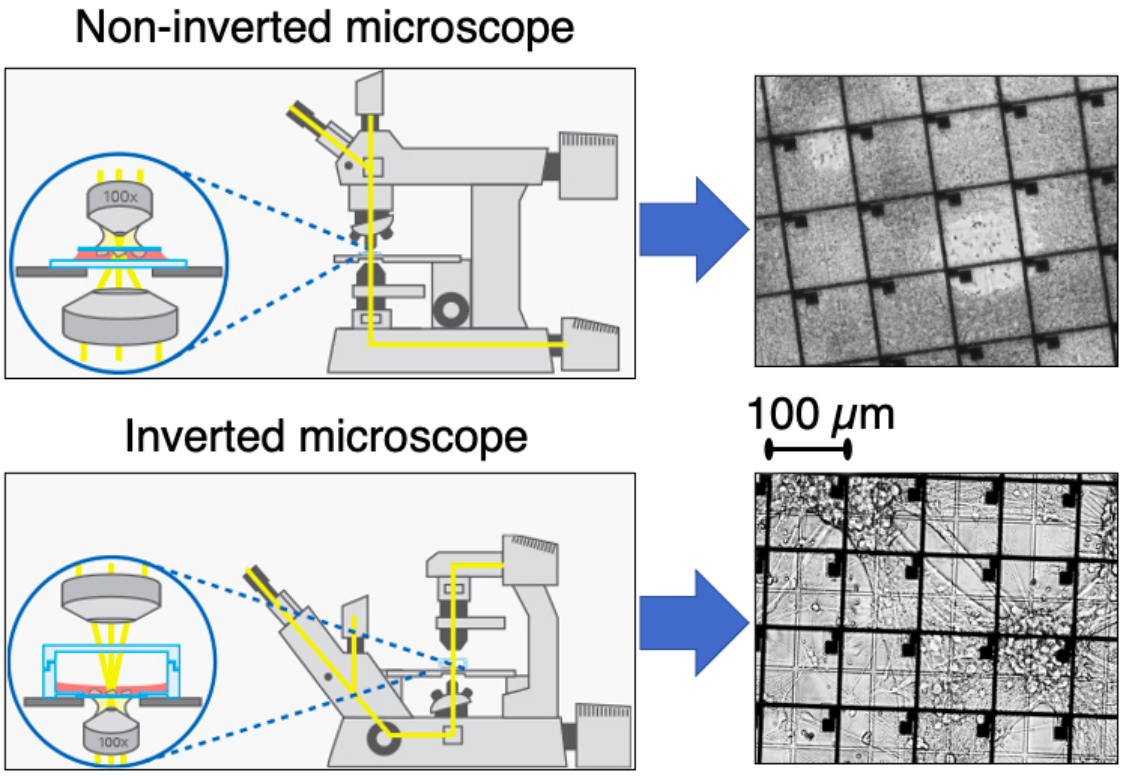

Figure 1.3: Importance of transparency of the substrate for analysis of cell cultures (example of neural cells)

- **Transparency**: Optical observation remains essential for study of cell cultures as it facilitates the examination of the cell viability and proliferation. This includes checking the cell confluency level, whether the cell morphology looks normal, if a contamination is present, or when the culture medium needs to be exchanged. This can be done by using an inverted microscope and a device with a transparent substrate for examining the cell culture condition after, before and during electrical measurements. **Figure 1.3** illustrates the importance of transparency of the substrate for analysis of cell cultures.

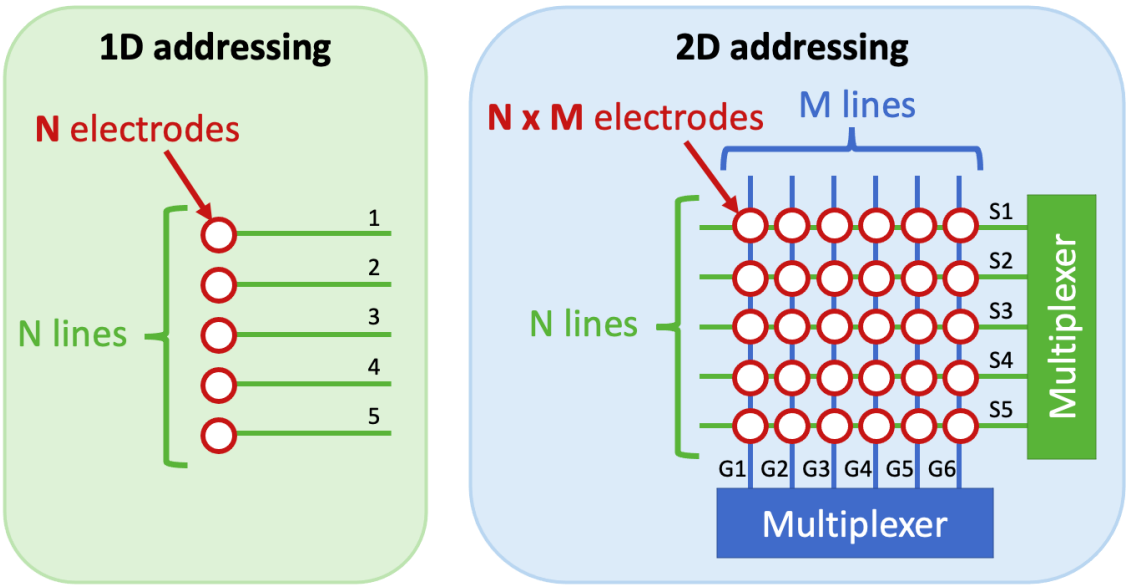

Figure 1.4: Comparison between 1D and 2D addressing: multiplexing feature allows to access N × M electrodes through only N + M addressing lines

- **Addressability**: The addressability of the electrodes is fundamental for the development of large-scale arrays with a high density of electrodes. Without multiplexing, the system would only give access to N electrodes through N addressing lines. However, with the use of multiplexers, N × M electrodes could be accessed through only N + M addressing lines, as shown in **Figure 1.4**.

- **Fill factor**: The fill factor (FF) is defined by the percent of addressable electrodes in the total substrate area. A high FF would thus guarantee the likelihood of measuring an event in a targeted area, while a low FF would lead to a loss of information from multiple areas not covered by electrodes.

- **Size of sensor array**: The development of a large sensor array is important as it can make the integration of microfluidic systems easier, which is useful for exchanging culture medium or for drug screening when dispensing specific drugs in the cell culture. Also, multiple measurements can be performed on different areas of the surface, allowing the use of one device instead of multiple ones. A large sensor array would also facilitate the integration of connected culture chambers on the same platform for study of co-cultures and organoids.

- **Spatial and temporal resolution**: The spatial resolution corresponds to the number of electrodes in a specific area, and is thus closely related to the size of the electrodes and the spacing between them. If the size of the electrode is too large, two events may occur simultaneously on that electrode, and it is thus not possible to distinguish one event from the other. However, if electrodes are small but too sparse, it is not possible to measure the events occurring in the regions not covered by electrodes. Therefore, measurements at cellular and subcellular levels necessitate a high spatial resolution. The temporal resolution corresponds to the speed of switching ON/OFF the addressable lines of the targeted electrodes. The gating and control system of the equipment is fundamental when it comes to obtain a temporal resolution that can cope with the speed of the biological phenomenon occurring on the surface. As many biological events such as action potentials in excitable cells are time-limited, the system needs to be on a similar timescale for reliable measurements.

- **Sensing and stimulation**: The ability to perform both electrical sensing and electrical stimulation by using the same device is a huge advantage for electrophysiological studies. Cells can be stimulated and their response can be directly measured, which offers the possibility to develop a closed-loop for automatic cell stimulation with real-time analysis. This feature is also essential for dielectrophoresis (DEP) to move cells and particles, as well as impedance spectroscopy to apply biphasic current pulse stimulation.

- **Multi-measurement array**: Other techniques continue to be developed and tested to improve the characterization of cell cultures. Indeed, cell communications also involve biochemical components. Moreover, if we want to study other parameters, such as cell morphological change or proliferation, we need different devices. It is thus of a great interest to have an MEA that allows both electrophysiological and electrochemical measurements by using the same platform, as well as additional techniques such as DEP, cell stimulation, or impedance spectroscopy. Indeed, the more types of measurements are performed on a cell culture, the better is the characterization of the electrical and biochemical properties of the cell network.

1.5 Research Challenges

As we have seen, several properties are required for the device technology itself and for using it for biological applications. However, in order to perform optimal measurements with the device and to surpass current technologies, we need to focus on the critical properties.

Biocompatibility is obviously an essential property for culturing biological cells on the substrate. If the material is not biocompatible, it is fundamental to explore the possibilities of surface treatments that can improve biocompatibility with the biological systems of study. The trade-off between transparency and the electrode density is also essential. This device is a MEA based on an array of transistors, which means that the addressing metal lines and the size of the transistors are a deciding factor for transparency. The size of the electrodes needs to be considered carefully in order to obtain a convenient spatial resolution. Similarly, the temporal resolution needs to be on a scale that is similar to the speed of action potentials occurring in networks of excitable cells. Otherwise, such events would become impossible to measure accurately. Additionally, a reliable control of the device is fundamental, especially as the number of electrodes increase. The use of a functional scanning system for switching ON/OFF the multiple transistors is thus essential. Finally, the possibility to perform different types of electrical measurements for various bioelectrochemical applications needs to be successfully demonstrated.

The main challenge of this work is thus to build a high resolution transparent microsystem for *in vitro* study of the bioelectrochemical properties of excitable cells, which is fundamental to make *in vitro* studies more efficient and get a better understanding of what happens at different biological scales.

1.6 Significance and Originality

In vitro recording of extracellular potentials with standard MEAs and CMOS-based MEAs is now well established for electrophysiological analyses. However, although they are widely used, they do not meet all the design requirements for an optimal recording of the bioelectric response of excitable cells; transparency, large surface area, and high density of small electrodes. To overcome the limitations of the current devices, this study proposes the TFT technology as a base for fabrication of integrated MEMS and the development of novel advanced microsystems for electrophysiological measurements.

This study demonstrates for the first time the use of 2D TFT-MEAs to simultaneously optically and electrically analyze cultures of excitable cells for *in vitro* studies. Measurements are repeatable under the same conditions, and experiments can be reproduced in their entirety. The originality of this work involves the novel use of the TFT technology for the development of MEMS for bioelectrochemical applications.

In vitro arrays developed with TFT technology have the advantages of having a high density of thousands transparent microelectrodes on a large surface [19] [20]. Moreover, these microelectrodes can be used for multiple measurement techniques for interdisciplinary characterization of biological cells, such as electrical recording, electrical stimulation, impedance spectroscopy, DEP, and electrochemistry. Ultimately, this work can be beneficial for the development of new instruments for pre-clinical and clinical studies in pharmacology, for the study of biophysical aspects in excitable cells, and for integration with non-biological systems as a controller to modulate cell network behavior.

1.7 Present Ongoing Research

1.7.1 Microelectrode Array

In 1972, Thomas et al. published the first article reporting the use of a MEA to describe the monitoring of the bioelectric activity of cultured cells. Their experimental system had 2 rows of 15 electrodes each, spaced 100 µm apart, with the first results obtained on chick myocytes [21]. In parallel to this work, other labs also working on MEAs published two other articles. The first recorded from 36 electrodes on isolated snail ganglion [22]. The second recorded from 2 parallel lines of 16 electrodes on dissociated neurons of the rat superior cervical ganglion [23]. These three pioneer MEAs had 7 µm to 10 µm square recording electrodes, 100 to 250 µm distant from each other.

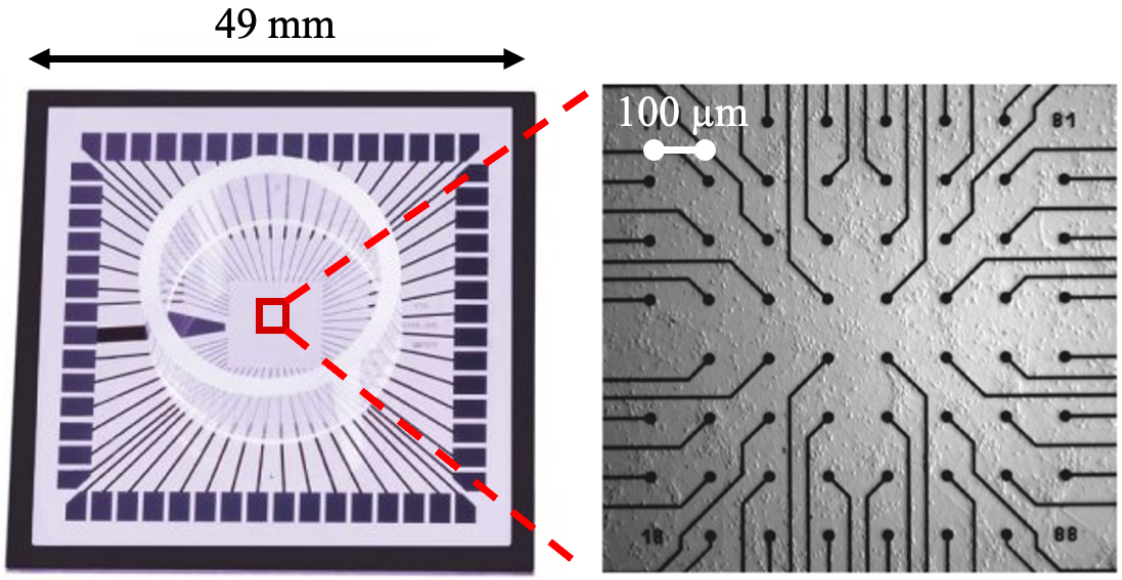

Figure 1.5: Example of commercially available standard MEA from Multi Channel Systems MCS GmbH

Since then, more research has been trying to improve the MEA technology to study more complex cell interactions within cell networks [24]. Standard MEAs are *in vitro* passive arrays. Compared to patch-clamping, they have the ability to select different recording sites within the array, the ability to receive data simultaneously from multiple recordings sites, and can integrate multiple microelectrodes for cellular-resolution electrophysiology [25]. Standard passive arrays thus provides information in a relatively high-throughput, optical transparency and low-cost manner [26]. An example of commercially available standard MEAs is shown in **Figure 1.5**.

The instrumentation strategy of this existing technology has been to wire all electrodes and select them externally, causing a severe trade-off between scale and resolution. MEAs are fabricated by deposition, lithography and etching with one level of metal. However, this technique of fabrication leads to a wiring congestion between the pads and electrodes, which limits the number and density of electrodes. Consequently, each electrode corresponds to one contact pad. Passive arrays have thus the clear advantage of being transparent, but have restrictions on routing off-chip, limiting their spatial resolution (pitch $>$ 30 µm) and number of integrated electrodes (usually less than 300).

1.7.2 Complementary Metal-Oxide-Semiconductor

CMOS based MEAs are active arrays that give access to some major benefits over passive arrays such as less parasitic capacitance, high density of electrodes, and robustness [18]. The first *in vitro* studies using a high-density CMOS-MEA provided simultaneously recordings from 4,096 electrodes [27] [28] [29]. These arrays are also fabricated by deposition, lithography, and etching, but they integrate multiple levels of metal, and include electronic components. CMOS-MEAs can thus provide several metal layers, improving drastically wire routing congestion thanks to the buried conduction tracks. As a consequence, a large number of microelectrodes, arranged in a much higher density but using less control lines is obtained with CMOS-MEAs.

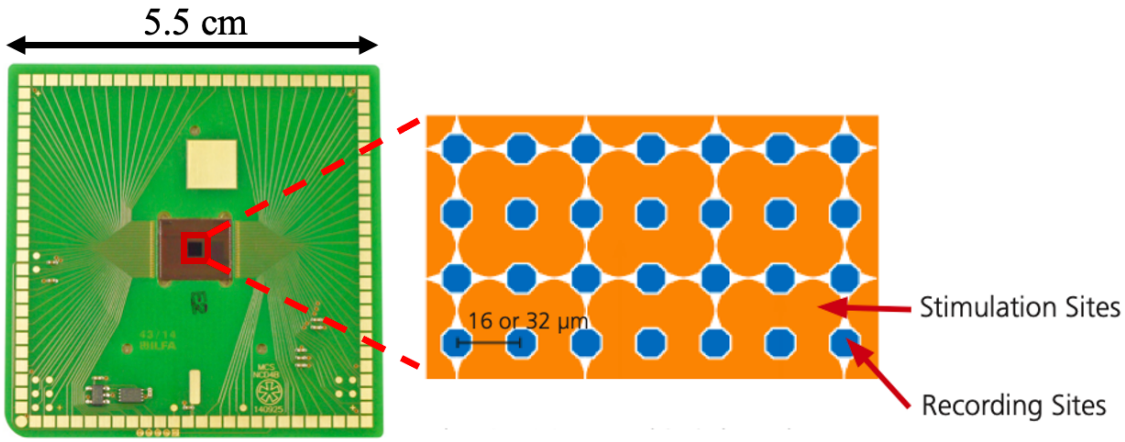

Figure 1.6: Example of commercially available CMOS-MEA chip from Multi Channel Systems MCS GmbH

By also reducing the dimension of electrodes, CMOS-MEAs can capture subtle signals at cellular, subcellular and network levels [30]. Moreover, CMOS-MEAs have the advantage to be designed with integrated components, like amplifiers or read-out system, which prevents the usage of external devices. The main drawbacks of CMOS-MEAs are the opacity of the devices, as they are based on silicon technology, and the small size of the sensing surface (mm size). An example of commercially available CMOS-MEAs can be seen in **Figure 1.6**.

1.7.3 Thin-Film Transistor

A TFT is a special type of metal-oxide-semiconductor field-effect transistor (MOSFET). TFTs are made by depositing thin films of layers: an active semiconductor layer (chanel) and a dielectric layer (insulator). Then, metallic contacts are integrated over a supporting (but non-conducting) substrate [31].

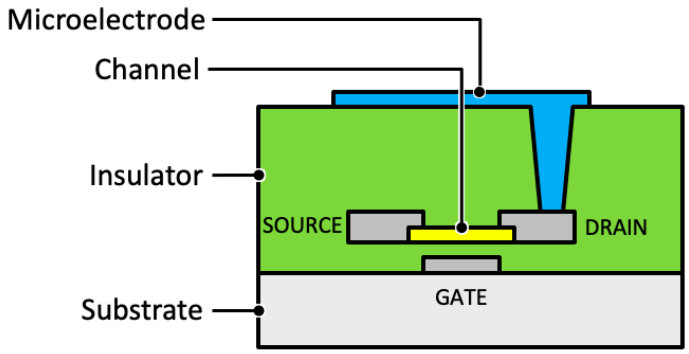

Figure 1.7: TFT structure

A schematic view of the TFT structure used in this study is shown in **Figure 1.7**. TFT technology has been mainly used in the field of display technology with a wide range of applications including liquid crystal display (LCD). Therefore, a common substrate used in that technology is glass. Indeed, by appropriately chosing the materials for the semiconductor, the metal, and the substrate materials, the TFT surface can be nearly transparent. This differs from the conventional CMOS-MEAs, where the semiconductor material typically is the substrate in silicon. Due to its large industrial applications, such TFT arrays can be fabricated with high yield [32]. In this study, we use the TFT technology for developing TFT based MEAs to study excitable cells, with an array of 22,500 indium tin oxyde (ITO) microelectrodes over 240 mm^2 area.

A comparison between standard MEAs, CMOS-MEAs, and TFT-MEAs is shown in **Table 1.2**.

	Standard MEAs	CMOS-MEAs	TFT-MEAs
Substrate	glass	silicon	glass
Transparency	transparent	opaque	transparent
Pixels	passives	actives	actives
Addressability	N	$\sqrt{N}$	$\sqrt{N}$
Number of electrodes	16 – 256	4,225 or more	22,500
Size of electrodes	10 µm – 200 µm	from 8 µm	50 – 100 µm
Spacing	30 µm – 300 µm	16 µm – 32 µm	5 µm – 15 µm
Density	< 25 %	> 90 %	> 90 %

Table 1.2: Comparison of state of the art devices: standard MEAs, CMOS-MEAs, TFT-MEAs

1.8 Thesis Structure

The dissertation starts with the context of this work, its scientific purpose, and the central contributions it offers in Chapter 1. Then the conceptual foundation of the work is presented in Chapter 2, followed by the methodology in Chapter 3. Chapter 4 presents the results obtained and the discussion is reported in Chapter 5. Finally, Chapter 6 summarizes the whole study and presents some prospects of future research. The thesis structure is shown in **Figure 1.8**.

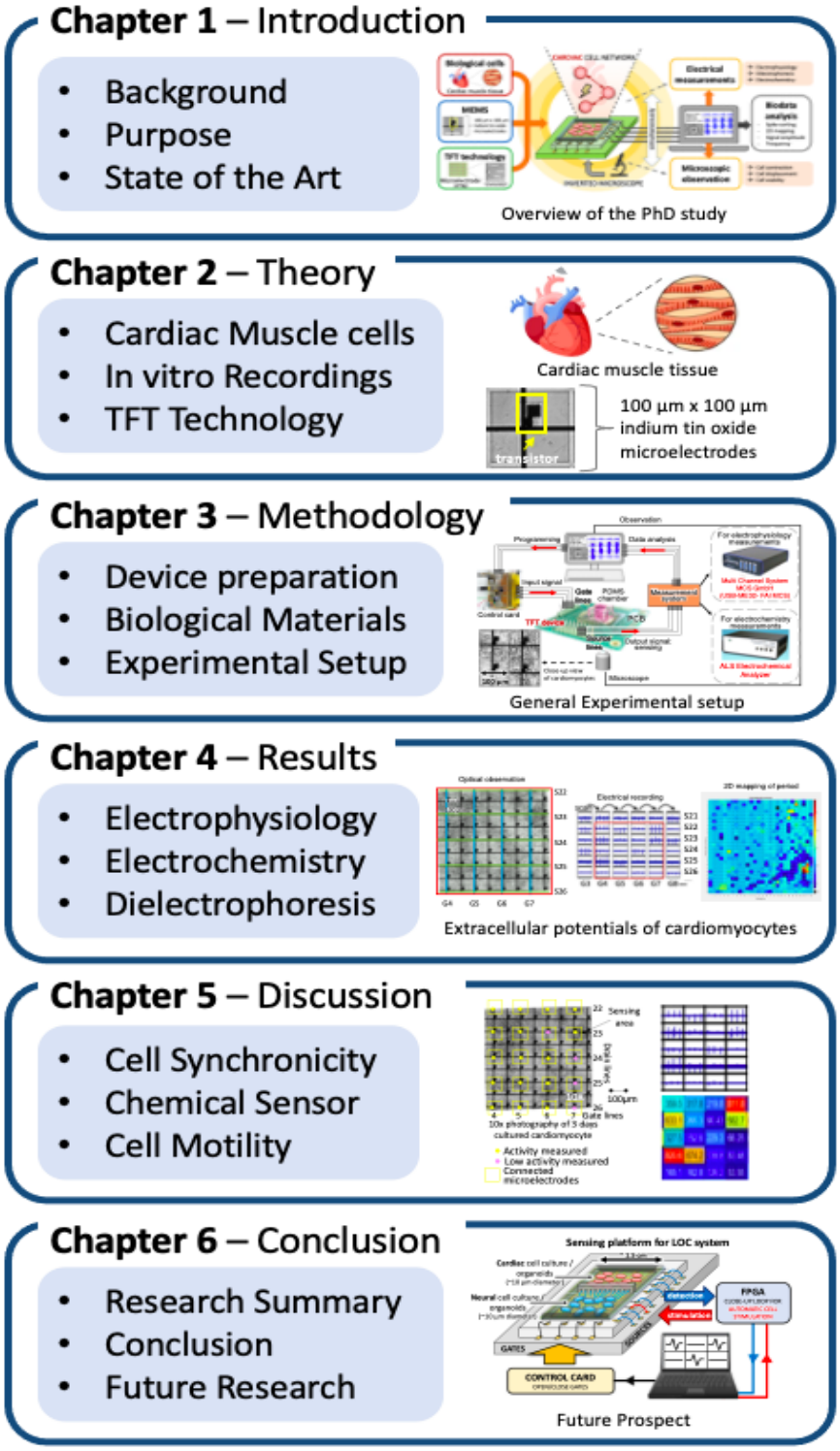

Figure 1.8: Chapter structure schematic

1.9 Chapter Summary

In this chapter, we provided a basic introduction of the research presented in this study. We also described state of the art devices used for cell bioanalysis and compared them with our proposed work.

Chapter 2

Theory

In this chapter, we provide the theory and principles behind the electrical analysis of cardiomyocytes. We start with the description of the structure, function, and properties of cardiomyocytes, as well as how they can be treated as an electrical system. Then, we discuss various technologies used for the analysis of the heart function and the recording of excitable cells in general. Finally, we introduce the basic structure and the different types of transistors used in the TFT technology.

2.1 Cardiac Muscle

2.1.1 Muscle Cells

All animals consist of vast numbers of cells forming tissues and working in concert with one another. Some cells can be electrically excited, which means they exhibit a change in membrane potential that is necessary for cellular responses in various tissues. Neurons, muscle cells (e.g. skeletal, smooth, cardiac), and some endocrine cells (e.g. insulin-releasing pancreatic β cells) are electrically *excitable* cells, also known as *electrogenic* cells. For example, muscle cells, or myocytes, form the muscle tissue and respond to excitation signals with a rapid depolarization, which is coupled with its physiological response: contraction. Muscle tissue can be classified by its morphology and function.

- The morphology can be striated or non-striated. Striated refers to the presence of visible banding, which occurs due to organization of myofibrils to produce a constant direction of tension. Striated muscle contracts and relaxes in short, intense bursts, whereas non-striated muscle sustains longer or even near-permanent contractions.

- The function can be voluntary or involuntary, which refers to whether the muscle is under conscious control or not.

It is thus possible to describe three types of muscle tissue recognized in vertebrates: skeletal, smooth, and cardiac. In this study, we focused our research on cardiac muscle cells, also called *cardiomyocytes*.

2.1.2 Cellular Organization in the Cardiac Muscle

Cardiomyocytes

The human heart contains approximately 2-3 billion cardiomyocytes, which form about 75 % of the total volume of cardiac muscle tissue [33] [34]. In order to pump the blood throughout the cardiovascular system, rapid, involuntary contraction and relaxation of the heart is vital. To accomplish this, the structure of cardiomyocytes has specific features that allow them to contract in a coordinated fashion and resist fatigue. **Figure 2.1** shows a schematic view of the multi-scale structure of the heart, which is dependent on its hierarchical architecture (organ, tissue, cellular, and molecular levels) [35].

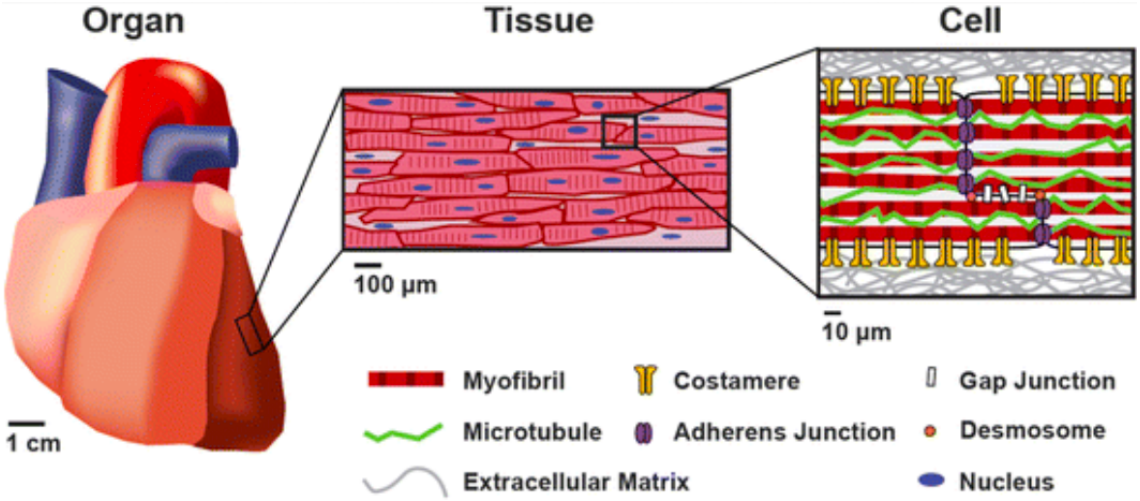

Figure 2.1: Multi-scale structure of the heart. The function of the heart is dependent on its hierarchical architecture: organ, tissue, cellular, and molecular levels [35]

Cardiomyocytes are typically up to 10-40 µm in diameter and 100-150 µm in length [36] [37] [38]. They are rectangular, branching cells with a tubular structure composed of chains of myofibrils, consisting of repeating sections of sarcomeres, which are the fundamental contractile units of muscle cells. Sarcomeres are composed of long proteins that organize into thick and thin filaments, called myofilaments. Thin myofilaments contain the protein actin, and thick myofilaments contain the protein myosin. Like skeletal muscle, the organization of thin and thick myofilaments overlapping within the sarcomere of the cell produces a striated appearance when viewed on microscopy. The myofilaments slide past each other as the muscle contracts and relaxes. The sliding of actin and myosin past each other produces the formation of "cross-bridges," which causes contraction of the heart and generation of force [39].

Neighboring cardiomyocytes are joined together at their ends by intercalated disks to create a syncytium of cardiac cells. Within the intercalated disc, there are gap junctions that permit intercellular communication by allowing ions from one cardiomyocyte to move to a neighboring cell without having to be excreted into the extracellular space first. Because of these junctions and bridges the heart muscle is able to act as a single coordinated unit [40].

Cardiac Fibroblasts

The majority of non-cardiomyocyte cells in the heart are cardiac fibroblasts. The relative number of fibroblasts in the heart varies between species. The number of non-cardiomyocytes is approximately 45 % of the cells in the mouse heart while they account for approximately 70 % in the rat heart [33] [34] [41].

Normal adult cardiac fibroblasts are flat and spindle shaped cells with multiple processes that form a network of cells within the extracellular matrix [42]. Cardiac fibroblasts play a fundamental role in the regulation and turnover of the extracellular matrix for maintenance of the structural integrity of the heart. The coordinated action of cardiac fibroblasts involves production and secretion of a variety of signaling molecules, cytokines and growth factors, such as collagens and fibronectin for maintenance of the extracellular matrix [43]. Moreover, even though fibroblasts have no contractile microfilaments or stress fibers, they support mechanical force distribution throughout the heart muscle [44].

Cardiac Cell Network

The maintenance of the heart tissue integrity and function relies on intercellular communication networks and mechanisms established between the different cardiac cell populations.

Intercellular communication in the heart can either occurs directly, via gap junction channels or tunneling nanotubes, or at longer distances involving soluble factors or extracellular vesicles. This cell-cell communication is vital to regulate cardiac repair after injury. In stress conditions, such as acute myocardial infarction, an orchestrated crosstalk between cardiac cells assumes particular importance to sustain efficient responses in wound healing and extracellular matrix remodeling [45]. As a result, intercellular communication players have emerged as attractive powerful therapeutic targets aimed at improving functional synchronization between the different cardiac cells in order to prevent or repair some of harmful consequences of heart ischemia and reperfusion.

2.1.3 Function of the Cardiac Muscle

Cardiac muscle has the specific ability to initiate an electrical potential at a fixed rate that spreads rapidly from cell to cell to trigger the heart contractile mechanism. This property is known as *autorhythmicity*. Unlike skeletal and smooth muscle which require neural input for contraction, cardiac fibers have specialized cells that spontaneously depolarize. However, these cells can still receive input from the autonomic nervous system to decrease or increase the heart rate depending on the requirements of the body. Specialized conducting components of the heart include the sinoatrial (SA) node, the internodal pathways, the atrioventricular (AV) node, the AV bundle of His, the right and left bundle branches, and the Purkinje fibers.

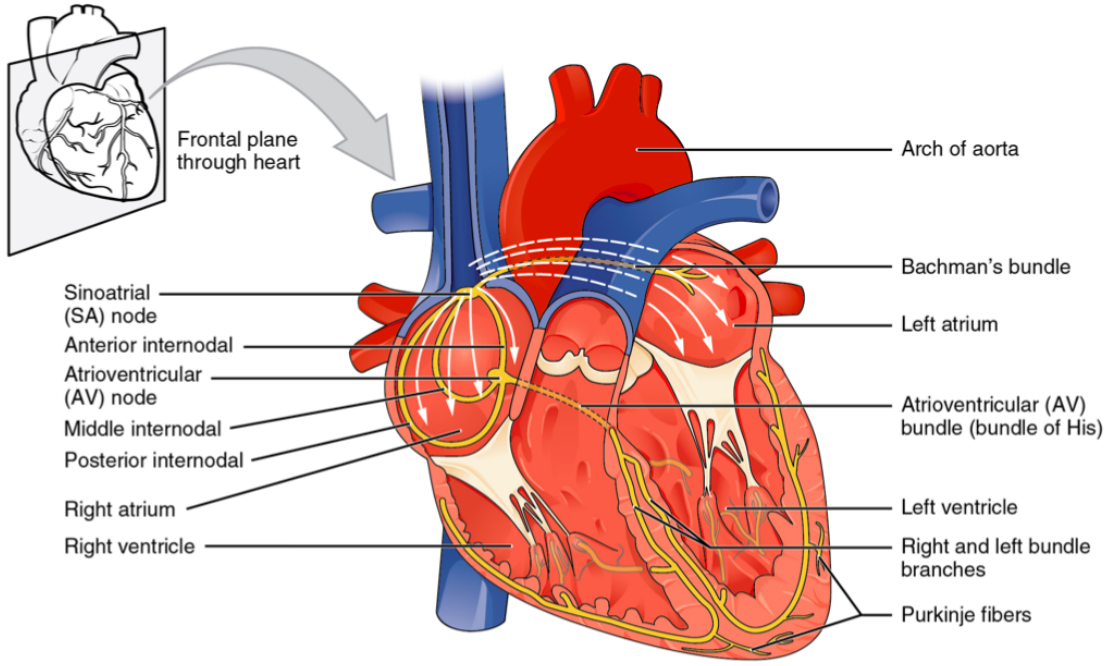

Figure 2.2: Conduction system of the heart [46]

Figure 2.2 shows the conduction system of the heart. There are two types of cardiomyocytes within the heart: the atrial and ventricular myocytes, and the cardiac pacemaker cells. Each cell assumes a distinct role in cardiac excitation and contraction.

- **Atrial and ventricular myocytes** make up the atria (the chambers in which blood enters the heart) and the ventricles (the chambers where blood is collected and pumped out of the heart). They are specialized to generate mechanical activity. For that reason, these cells must be able to shorten and lengthen their fibers and the fibers must be flexible enough to stretch. These functions are critical to the proper contraction and relaxation during the beating of the heart.

- **Cardiac pacemaker cells** carry the impulses that are responsible for the heart beating. They are able to spontaneously generate, send out, and transfer electrical impulses from cell to cell. They can also receive and respond to electrical impulses from the brain. This occurs in the SA node, the AV node and the AV bundle of His.

The myocardial action potential occurs in five steps. (1) The SA node and the remainder of the conduction system are at rest. (2) The SA node initiates the action potential, which sweeps across the atria. (3) After reaching the AV node, there is a delay of approximately 100 ms that allows the atria to complete pumping blood before the impulse is transmitted to the AV bundle. (4) The impulse travels through the AV bundle and bundle branches to the Purkinje fibers, and reaches the right papillary muscle via the moderator band. (5) The impulse spreads to the contractile fibers of the ventricle. (6) Ventricular contraction begins.

The concentration of calcium in the myocyte is the critical factor that determines how much force is generated with each contraction. Cardiac muscle cells can increase contractility through beta-1 adrenergic receptors on the surface with a Gs G-protein. When stimulated by either the sympathetic nervous system or beta-1 agonist drugs, the Gs activate the enzyme adenylyl cyclase, which converts ATP to cAMP. Intracellular cAMP increases the activity of protein kinase A, which then phosphorylates calcium channels permitting more calcium to enter the cell, leading to increased contraction [47].

2.2 Electrical Properties of Cardiomyocytes

2.2.1 Membrane Potential

Animal cells are surrounded by a membrane composed of a lipid bilayer, which serves as an insulator and a diffusion barrier to the movement of ions through two types of proteins embedded in cell membranes: ion pumps and ion channels. Ion pumps are transmembrane proteins that actively push ions across the membrane and establish concentration gradients across the membrane, while ion channels allow ions to move across the membrane down those concentration gradients. Ion pumps and ion channels are electrically equivalent to a set of batteries and resistors inserted in the membrane, and therefore create a voltage between the two sides of the membrane as shown in **Figure 2.3** [48].

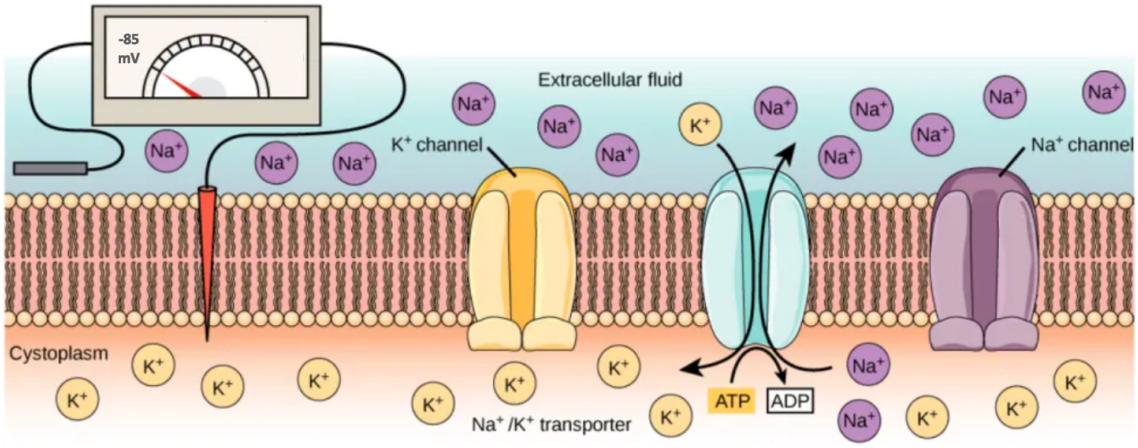

Figure 2.3: Schematic view of resting membrane potential and ion movement in cardiomyocytes (illustration provided by OpenStax)

In electrically excitable cells, such as neurons and cardiomyocytes, the membrane potential is used for transmitting signals between different parts of a cell. These cells can transition from a resting state to an excited state. The resting membrane potential of a cell is defined as the electrical potential difference across the plasma membrane when the cell is in a non-excited state. Traditionally, the electrical potential difference across a cell membrane is expressed by its value inside the cell relative to the extracellular environment, with the inside usually negative with respect to the outside. Signals are generated by opening and closing of ion pumps and ion channels in the membrane, producing a local change in the membrane potential. They then open and close in response to the potential change, reproducing the signal [49] [50].

The most important ions that contribute to the membrane potential are Na^+, K^+, Ca^{2+}, and Cl^-. In a typical cell, the concentration of K^+ is higher inside than outside. the cell. In contrast, Na^+, Ca^{2+}, and Cl^- have higher concentrations outside than inside the cell. All cells within the body have a characteristic resting membrane potential depending on their cell type. The resting potential E_{m} can be determined from the Goldman equation:

$$E_{\mathrm{m}} = g'_{\mathrm{K}^+} E_{\mathrm{K}^+} + g'_{\mathrm{Na}^+} E_{\mathrm{Na}^+} + g'_{\mathrm{Ca}^{2+}} E_{\mathrm{Ca}^{2+}} + g'_{\mathrm{Cl}^-} E_{\mathrm{Cl}^-}$$

This equation uses the Nernst equation used to calculate the potential of an ion of charge z across a membrane.

This potential is determined using the concentration of the ion both inside and outside the cell:

$$E_{\text{ion}} = \frac{RT}{zF} \ln \frac{[\text{ion outside cell}]}{[\text{ion inside cell}]}$$

where R is the ideal gas constant (joules per kelvin per mole), T is the temperature kelvins), and F is the Faraday's constant (coulombs per mole). Therefore, the membrane potential E_{m} depends on the sum of the individual equilibrium potentials times the relative membrane conductance of each ionic species. The relative conductance g'_{X} of a given ionic species is the conductance for that single ion divided by the total conductance for all of the ionic species X, with $g'_{\text{X}} = g_{\text{X}}/g_{\text{total}}$. The resting membrane potential of atrial and ventricular cardiomyocytes and in cells from the His-Purkinje system is typically between -80 mV and -90 mV [51].

2.2.2 Action Potential

In response to a stimulus, cardiomyocytes can generate an action potential associated with a contractile response of the heart. An action potential is a reversible change of the membrane potential characterized by a depolarization and repolarization of the cell membrane. During cellular depolarization the resting membrane potential moves from negative values (-85 mV) to positive values (up to +30 mV) and then recover back to the basal resting membrane potential during the repolarizing process.

Cell stimulation above a threshold value is needed to generate an action potential. This stimulation induces the opening of voltage-gated ion channels and a flood of cations into the cell that causes the depolarization of the cell membrane. Due to the cellular depolarization, voltage-gated calcium channels open and Ca^{2+} is released from the t-tubules. This influx of calcium leads to additional calcium release from the sarcoplasmic reticulum [52]. After a delay, K^+ channels reopen, and the resulting flow of K^+ out of the cell causes repolarization to the resting state. The duration of an action potential can range from 200 to 400 ms [51]. The generation of action potential sequentially and the corresponding electrical activity can be seen on the surface electrocardiogram (ECG) with the typical series of upward and downward spikes (labelled P, Q, R, S and T) as shown in **Figure 2.4** [53].

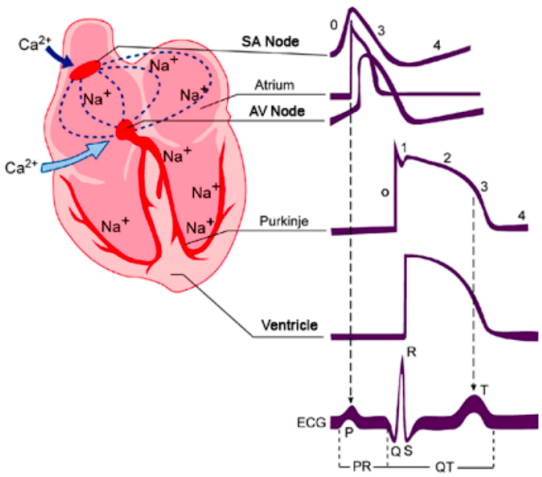

Figure 2.4: Ca^{2+}-dependent (SA and AV nodes) and Na^+-dependent action potentials (atria, ventricles and His-Purkinje system) recorded in cardiac tissues (illustration provided from ITACA Consortium)

2.2.3 Electrical Model

Electrophysiologists observed that the current carried by a particular ion varies with the cell membrane voltage, which suggests that the contribution of each ion to the electrical properties of the cell membrane may be represented by elements of an electrical circuit. The membrane of excitable cells can thus be modeled in terms of an equivalent circuit model for understanding the electrical properties and ionic basis of membrane potentials. This model transcripts the effects of ionic concentration differences, ion pumps/channels, and membrane capacitance. The equivalent circuit consists of a capacitor in parallel with four pathways each consisting of a battery in series with a variable conductance as shown in **Figure 2.5**.

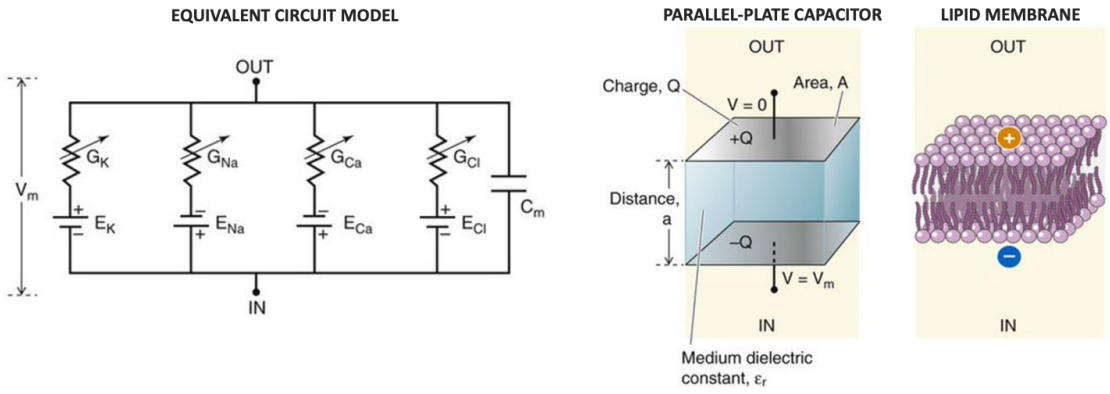

(a) (b)

Figure 2.5: Electrical model of cardiomyocytes: (a) equivalent circuit for a cell membrane, consisting of a fixed capacitance in parallel with four pathways each containing a battery in series with a variable conductance; and (b) idealized capacitor that is formed by two parallel conductive plates, and a capacitor that is formed by a piece of lipid membrane [54]

The voltage of each ionic pathway is determined by the concentrations of the ion on each side of the membrane. Each of the four parallel pathways comes from one of the principal ions, in this case K^+, Na^+, Ca^{2+}, and Cl^-, each one represented by its own component of the circuit, all in parallel with each other [54]. Therefore, there are three main components to the model:

- **Capacitor**: the plates of a capacitor correspond roughly to the inner and outer faces of the cell membrane, which are formed by the polar head groups of the constituent phospholipids that comprise the bilayer structure of the cell membrane. The capacitance is taken to be fixed.

- **Variable conductances**: the conductance of each ionic pathway at any point in time is determined by the states of all the ion channels that are potentially permeable to that ion, including leakage channels, ion channels, and ion pumps.

- **Electromotive forces**: the various ionic gradients across the membrane provide a form of stored electrical energy, much like that of a battery. The equilibrium potential of a given ion can be considered a voltage source, or electromotive force, for that ion. Each of these batteries produces its own ionic current across the membrane, and the sum of these individual ionic currents is the total ionic current.

2.3 Recording Techniques

2.3.1 Electrocardiogram

Medical Use

Einthoven developped the first ECG in 1895. Since then, it evolved into the 12-lead electrocardiogram as we know it today [55]. Electrocardiography is now an essential part of the initial evaluation for patients presenting with cardiac complaints. Specifically, it plays an important role as a non-invasive, cost-effective tool to evaluate changes in the normal ECG pattern that occur in numerous cardiac abnormalities, including arrhythmias and ischemic heart disease [56].

Electrocardiography has played a fundamental role in our understanding of heart disease,s and together with electrophysiology, they remain the standard techniques for evaluation of the nature of rhythm disturbances. Moreover, ECG has been among the first methods to provide objective data on the function and structure of the human body [57]. An ECG can be used to measure the rate and rhythm of heartbeats, the size and position of the heart chambers, and to evaluate the presence of damages to the cardiac muscle cells or conduction system, the effects of heart drugs, and the function of implanted pacemakers [58].

Principle

An electrocardiogram is a graph of voltage versus time of the electrical activity of the heart using electrodes placed on the skin. These electrodes detect the small electrical changes that are a consequence of cardiac muscle depolarization and repolarization during each heartbeat.

In a conventional 12-lead ECG, 10 electrodes are placed on the patient's limbs and on the surface of the chest. The overall magnitude of the heart electrical potential is then measured from 12 different angles ("leads") and is recorded over 10 seconds approximately. The overall magnitude and direction of the electrical depolarization is captured at each moment throughout the cardiac cycle. During each heartbeat, a healthy heart has an orderly progression of depolarization that starts with pacemaker cells in the SA node, spreads throughout the atrium, and passes through the AV node down into the bundle of His and into the Purkinje fibers, spreading down and to the left throughout the ventricles [59]. This orderly pattern of depolarization gives rise to the characteristic ECG tracing.

Interpretations

Interpretation of the ECG is fundamentally about understanding the electrical conduction system of the heart. Normal conduction starts and propagates in a predictable pattern, and deviation from this pattern can be a normal variation or be pathological.

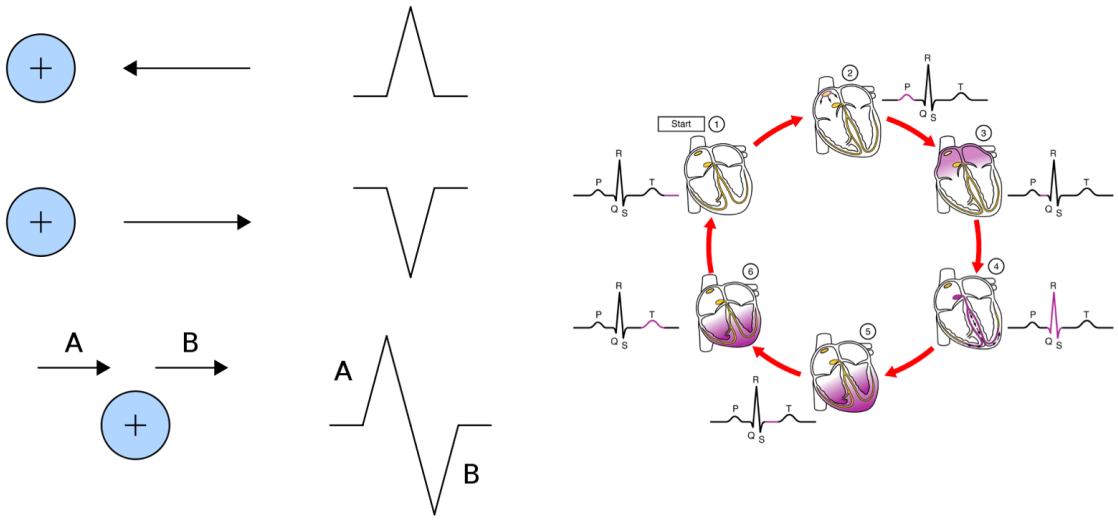

(a) (b)

Figure 2.6: Pattern recognition in ECG: (a) depolarization and repolarization of the heart according to the position of the positive electrode; (b) ECG tracing correlated to the heart conduction system [46]

The theory is rooted in electromagnetics and can be summarized in the four following points as shown in **Figure 2.6**:

1. Depolarization of the heart towards a positive electrode produces a positive deflection.

2. Depolarization of the heart away from a positive electrode produces a negative deflection.

3. Repolarization of the heart towards a positive electrode produces a negative deflection.

4. Repolarization of the heart away from a positive electrode produces a positive deflection.

Additionally, normal rhythm produces 4 components:

1. The P wave that represents atrial depolarization,
2. The QRS complex that represents ventricular depolarization,
3. The T wave that represents ventricular repolarization,
4. The U wave that represents papillary muscle repolarization.

The U wave is not typically seen and its absence is generally ignored. Moreover, changes in the structure of the heart and its surroundings (including blood composition) change the patterns of these four entities. Indeed, some arrhythmias can be observed in ECG. For example, the absence of P waves with irregular QRS complexes can be linked to atrial fibrillation. Also, the absence of P waves associated with wide QRS complexes and a fast heart rate can be related to ventricular tachycardia [60].

2.3.2 Fluorescence Microscope

Calcium imaging is one of the main microscopy technique used to optically measure the calcium Ca^{2+} status of cell cultures, or tissues of excitable cells. This technique uses calcium indicators that are fluorescent molecules which respond to the binding of Ca^{2+} ions by changing their fluorescence properties. This technique is useful for studies of calcium signalling in excitable cells.

Electrical activity in excitable cells is always accompanied by an influx of Ca^{2+} ions. In cardiomyocytes, calcium plays a key role as a second messenger of excitation contraction coupling. Thus, calcium imaging can be used to monitor the electrical activity in cultures of cardiomyocytes, which makes possible to dissect the function of cardiac cell networks. This technique can also be used as a powerful tool for high *in vitro* drug screening analyses, as drug effects can be reflected through changes in calcium fluxes in cardiomyocytes [61].

Chemical indicators are small molecules on an egtazic acid homologue called BAPTA, with high selectivity for Ca^{2+} ions versus Mg^{2+} ions. Binding of a Ca^{2+} ion to a fluorescent indicator molecule leads to either an increase in quantum yield of fluorescence or emission/excitation wavelength shift. The first real-time Ca^{2+} imaging was carried out in 1986 in cardiac muscle [62]. Later development of the technique using laser scanning confocal microscopes revealed sub-cellular Ca^{2+} signals in the form of Ca^{2+} sparks and blips. It is also used to perform research on myocardial tissue to create 2D mapping of cell electrical activity [63]. Special high throughput imaging apparatuses allow simultaneous reading of calcium transients from up to hundreds of samples [64], allowing the study of several disease models and drugs in a short time period compared to conventional microscopes. However, high content screening produces massive amounts of data, which require advanced automated software for data analysis [65].

2.3.3 Patch-clamp Technique

The patch-clamp technique was invented by Erwin Neher and Bert Sakmann in 1976 [66]. They won the Nobel Prize in 1991 based on the invention of this technique. This method was originally designed to detect the activity of single-ion channel proteins in the cell membrane. It was then widely applied to cell analysis, which revolutionized research in physiology at the cellular and molecular levels [67] [68] [69]. The technique is now widely used in the field of single cell and ion channel research. Thanks to this technique, it is possible to monitor changes of intracellular voltage, current, and capacitance in membranes of excitable cells with a high time resolution.

The basic principle of patch-clamp technique uses a glass microcapillary tube as an electrode. A portion of the cell membrane is suctioned into the pipette, creating an omega-shaped area of membrane which creates a resistance R_{seal} in the 10 GΩ - 100 GΩ range ("gigaohm seal") between the inside and outside of the electrode. Thanks to the high resistance of this seal, it is possible to isolate electronically the currents measured across the membrane patch with little competing noise, while providing some mechanical stability to the recording [70]. The region of the membrane in the inner tip of the electrode is then voltage-clamped, and levels of ionic currents through the ion channels in the patch membrane are detected through an amplifier. With this technique, picoampere levels of current can be measured.

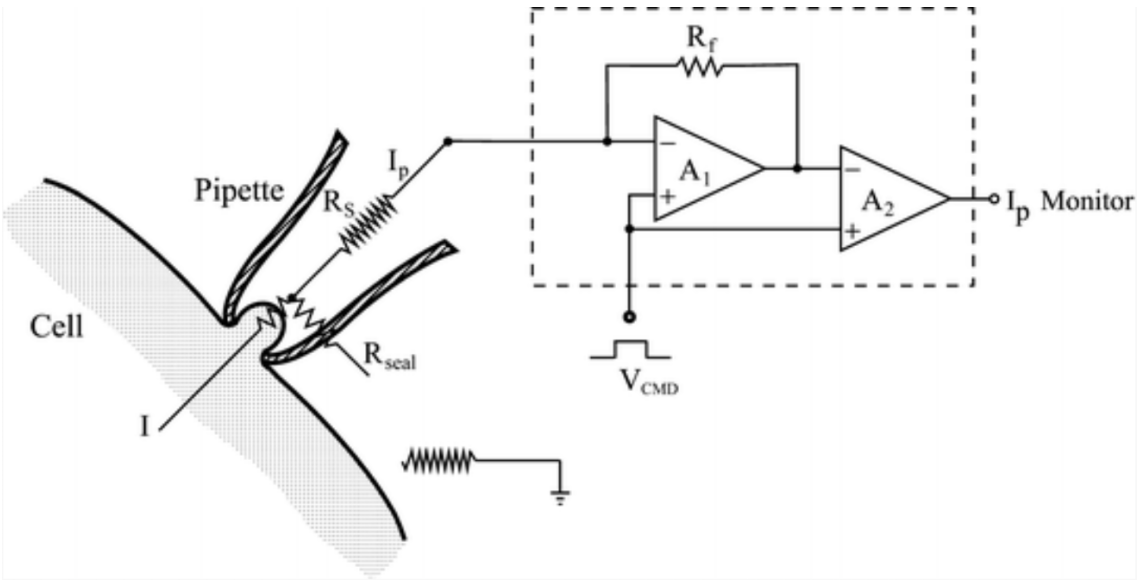

Figure 2.7: Principle of patch-clamp technique [71]

The basic amplifier for patch-clamp is a current to voltage converter circuit with several operational amplifiers (**Figure 2.7**). The design involves transmitting the command voltage V_{CMD} into the positive input of A_1 and the negative input of A_2. The output voltage of A_1 is fed into the pipette and the negative terminal of A_1, so that the voltage matches V_{CMD}. The output of A_1 is then transmitted to the negative terminal of A_2 so that V_{CMD} can be subtracted off of the signal coming from the electrode. If the series resistance R_S between A_1 and the electrode tip is too high, the voltage drops across R_S and the voltage membrane does not equal V_{CMD}. Compensation circuitry can be used to partially correct this problem with R_S around 1 MΩ to 5 MΩ. When the electrode tip is sealed with the patch membrane at more than 10 GΩ, the current through the seal becomes negligible and the recorded current I_p purely reflects in magnitude the current through the cell membrane [71].

2.3.4 Microelectrode Arrays

Excitable cells create ion currents through their membranes when excited, causing a change in voltage between the inside and the outside of the cell. When recording, the electrodes on MEAs transduce the change in voltage from the environment carried by ions into currents carried by electrons. When stimulating, electrodes transduce electronic currents into ionic currents through the media. This triggers the voltage-gated ion channels on the membranes of the excitable cells, causing the cell to depolarize. An MEA can be used to perform electrophysiological experiments on tissue slices or dissociated cell cultures.

The size and shape of a recorded signal depend upon several factors: the nature of the medium in which the cells are located (e.g. the medium's electrical conductivity, capacitance, and homogeneity); the nature of contact between the cells and the MEA electrode (e.g. area of contact and tightness); the nature of the MEA electrode itself (e.g. its geometry, impedance, and noise); the analog signal processing (e.g. the system's gain, bandwidth, and behavior outside of cutoff frequencies); and the data sampling properties (e.g. sampling rate and digital signal processing) [72]. It can be seen that the voltage amplitude an electrode experiences is inversely related to the distance from which a cell depolarizes [24]. Thus, it may be necessary for the cells to be cultured or otherwise placed as close to the electrodes as possible.

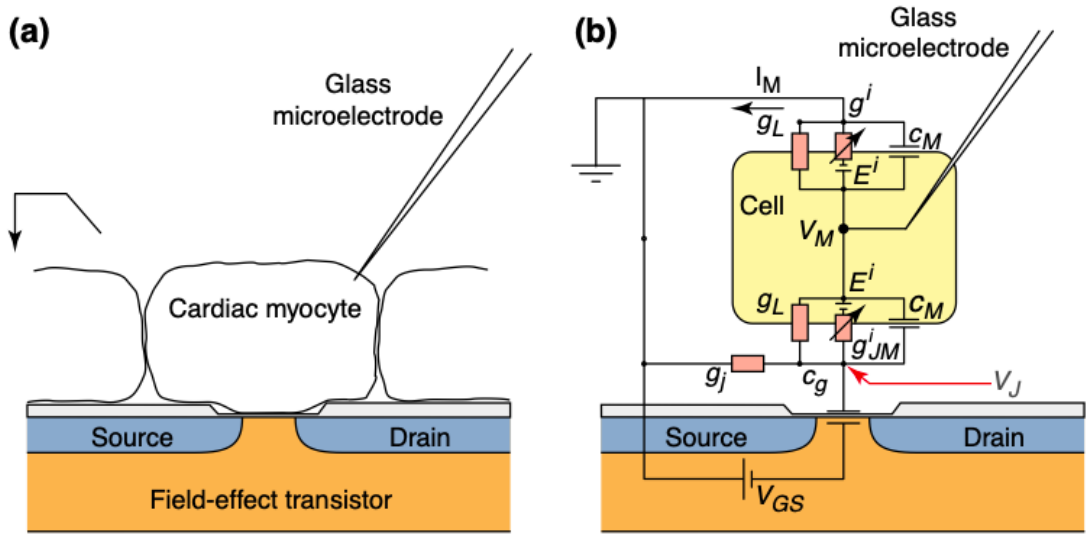

Figure 2.8: Electrical equivalent circuit of a FET-based MEAMEA: cell transistor hybrid system: (a) monolayer of cardiomyocytes cultured on the FET-based MEA substrate; and (b) electrical equivalence circuit of one cardiomyocyte on the FET electrode: the space between the cell and the gate constituted by the electrolyte has a conductance g_j, the membrane has a capacitance C_M, the gate oxide a capacitance c_g, specific ion conductances g_i, and the extracellular voltage V_M is the voltage measured at the gate [73]

Figure 2.8 shows the circuit model of one cardiac muscle cell cultured on an MEA based on field effect transistor (FET) technology. The attached/free membrane of the cell is defined by the membrane capacitance, the leakage conductance and the ionic conductance. The gate oxide is defined by its capacitance and the junction by seal conductance. The extracellular voltage is then recorded by the transistor [73].

The signal detected is an extracellular field potential. This signal is similar in shape with an ECG. Indeed, multiple investigators have showed the correlation between field action potential and ECG [74] [75] [76]. The depolarization is thus compared to QRS complex, whereas the repolarization is referred to as T wave. The field potential is the first negative derivative of the action potential.

Recently, high density MEAs have been developed, backed by the rise of microelectronics such as the CMOS microchips commonly used in digital cameras. Every single electrode has an active, intelligent technology behind it. Amplifiers are located right below each electrode, allowing enhancement of the signal at the source (right underneath the cells) without amplifying any additional noise, and preventing signal attenuation during the propagation of the signal. Using a switch-matrix, high density MEAs allow optimal electrode utilization and signal amplification by achieving exceptional signal to noise ratio (SNR) and integrating circuitry with thousands of electrodes per square millimeter on the same chip. It is thus possible to conduct experiments requiring cellular and subcellular level resolution. For example, 3Brain Company proposes CMOS-MEAs with square electrodes of 21 µm, arranged in a 64 by 64 layout with an electrode pitch comprised between 42 µm and 81 µm. Signals can be recorded at a sampling rate of 18 to 64 KHz for each pixel.

2.3.5 Electrochemical Sensors

Electrochemistry is an important technique for fundamental studies of single cell communication, exchange of chemical messenger molecules, as well as small-scale electroporation applications. The development of electrochemical methods for detection of chemical messengers began with the work of Adams in 1976 and has progressed to the detection of molecules from a single vesicle with the work of Wightman et al. [77] [78]. Since then, fully automated microchips have been designed and manufactured for the detection of electroactive species secreted from single cells and small ensembles of cells [79].

Amperometric detection is a common electrochemical technique, which is applied to the detection of electroactive analytes that can be electrochemically reduced or oxidized. Amperometric detection consists in applying voltage steps to the indicator electrode and measuring the resulting Faradaic current, which is directly proportional to the concentration of the analyte [80]. The simplest reaction that can occur at the working electrode surface polarized at appropriate potential can take the following form:

$$O_x + \mathrm{n}e \rightleftharpoons R_{ed}$$

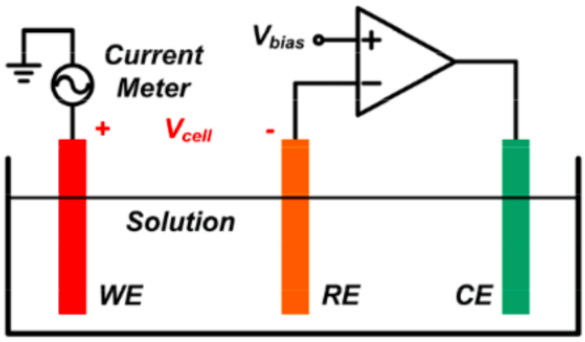

Figure 2.9: Electrodes for amperometric electrochemical sensor [81]

Figure 2.9 shows the basic structure of an amperometric sensor with three electrode cells. The first electrode cell is a working electrode (WE) that serves as a platform on which the electrochemical reaction takes place. The second is a reference electrode (RE) that sets the potential to zero. The third electrode is a counter electrode (CE) that acts as an electron source/sink [81]. A constant potential is applied to the WE to provide energy to the electrochemical process of interest. Current flows between the CE and WE while potential is applied between the RE and WE. The response current is measured through the CE as a function of time.

Amperometry is well suited to quantifying release from vesicles on the millisecond time scale [82]. This approach also offers high selectivity, high sensitivity, and accurate quantification, which is a clear advantage as biological phenomena generally involve small amounts of molecules at very high local concentrations [83].

2.3.6 Impedance-based Techniques

Electrical impedance measurements are used to quantify the resistance of a material to an injected electrical stimulus. In a DC circuit, Ohm's law is used to describe the relationship between resistance (R), voltage (V), and current (I). In the case of an AC circuit, the same general equation applies, but resistance is, in this case, replaced by impedance (Z). Unlike DC resistance, AC impedance is complex and has a real and an imaginary part. The real part of complex impedance is the resistance, whereas the imaginary part arises from inductive and capacitive effects and is referred to as reactance [84], such as:

$$Z(\omega) = Z_{real}(\omega) + jZ_{imag}(\omega)$$

To simplify calculations, sinusoidal voltage and current waves are commonly represented as complex-valued functions of time. The impedance is defined as the ratio of these quantities:

$$Z = \frac{V}{I} = \frac{|V|e^{j(\omega t+\phi_V)}}{|I|e^{j(\omega t+\phi_I)}} = \frac{|V|}{|I|}e^{j(\phi_V-\phi_I)}$$

Hence, we have:

$$|Z| = \frac{|V|}{|I|}$$

$$\phi_Z = \phi_V - \phi_I$$

The first equation is the Ohm's law applied to the voltage and current amplitudes, while the second equation defines the phase relationship.

The rationale for impedance measurements in biological cells is based on the fact that impedance is directly proportional to resistance and inversely proportional to capacitance, and that resistance and capacitance are inversely and directly proportional to the free electrode area. Therefore, when cells adhere and spread to the electrode surface during cell growth, the impedance magnitude or resistance at intermediate frequencies increases because the cells, which have an insulating membrane, disturb the current flow through the electrode. As cells proliferate sufficiently such that the cell density on the limited area of the electrode surface is saturated, the increase in impedance or resistance is halted [85]. Similarly, cells may become detached from the electrode surface, resulting to a decrease of the impedance or resistance as the electric current can flow freely through the uncovered electrode surface.

Impedance-based devices are thus commonly used for the characterization of cells and tissues, and for monitoring changes in shape, growth, proliferation, or differentiation of cells [86] [87] [88] [89]. Using a waveform generator, cells on electrodes are subjected to mV amplitude signals in the kHz range, and resistance, capacitance and impedance data are collected. Giaever and Keese pioneered electrical cell-substrate impedance-based sensing by developing a real-time method for characterization of cellular behavior and responses to drug candidates [90].

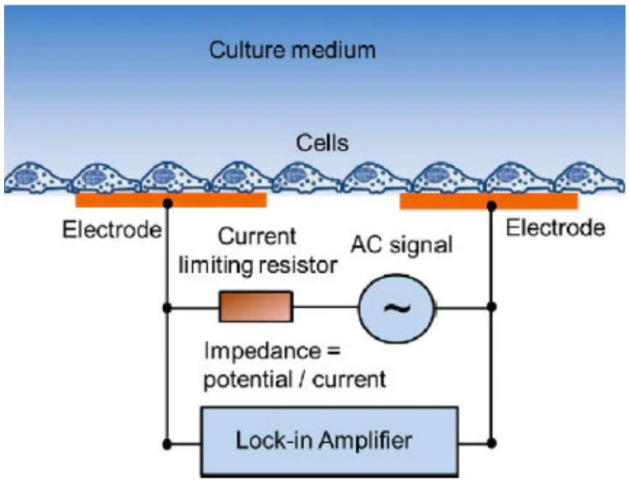

Figure 2.10: Schematic of electrical cell-substrate impedance-based sensing which consists of electrodes, function generator, current limiting resistor, and lock-in amplifier [91]

As shown in **Figure 2.10**, the alternating current flowing through the electrodes and cells is restricted by the current limiting resistor serially connected to the function generator. When a weak alternating current is applied across the electrodes from the signal generator, the responsive potential is recorded by the lock-in amplifier to determine the electrical impedance by using the ratio of the voltage to the current [91].

2.3.7 Dielectrophoresis

DEP is a phenomena which results in the motion of dielectric particles relative to the solvent in which they are immersed. Because biological cells have dielectric properties [92], they can be moved by DEP through polarization forces appearing on the cells and produced by an inhomogeneous electric field.

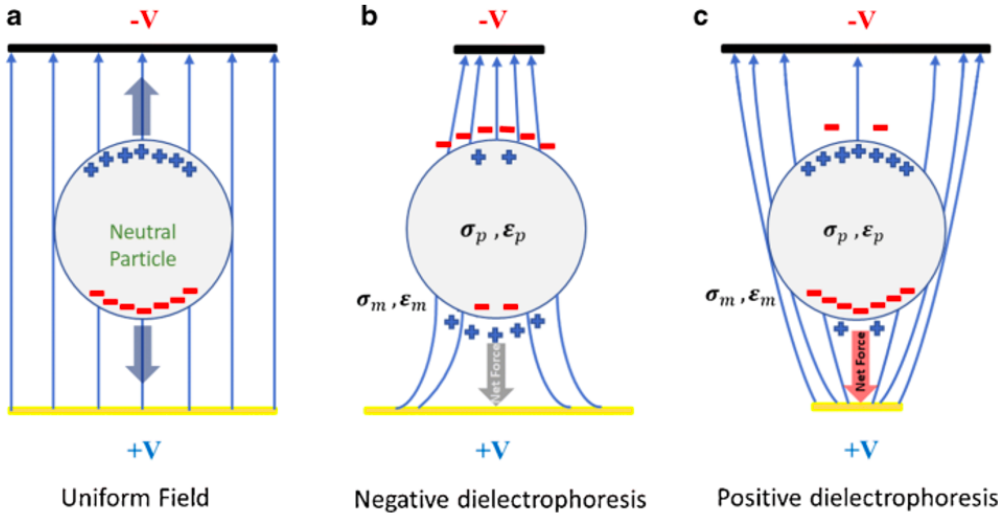

Figure 2.11: Dielectric properties of cells [93]

Inhomogeneous electric field appears when an electrical signal is applied in between patterned microelectrodes. That electric field will exert a DEP force on the particles which will become either attracted towards the maximum of electric field (positive DEP) or repulsed (negative DEP), according to the permittivity of the cells versus the one of the medium (**Figure 2.11**). This phenomena is governed by a force, the DEP force expressed by:

$$\langle F_{\mathrm{DEP}} \rangle = 2\pi r^3 \varepsilon_m \mathrm{Re}\left\{ \frac{\varepsilon_p^* - \varepsilon_m^*}{\varepsilon_p^* + 2\varepsilon_m^*} \right\} \nabla \left| \vec{E}_{rms} \right|^2$$

in which, $\langle F_{\mathrm{DEP}} \rangle$ is the time-average DEP force acting on one dielectric particle, r is the radius of the particle, ε_m is the absolute permittivity of the surrounding medium. Re is the real part of the electric field:

$$R_e = Ecos(\omega t)$$

where ε_p^* and ε_m^* are the complex permittivity of respectively the particle and the medium, and ∇E is the gradient of the amplitude of the electric field. The strength of the force and its repulsive or attractive aspects are strongly dependent on the particles and medium electrical properties, size and shape of the particles, and the frequency of the electric field. The strength and the orientation of the force (positive or negative) can be modeled using the Clausius-Mossotti (CM) factor which contains all the frequency dependency of the DEP force:

$$CM = \left\{ \frac{\varepsilon_p^* - \varepsilon_m^*}{\varepsilon_p^* + 2\varepsilon_m^*} \right\}$$

ϵ^* is dependent on the permittivity and the conductivity of the particles (p) and medium (m), as well as the frequency of the signal. The permittivity and the conductivity of a particle depends on its material, its size and its structure. The "crossover frequency" corresponds to the frequency at which CM equals to zero. Above that frequency, CM changes sign, as well as the DEP force. According to the literature, biological cells present a crossover frequency between 100 kHz and 1 MHz [94] [95].

DEP can be used to separate particles with different sign polarizabilities as they move in different directions at a given frequency of the AC field applied. DEP has been applied for the separation of living and dead cells, with the remaining living cells still viable after separation [96], for cell patterning, or for forcing contact between selected single cells to study cell-cell interaction [97].

2.4 Thin-Film Transistor Technology

2.4.1 Basic Structure

The basic structure of a TFT is a three terminal component (gate, source, and drain) that can be classified by two factors: the planarity of the semiconducting channel (coplanar/staggered) and the gate position (bottom/top) in the semiconductor. In a coplanar situation, the conducting channel is directly between the source and drain terminals, while in a staggered situation the conducting channel is above or below the source and drain terminals depending on the gate position. A bottom-gate configuration is one in which the gate is placed below the semiconducting channel, while a top-gate configuration is one in which the gate is placed above the semiconducting channel [98]. The different configurations of TFTs are shown in **Figure 2.12**.

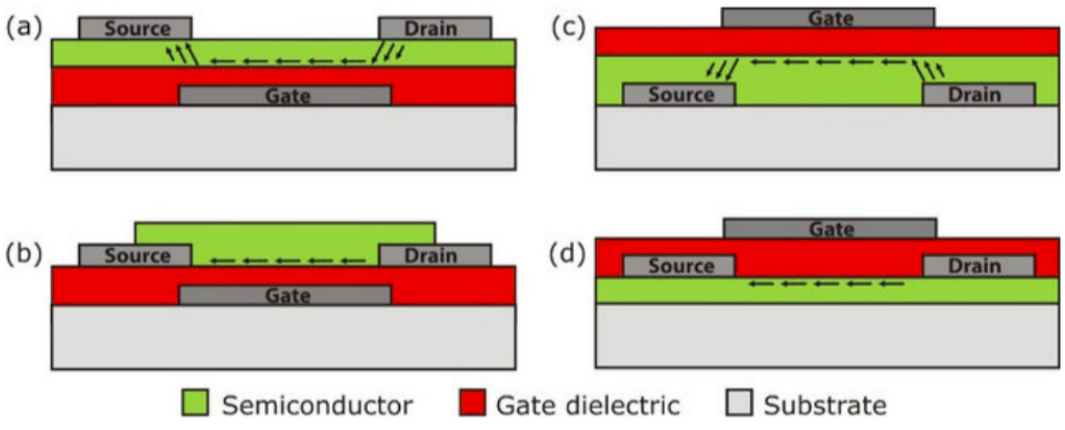

Figure 2.12: General TFT configurations: (a) staggered bottom-gate; (b) coplanar bottom-gate; (c) staggered top-gate and (d) coplanar top-gate [98]

2.4.2 Types of Thin-Film Transistors

A wide variety of semiconductor materials can be used for developing TFTs. One common material used for TFTs is silicon. In this case, the silicon's crystalline state is an important factor to the TFT characteristics. Indeed, the semiconductor layer can be either amorphous silicon, microcrystalline silicon, or it can be annealed into polysilicon [99]. Amorphous silicon-based TFTs have the advantage of being easy to manufacture on a large scale, as well as being transparent [100]. They also have a very high field effect mobility of 4.7 cm^2/Vs in top-gate configuration, and 1.5 cm^2/Vs in bottom-gate configuration [101]. Polysilicon-based TFTs have a much higher mobility: 46 cm^2/Vs [102]. This field effect mobility characterizes how quickly an electron can move through the semiconductor when pulled by an electric field. For semiconductors, the behavior of transistors and other devices can be very different depending on whether there are many electrons with low mobility or few electrons with high mobility. Therefore mobility is a very important parameter for semiconductor materials. Almost always, higher mobility leads to better device performance, with other things equal.

TFTs have also been made using organic materials, referred to as organic field-effect transistors (OFETs), opening possible applications with flexible electronics [103]. However, they may be less stable if integrated on flexible substrates. Organic TFTs can have a mobility as high as 10 cm^2/Vs, which surpasses amorphous silicon-based TFTs [104].

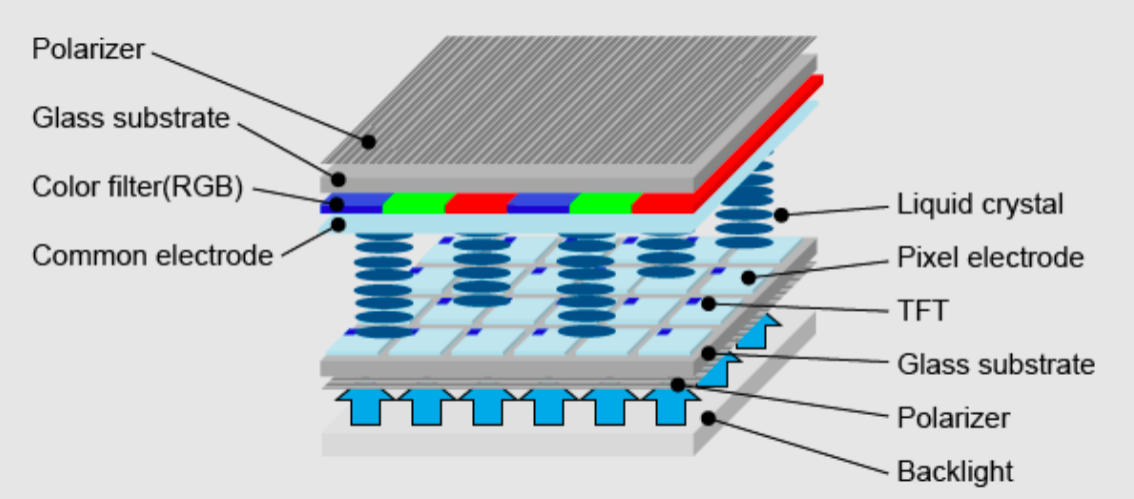

Figure 2.13: Structure of a TFT LCD (Japan Display Inc.)

Other materials which have been used as semiconductors in TFTs include compound semiconductors such as metal oxides. Some examples of oxide compounds are zinc, cadmium, or indium [105] [106] [107].

By combining transparent semiconductors with transparent electrodes, such as indium tin oxide (ITO), TFT devices can be made transparent. As a result, they can be used for construction of video display panels for televisions or computer screens. **Figure 2.13** shows the structure of a TFT LCD. The first solution-processed of completely transparent TFTs, based on zinc oxide, were reported in 2005 at the NOVA University Lisbon. The TFT could be produced at room temperature [108].

Recently we have seen a growing interest in indium oxide compound indium gallium zinc oxide (IGZO). The first amorphous IGZO TFTs were developed in 2004 [109], with a mobility of 8.3 cm^2/Vs,. The device was transparent and could be fabricated at room temperature. Sharp corporation then started the fabrication and commercialization of TFT LCD panels using IGZO semiconductors in 2012. In this research in collaboration with Sharp corporation, transparent TFT devices are used for the study of biological systems.

2.5 Chapter Summary

In this chapter, we presented the theory related to the structure, function and properties of cardiomyocytes. The recording techniques used for *in vitro* analysis of excitable cells have then been described. Finally, we introduced the TFT technology used in this research and discussed about the different types of TFTs.

Chapter 3

Methodology

In this chapter, we describe the structure, working principle, and fabrication of the TFT-MEA platform used in this research. Then we explain how experiments of electrophysiology, electrochemistry, and dielectrophoresis are performed. For each type of measurement, we describe the preparation of the device, the preparation of biological materials, and the experimental setup. Finally, we present the tools used for data analysis of electrophysiological measurements.

3.1 Thin-Film Transistor based MEAs

3.1.1 Structure

The substrates of TFT arrays used in this study were designed and fabricated by Sharp Corporation for the purpose of biological applications. This work involves the use of substrates with a large, dense array of 150 × 150 square transparent electrodes of 100 µm with an electrode pitch of 5 µm. Each electrode is individually connected to a TFT, which controls the open/close states of the electrode. The principal substrate used for this study is 27 mm × 25 mm and the electrodes cover a surface of roughly 225 mm^2.

The transistor is a three terminal component (gate, source, and drain) on a bottom-gate configuration. The surface electrodes are ITO, which is a transparent conductor. Each electrode is connected to the drain of a transistor through a via of Mo/Al/Mo. Multiple insulation layers are placed between the surface electrode and the gate and source lines in order to prevent possible interference. Insulation layers are SiN, structural polymer, and SiN/SiO. The gate, source, drain, and their addressing lines are constructed of Mo/Al. The channel is an N-type semiconducting channel of IGZO, which has the property to be nearly transparent. For the sake of transparency, the size of transistors cannot be too large. However, a too small transistor can interfere with the source-drain transmission. Here, the transistors varied from 5 to 15 µm.

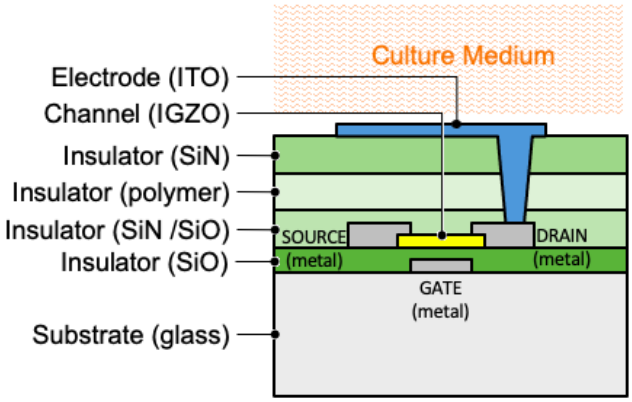

Figure 3.1: Structure of transistor in a TFT-MEA

A schematic view of the TFT structure can be seen in **Figure 3.1**. The TFTs used in this research are N-channel transistors, which means that the conventional flow of drain current is in the positive direction so a positive gate voltage is applied to switch the transistor ON.

3.1.2 Working Principle

In this research, each electrode is independently connected to an integrated TFT, which controls the current/voltage of that single electrode. TFTs are thus used for switching ON/OFF the electrodes. TFTs consist of three terminals: a gate, a source, and a drain. Gate terminals are addressed through column-parallel connected lines, while source terminals are addressed through row-parallel connected lines. The drain terminal of each TFT is connected to the corresponding ITO electrode. By applying a positive voltage to the gate line (column), all TFTs connected to this line are switched ON.

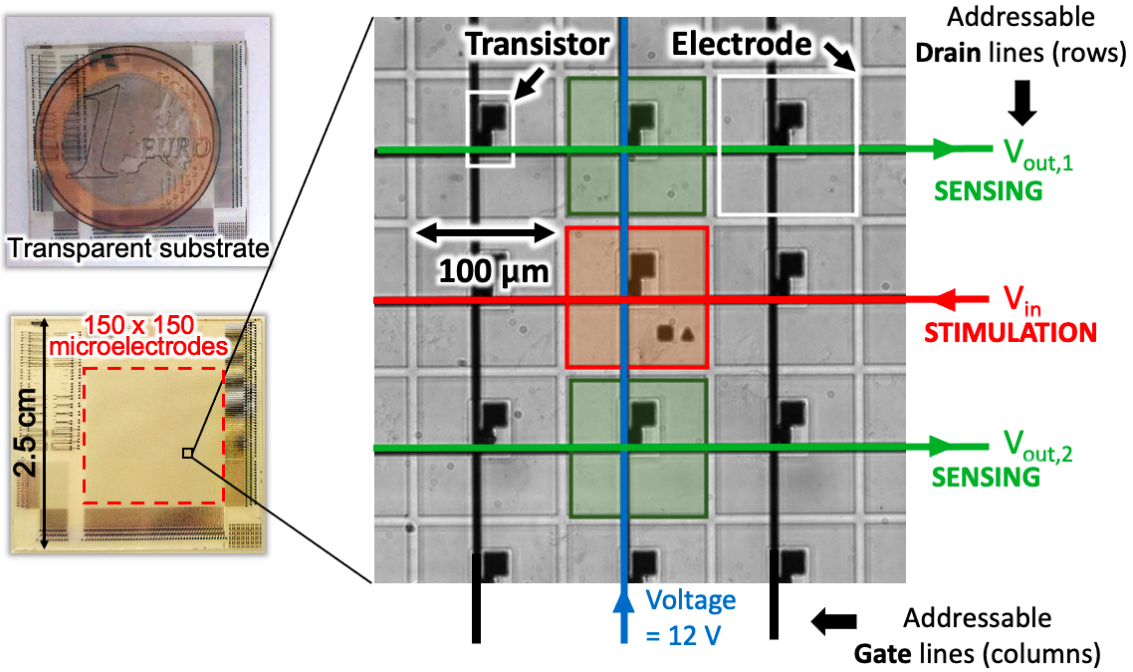

Figure 3.2: Working Principle of TFT-MEAs

With a measurement system, or a signal generator connected to the source lines, the electrodes at the intersection of the gate/source lines can be used for sensing or for applying an electrical signal respectively. **Figure 3.2** shows the working principle of our TFT-MEAs.

3.1.3 Fabrication

Fabrication on PCB

To access the pads connected to the gate and source lines, the TFT substrate is mounted on a commercially available printed circuit board (PCB). A 20 mm × 20 mm hole is made in the PCB beforehand, so that optical transparency of the whole device remains possible. Connectors are then placed on the PCB using a solder.

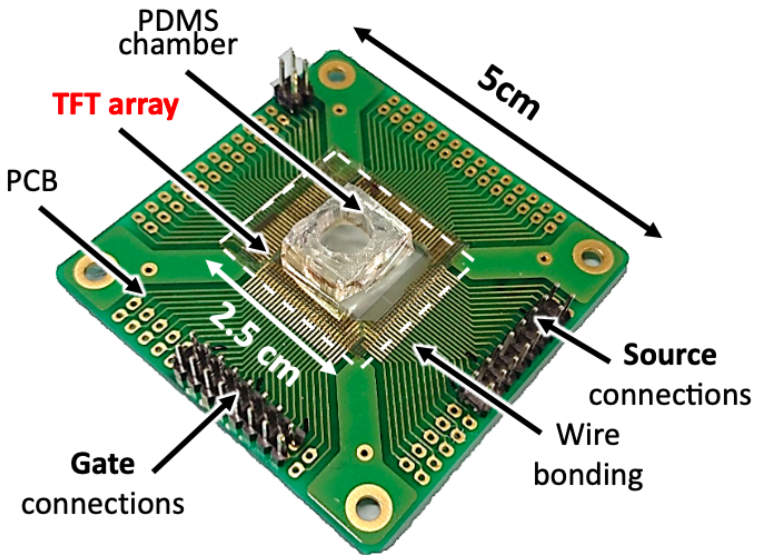

Figure 3.3: Photo of the TFT-MEA platform after post-processing

The TFT substrate is finally attached to the PCB and the connections between the pads of the TFT substrate and the pads of the PCB are done by wire bonding (WEST BOND, Product No.-10267).

PDMS chamber

A PDMS chamber is placed on the TFT substrate to culture cells on the device. PDMS is prepared by mixing a curing and a base agent (SILPOT 184) in the ratio 1:10. After removing potential bubbles with a vacuum chamber, the mixture is placed on a hot plate at +90°C for a few hours for fast curing. A square-shaped PDMS culture chamber of 20 mm with a 16 mm diameter hole in the middle is then prepared and placed on the TFT substrate. Finally, PDMS is added around the culture chamber for fixing it to the TFT substrate and for protecting the bonding wires. **Figure 3.3** presents the TFT-MEA after post-processing.

3.1.4 Characterization

After fabrication of the TFT-MEA, characterization of the device can be performed. The accurate determination of the TFT threshold voltage (V_{TH}) is essential for TFT device operation, as it is the minimum gate-to-source voltage that is needed to create a conducting path between the source and drain terminals. Among numerous V_{TH} extraction techniques, the transconductance change method is recognized as one of the most useful and accurate because it is considered to be unaffected by mobility degradation and series resistance effects [110]. The electrical characterization of the TFT platform was performed by evaluating the current-voltage (IV) characteristics of TFTs using a Keysight B1500A semiconductor analyzer (Keysight Technologies, USA).

The characterization of TFTs requires the post-processing of gold patterns to "loop-back" connect two electrodes together and to have access to separate source and drain lines [111]. For this study, we evaluated the drain current (I_d) and gate voltage (V_g) characteristics with a drain voltage (V_d) of 1 V on several TFTs. We calculated the transconductance (gm), which quantifies the I_d variation with a gate-source voltage (V_{gs}) variation while keeping the drain-source voltage (V_{ds}) constant. As a result of these measurements, we calculated a V_{TH} value of 4.8 V. Nine TFTs were also chosen on various position on the device for determination of $I_d - V_d$ variations. We obtained a variation of saturation current (I_{dsat}) of approximately 10 %.

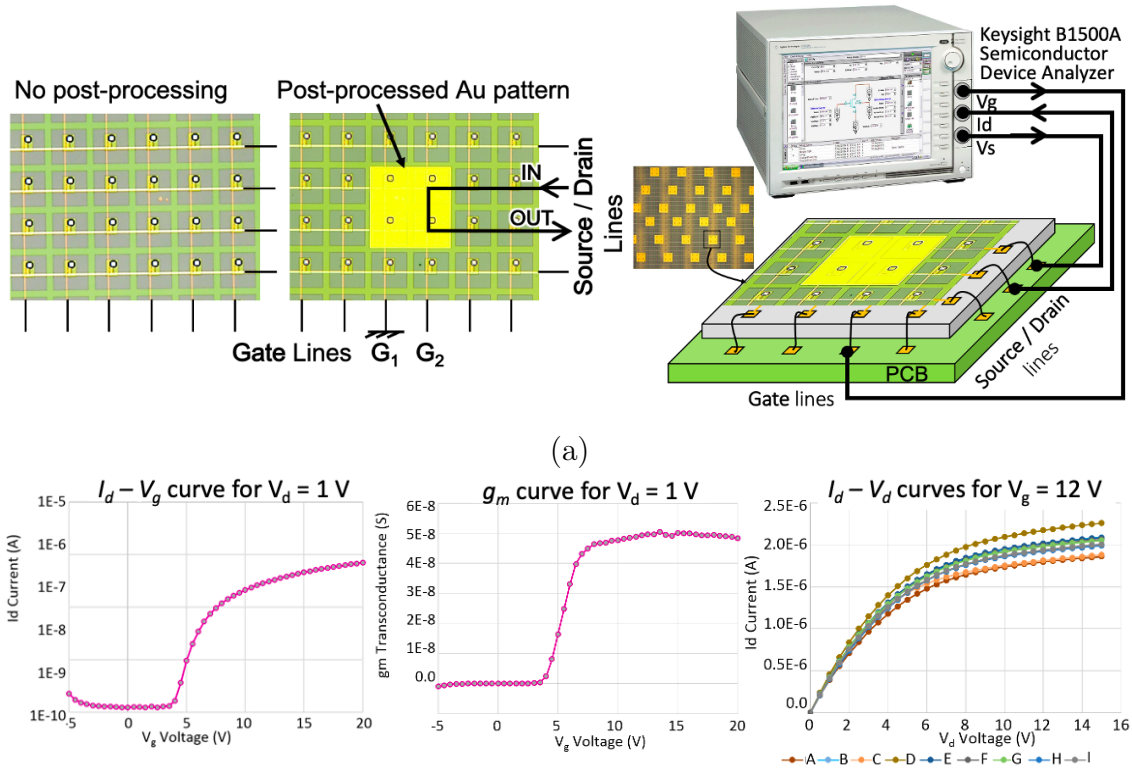

Figure 3.4: TFT array characterization: (a) experimental setup for TFT characterization with a semiconductor analyzer; (b) characterization results for $I_d - V_g$ (left), $g_m - V_g$ (middle), and $I_d - V_d$ (right).

Figure 3.4 presents the experimental setup, as well as the $I_d - V_g$, $g_m - V_g$ and $I_d - V_d$ curves obtained for the IV measurements. This characterization justifies the choice of 12 V applied to the gate lines for reaching the saturation region and switching ON all the transistors. It also demonstrates the variation of characteristics among transistors. This has to be taken into account when transistors are used as circuit elements like in the case of sensing applications.

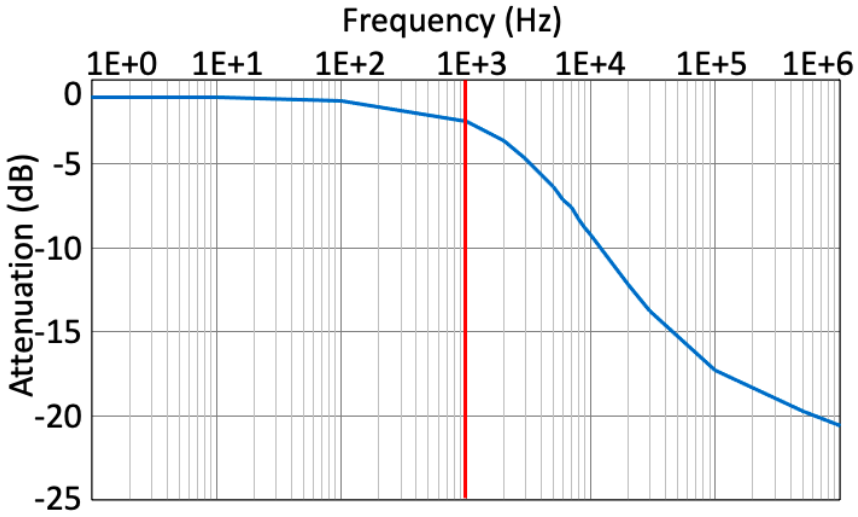

Figure 3.5: Bode diagram for one transistor

TFTs used for LCD are working in DC mode. However, an AC signal is required for some applications, such as DEP experiments. Therefore, the range of frequencies that is compatible with our TFT-MEA needs to be determined. To accomplish this, a Bode diagram was built. A probe was placed on one electrode in dry environment. The corresponding gate line was then supplied with 25 V DC voltage and the source line was supplied with 10 V AC voltage. The range of frequencies of the AC voltage was [1 Hz : 1 MHz], which is a typical result from low pas filter systems. **Figure 3.5** shows the Bode diagram obtained in our experiments. We observe -10 dB attenuation at 10 kHz and -20 dB attenuation at 1 MHz. As a result, DEP can be performed with signals of 100 kHz maximum. Regarding electrophysiological measurements, we notice that signals at 1 kHz are almost not attenuated. As the signal frequency of cardiomyocytes is around 1 kHz or lower range, it is possible to perform efficient voltage sensing of the cell electrical activity.

3.2 Experiments for Electrophysiology

3.2.1 Preparation of the Device

TFT-MEAs and standard MEAs were used for electrophysiological experiments with cardiomyocytes. Among the standard MEAs tested, we used commercially available devices from two companies: Alpha MED Scientific Inc. and Multichannel Systems MCS GmbH.

The surface of TFT-MEAs and commercially available MEAs is usually hydrophobic and they tend to become more hydrophobic again during storage. However, an hydrophobic surface prevents attachment and growth of the cells, which are hydrophilic. The first step in preparing a substrate for use is therefore to ensure that the surface is hydrophilic enough for coating and cell adhesion [112]. The MEAs are thus placed in a plasma-cleaning chamber available in our laboratory and are exposed to a gas plasma discharge, which makes the surface polar and thus more hydrophilic. MEAs are usually treated with low-vacuum plasma for 1 minute at 0.2 mbar and 50 W to 100 W. The treatment gives a very clean and sterile surface that can be coated readily with water-soluble molecules if needed.

MEAs are then sterilized with standard methods for cell culture materials using rinsing with alcohol and UV light. 70 % ethanol is placed in the PDMS culture chamber for 1 hour. The whole device is then rinsed once with 70 % ethanol, and then rinsed 3 times with autoclaved deionized water. MEA devices are not fully immerse into alcohol for a longer time as bonding wires of TFT-MEAs, even though covered by PDMS, can be damaged, and the ring on the commercial MEAs may get off. MEAs are then let air-dry for a few hours in a laminar flow hood with UV light turned on.

Coating of MEAs with various materials can be used for improving the attachment and growth of cell cultures. Fibronectin is a typical biological coating used for heart tissues. The adhesion tends to be very stable, which allows longer cultivation times. A concentration of 10 µg/ml fibronectin (Sigma, F1141-1MG) is prepared in phosphate buffered saline (PBS) and the MEA surface is covered with 300 µl fibronectin solution and incubated at +37°C for at least 1 hour. The surface is then rinsed 2 times with PBS and cells are plated onto the surface immediately after coating [112]. We noticed that no clear difference was observed, regarding cell attachment, cell viability, and cell electrical activity, between cells cultured on a coated substrate and cells cultured on a non-coated substrate. Therefore, most experiments were performed without surface coating with fibronectin.

3.2.2 Preparation of Cardiac Muscle Cells

In this study, cardiomyocytes are used for electrophysiological measurements with our TFT-MEAs. For these experiments, cardiomyocytes are isolated from neonatal mouse hearts and dissociated into single cell suspension for cultivation of beating cardiomyocytes. Neonatal hearts are dissociated using the neonatal heart dissociation kit for mouse from Miltenyi Biotec GmbH (Bergisch Gladbach, Germany). Cardiomyocyte isolation was performed by a collaborator from the Department of Cardiovascular Medicine at the University of Tokyo. An illustration of the steps for cell dissociation is found in **Figure 3.6**.

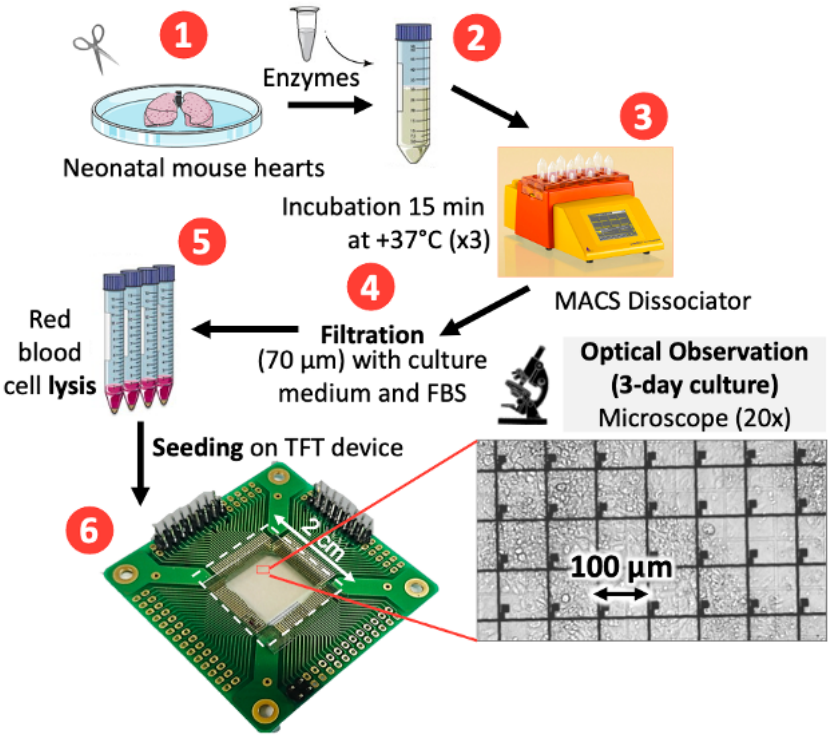

Figure 3.6: Flowchart for neonatal heart dissociation

The cells are then plated onto the surface at a very high concentration to ensure a good network connection among the cells. A cell density in the range of 2.5×10^5 - 1.0×10^6 cells/device used to give the best results for our experiments with TFT-MEAs. In other words, good synchronicity and strong cell contraction of the cardiomyocyte cultures could be observed. A droplet of 30 µL of cell solution is placed on top of the targeted electrodes of TFT-MEAs. The devices are then incubated at +37°C for 15-30 minutes to let the cells fall onto the electrodes and prevent them to escape the targeted region of study. Indeed, it has been observed that cells tend to avoid attaching to electrodes and prefer growing onto electrode-free regions of the TFT substrates. Culture medium is then carefully and slowly added into the culture chamber to avoid detaching the cells from the surface electrodes.

Finally, each device is placed in a petri disch and stored in the incubator at +37°C with 5% CO2 and 90% humidity. Despite the harsh environment of the incubator, no substantial damage was observed at the level of the connection pins of the PCB, or the bonding wires covered with PDMS.

Reagent	Supplier	Reference
DMEM (1X) 500mL	Gibco	11995-065
Pen/Strep	Gibco	15140-122 100ML
L-Glutamine 200mM (100X)	Gibco	25030-081 100ML C
Fetal Bovine Serum (FBS)	Gibco	26140-079

Table 3.1: Reagents for cell culture of cardiomyocytes

Cardiomyocytes are cultured for at least 3 days on the TFT devices. Half of culture medium is carefully changed every day during the whole period of electrophysiological measurements. Culture medium for cardiomyocytes was prepared by mixing 500 mL DMEM with 50 mL FBS, 5 mL Pen/Strep, and 3.5 mL L-Glutamine. The list of reagents can be found in **Table 3.1**.

3.2.3 Experimental Setup

A control card, called JAPASTIM, was developed in our laboratory to obtain a dynamic access to the TFTs and control the ON/OFF status of the gate and source lines, thus offering a 2D controllable area. The control card is a waveform generator with 28 $\times$ 28 modular outputs. It has a range of amplitudes between -5 V and +27 V and allows the application of various shapes of electrical signals, such as DC, AC, and pulses. The control card is then programmed by means of the open-source software, Tera Term. The electrodes can then be controlled in a flexible way and can be used for local sensing, stimulation, or DEP.

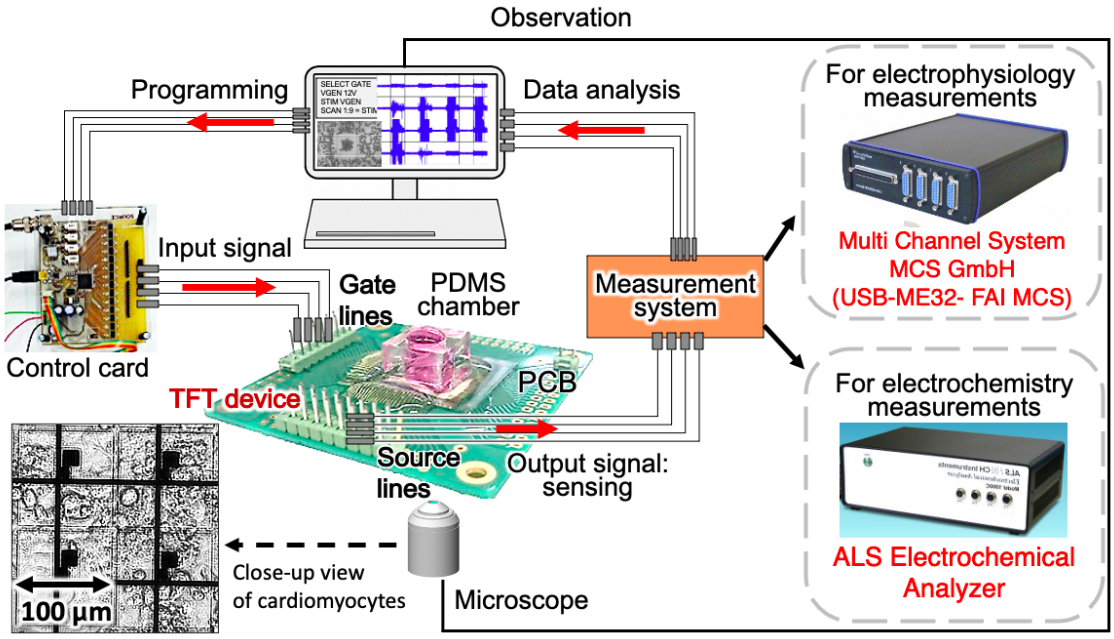

Figure 3.7: General experimental setup scheme for electrophysiological and electrochemical measurements with a TFT-MEA: a data acquisition system (Multi Channel Systems MCS GmbH) is used for extracellular electrophysiology, and an electrochemical analyzer (ALS Co., Ltd) is used for electrochemistry

In this section, we focus on the voltage sensing of cardiomyocyte electrical activity. The control card is composed of two parts: the "source card" that can control the source/gate lines, and the "gate card" that controls the gate lines of the TFTs. The measurements of the electrical activity of cardiomyocytes is performed using the experimental setup described in **Figure 3.7**. The gate lines are connected to the "gate card" of the control card, while the source lines are connected to a USB-ME32-FAI acquisition system (Multi Channel System MCS GmbH) for data measurement using a sampling frequency of 10-20 kHz. The "source card" is thus not needed in these experiments.

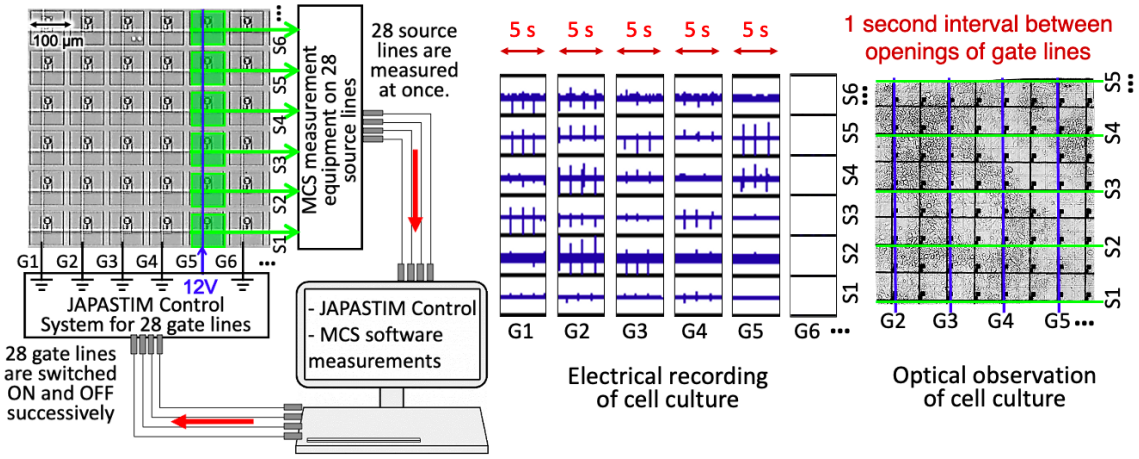

Figure 3.8: Schematic view of 6 × 6 connected electrodes for electrophysiological measurements

The number of channels available on the MCS acquisition system is limited to 32. In most experiments we connected 28 gate lines and 28 source lines, which confers an array of 784 electrodes available for measurement. For voltage sensing experiments, gate lines have to be opened successfully. The JAPASTIM control card is thus programmed to scan the gate lines by switching ON and OFF each gate one after another. Measurements are taken through the source lines during the entire period of gate scanning. **Figure 3.8** shows a schematic view of the connected electrodes for a set of experiments with cardiomyocytes. In this example, we connected one every two electrodes for both the gate and source lines. As a result, the array of connected electrodes covered a total area of 5.8 mm × 5.8 mm, with half of the surface directly available for measurements.

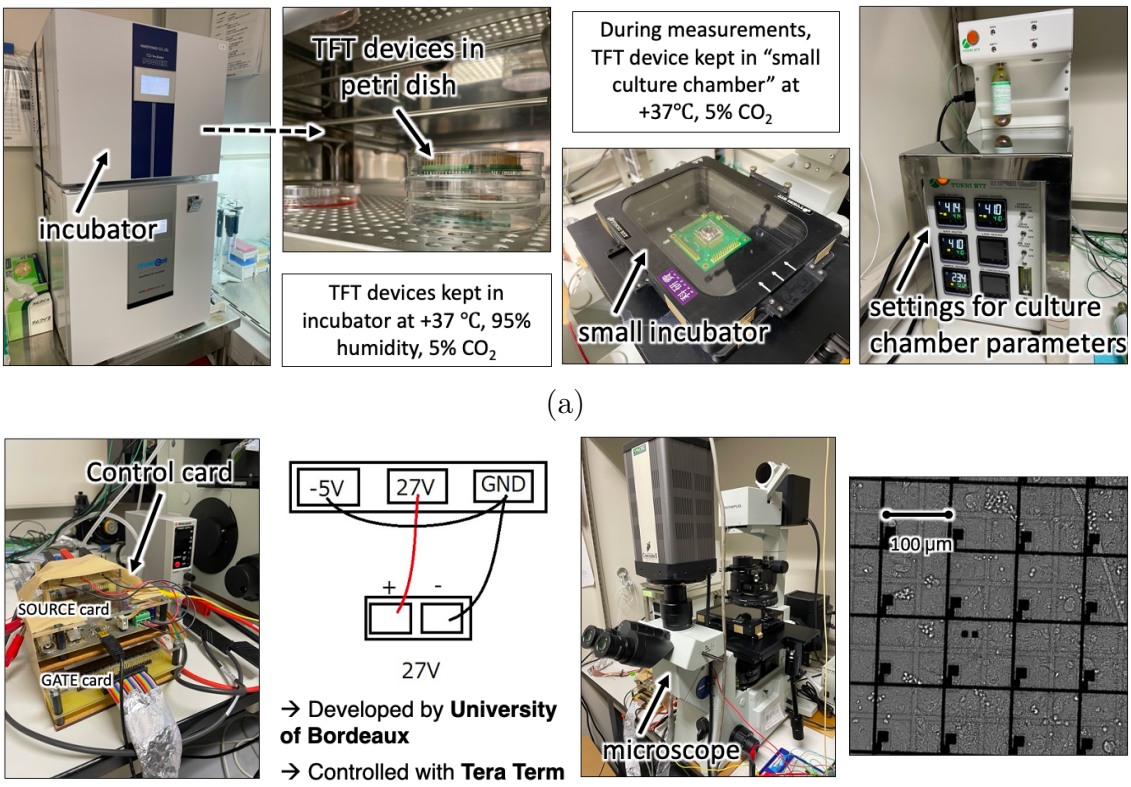

Figure 3.9: Photos of equipment used for electrophysiological measurements with cardiomyocytes: (a) TFT device placed in the laboratory incubator between measurements and in a small incubator during measurements; and (b) JAPASTIM control card for switching ON/OFF the TFTs, and the inverted microscope for optical observation

Electrical recordings are performed under an inverted microscope to observe the contraction of cardiomyocytes simultaneously. For measurements, the TFT-MEA is placed in a small incubator under the microscope to keep the cell environment at +37°C, and a thin wire of Ag/AgCl placed in the culture medium is used as reference electrode. **Figure 3.9** shows photos of the incubators, JAPASTIM control card, and microscope used for electrophysiological experiments with cardiomyocytes.

3.3 Experiments for Electrochemistry

3.3.1 Preparation of the Device

In this study, electrochemical experiments did not involve culture of biological cells on our TFT-MEAs. Less surface treatment was thus needed for this type of analysis. For these measurements, we wanted to test the feasibility of integrating a reference electrode directly onto the substrate of TFT-MEAs. For performing this test, an Ag/AgCl ink (ALS Co. Ltd, 011464) is thus painted directly onto the region of TFT-MEAs that is specifically dedicated for reference electrode. The Ag/AgCl ink is then let air-dried for a day.

3.3.2 Preparation of Tyramine

Electrochemical analyses for amperometry experiments were realized with tyramine, which is a vasoactive amine derived from the amino acid tyrosine. This molecule is acquired through alimentation and is metabolized in digestive system by various enzymes, including monoamine oxidases. Tyramine was chosen due to its direct availability in our laboratory and its effects on heart rate and blood pressure when administered in large quantity [113] [114]. Tyramine (Tokyo Chemical Industry, A0305) is prepared in 1X PBS solution at different concentrations: 10 µM, 100 µM, and 1 mM.

3.3.3 Experimental Setup

Integration of Electrochemical Sensors

The experimental setup for electrochemical sensing is similar to the one used for voltage sensing. The experimental setup is described in **Figure 3.7** and **Figure 3.10**. In general, electrochemical measurements require three electrodes: a counter electrode (CE), a working electrode (WE) and a reference electrode (RE). Current flows between the CE and WE. Here, the CE is a platinum wire placed inside an electrolyte solution. The WE is either a standard gold electrode (ALS Co., Ltd, AUE gold electrode 2014) or an ITO electrode from our TFT-MEA. The RE is either an Ag/AgCl glass electrode or integrated Ag/AgCl RE made with Ag/AgCl ink placed directly on a specially dedicated RE area of the TFT substrate.

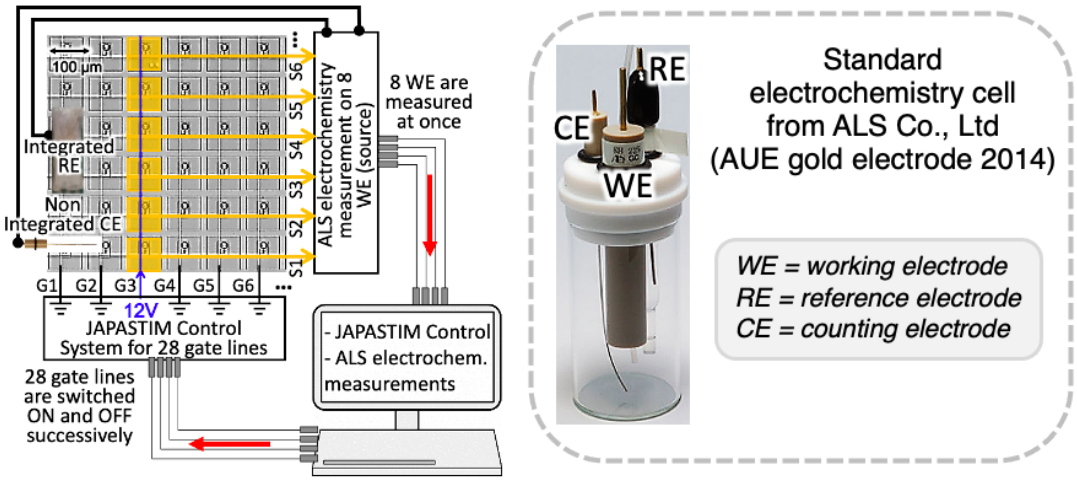

Figure 3.10: Schematic view of 6 × 6 connected electrodes for electrochemical measurements and photo of standard electrochemistry cell

Voltammetry and Amperometry

In this study, two electrochemical methods are performed: cyclic voltammetry and amperometry.

- **Cyclic Voltammetry**: the potential difference between the WE and RE is changed periodically, and the current between the WE and CE is monitored. Cyclic voltammetry experiments are performed with 2 mM K3Fe(CN)6 in 1 mM KCl solution, which is a standard material for electrochemical calibration. The range of potential applied during measurements is comprised between [-0.6 V : +0.6 V], with a scan rate of 0.1 V/s.

- **Amperometry**: a constant potential difference is applied between WE and RE. The current between the WE and CE is monitored as it is an indication of the analyte concentration through the reaction progress. Amperometric experiments are realized with tyramine in PBS. Different concentrations of tyramine are analyzed and compared using either standard gold WE or ITO WE of the TFT-MEA. The applied potential is +0.3 V with a scan rate of 0.05 V/s.

3.4 Experiments for Dielectrophoresis

3.4.1 Preparation of the Device

Successful DEP results were already obtained with microbeads and yeast cells using our TFT-MEAs [115]. However, when using mammalian cells, efficient transport required larger voltages, which damaged the electrodes due to electrolysis. To overcome this problem, TFT substrate is coated with a thin insulation layer to protect the substrate from the culture medium and electrolysis. Therefore, to prevent damage of the electrodes, a 400 nm layer of Teflon is coated on the TFT substrate, allowing the application of a voltage higher than 3 V.

Before plating the mammalian cells, the TFT-MEAs are sterilized to avoid contamination and sustain viability of the cells. The sterilization process is the same as the one used for electrophysiological experiments. 70 % ethanol is placed in the culture chamber for 1 hour. The whole device is then immersed once with 70 % ethanol, and then rinsed 3 times with autoclaved deionized water. Finally, the TFT devices are let air-dry under UV light for a few hours in a laminar flow hood.

3.4.2 Preparation of Liver and Skeletal Muscle Cells

HepG2 Liver Cells

DEP experiments have been first performed with HepG2 cells due to their direct availability in our laboratory. HepG2 is a human liver cancer cell line, which is usually used as an *in vitro* model system for the study of polarized human hepatocytes [116]. Hepg2 are cultured in a 25 cm^2 flask in HepG2 Human Hepatocellular Carcinoma Expansion Media until they reach 80% confluency. Then, HepG2 are gently washed once with PBS and subcultured at a 1:3 split ratio using 0.25% Trypsin/EDTA. The list of reagents is found in **Table 3.2**.

Skeletal Muscle Cells

C2C12 cells have then been used to confirm the results previously obtained with HepG2. C2C12 is an immortalized mouse myoblast cell line that is capable of rapid proliferation under high serum conditions and differentiation into myotubes under low serum conditions. C2C12 cells also demonstrate rapid development and maturation into functional skeletal muscle cells and have the ability to contract and generate force, which is useful in biomedical research [117]. C2C12 are cultured in a 25 cm^2 flask in culture medium (500 mL DMEM, 50 mL FBS, 5 mL Pen/Strep, 3.5 mL L-Glutamine). When they reach 70% confluency, C2C12 are subcultured at a 1:10 split ratio using 0.05% Trypsin/EDTA. Reagents used for culture of C2C12 cells are listed in **Table 3.2**.

Reagent for HepG2	Supplier	Reference
HepG2 Human Hepatocellular Carcinoma Expansion Media	Cellular Engineering Technologies	HEPG2.E.Media-450
0.25% Trypsin-EDTA (1X)	Gibco	25200-056 100ML
PBS, pH 7.4	Gibco	10010-023

(a)

Reagent for C2C12	Supplier	Reference
DMEM (1X) 500mL	Gibco	11995-065
Pen/Strep	Gibco	15140-122 100ML
L-Glutamine 200mM (100X)	Gibco	25030-081 100ML C
Fetal Bovine Serum	Gibco	26140-079
Horse Serum	Gibco	16050-122 500ML
0.05% Trypsin-EDTA (1X)	Gibco	25300-054 100ML
PBS, pH 7.4	Gibco	10010-023

(b)

Table 3.2: Reagents for cell culture of (a) HepG2 liver cells, and (b) C2C12 skeletal muscle cells

Buffers and Cell Platting

For DEP experiments with TFT substrates, it is necessary to work with a low conductive buffer. Indeed, a low conductivity buffer allows a large Clausius-Mossotti factor in the range of working frequency and provides efficient effects. A low conductivity buffer solutions has thus been prepared and tested for our DEP experiments.

DEP of yeast is possible in deionized water with a conductivity of 0.055 µS/cm. However, deionized water is hypotonic compared to the inner of mammal cells. Consequently, mammalian cells would swell and burst in this type buffer due to the diffusion of water by osmosis in the cells. Because yeast cells have a double membrane to protect them, these cells are not subjected to the same effects. A low conductivity buffer solution of 300 mM D-Mannitol (Sigma-Aldrich, M4125-10MG) has thus been prepared for experiments. This 300 mM D-Mannitol solution has a relatively low conductivity of 10 µS/cm that keeps the osmolarity of the cells.

Solutions of 1.0×10^6 cells/mL are prepared in 300 mM D-Mannitol and placed in the PDMS culture chamber of the TFT-MEA. Experiments are performed for no longer than 1 hour for preventing possible damage to the cells due to the D-Mannitol solution. For some experiments, 10 µm polystyrene microbeads (Bangs Laboratories, Inc.) are added to the cell solution at a concentration of 4%. Solution of propidium iodide (PI) has also been used in our DEP experiments. PI is a fluorescent agent that binds to DNA by intercalating between the bases with little or no sequence preference. PI has a fluorescent excitation/emission maximum of 493 nm (blue-green) / 636 nm (red). After binding DNA, the excitation/emission maximum of PI is shifted to 535 nm (green) / 617 nm (orange-red) [118]. PI has thus been used as a DNA stain to evaluate cell viability in the solution of D-Mannitol.

3.4.3 Experimental Setup

The experimental setup for DEP experiments with TFT-MEAS is shown in **Figure 3.11**. It consists of five main parts: (1) electrical sources for applying the desired voltage through the source lines, (2) the JAPAS-TIM control card composed of a "gate card" and "source card" that activates the electrodes through the gate and source lines, (3) a TFT-MEA prepared for DEP experiments, (4) a computer to send the commands to the control card, and (5) a microscope for optical observation. Unlike voltage sensing for electrophysiology, DEP experiments require an output AC signal on the electrodes of the TFT-MEA. It is thus necessary to apply a DC signal with the "gate card", and an AC signal with the "source card" to the gate and source lines respectively.

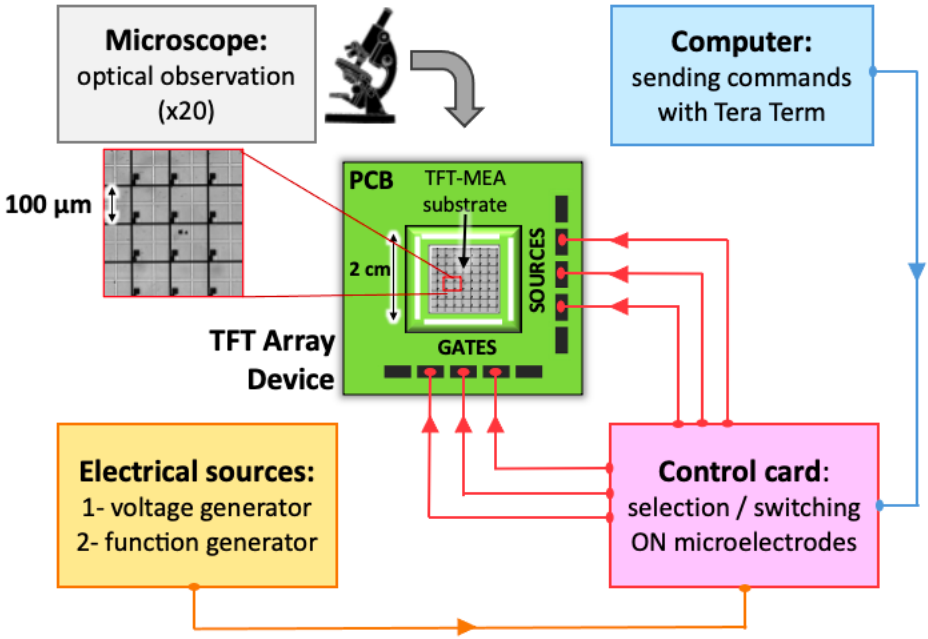

Figure 3.11: Experimental setup for DEP

The JAPASTIM control card is programmed on the computer with Tera Term. This system can provide: 0 V (ground), [-5 V : +5 V] (low voltage), and [+5 V : +24 V] (high voltage). For AC signal, the coaxial external input needs to be connected to a function generator with the card programmed in "external signal mode". AC electro-osmosis (ACEO) force is dominant for frequencies from DC to 1 kHz, which means that vortexes can appear at the edge of electrodes [119]. This phenomenon may thus make the mobility of cells difficult. Additionally, according to the measurements for TFT characterization, strong attenuation of the signal is observed for frequencies above 100 kHz. As a result, frequencies in the range of [1 kHz : 100 kHz] are thus applied for our DEP experiments.

3.5 Data Analysis for Electrophysiology

3.5.1 Wave Propagation

As measurements are performed simultaneously on the electrodes of the same column, the propagation velocity of the cell electrical signal is calculated for columns of electrodes (e.g. on 4 columns of electrodes with 4 electrodes on each column). To accomplish this, we select the first electrode that detects an electrical signal, and we calculate the delay between the start of this first electrical signal and the start of the electrical signal detected on the other electrodes of the same column.

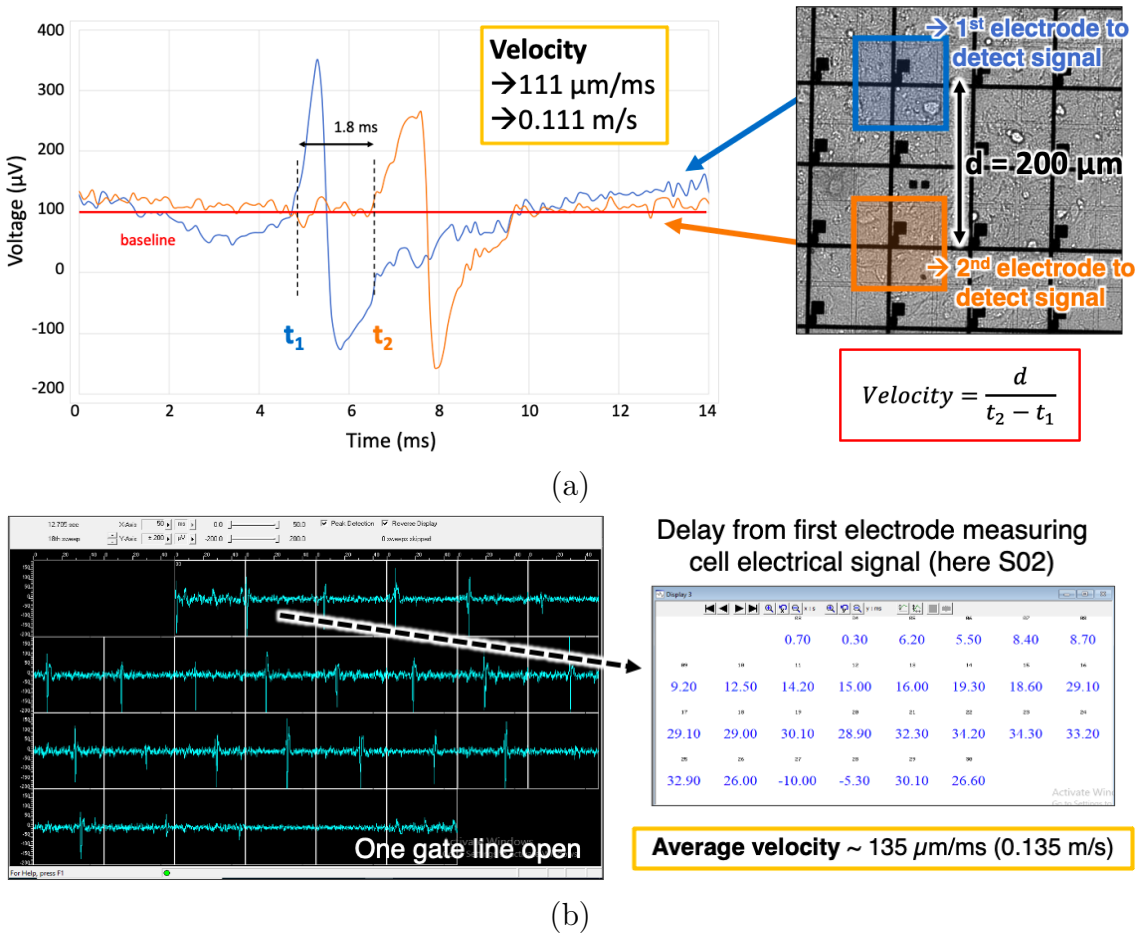

Figure 3.12: Calculation of signal propagation with (a) Excel, and (b) Multi Channel System MCS GmbH

Calculation on a small electrode arrays is first performed with Excel. By using the MC Rack software analysis from Multi Channel System MCS GmbH, calculation can then be performed on every column, which means on the 28 connected gate lines of our TFT-MEAs. **Figure 3.12** shows the calculation performed with Excel and the MC Rack Software to determine the delay between the cell electrical signals on columns of electrodes. Knowing the delay of signals and the distance between each electrode, the signal velocity can be calculated on each column.

3.5.2 Spike Sorting Algorithm

Analysis of data obtained with a large array of TFT electrodes is not easily processed using available software from Multi Channel System MCS GmbH. To overcome this, an algorithm has been developed by a collaborator from the University of Bordeaux. This algorithm includes specific functions adapted to the TFT-MEA functioning for voltage sensing and can also be applied to larger TFT arrays. The flowchart of the algorithm working process is described in **Figure 3.13**. The algorithm working principle consists of: (1) read the raw data file containing the data of all 28 × 28 electrodes; (2) separate the data in different files for each source line; (3) extract the information for each electrode in each source line.

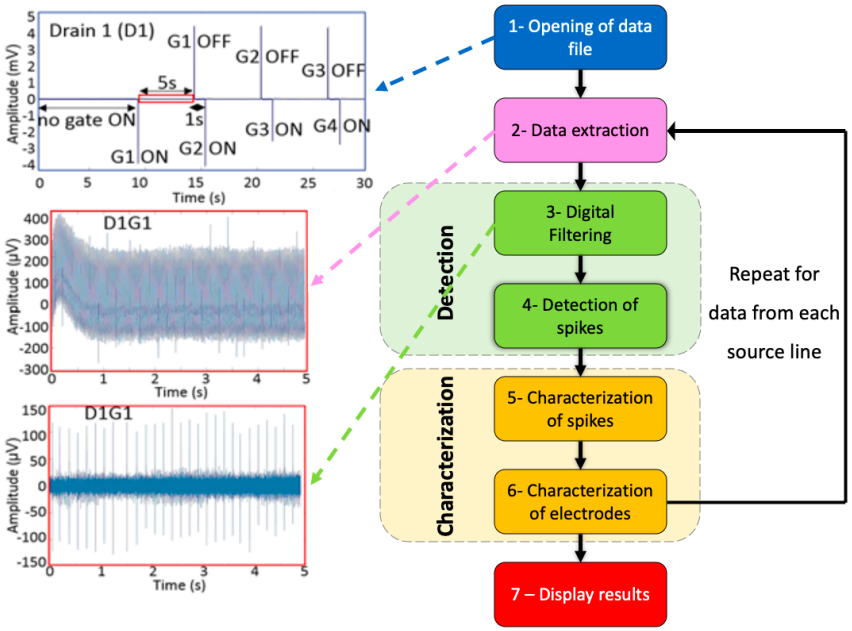

Figure 3.13: Biosignal processing with Matlab program

The data of each electrode can easily be recognized as they are placed in between the two commutation spikes that have a voltage > 2 mV when gates are switched ON/OFF. Then the data are filtered with a band-pass digital finite impulse response (FIR) filter. The advantage of this filter is its symmetrical coefficients that do not disturb too much the signal thanks to a constant group delay. The spikes are then detected and their amplitude and period are characterized. Finally, the results are stored in an Excel file and displayed by heat-map graphs.

3.6 Chapter Summary

In this chapter, we described the structure of the transistor, as well as the working principle, and post-processing of the TFT-MEAs. We then evaluated the device with the characterization data we obtained from it. After this, we presented the preparation of the device, the preparation of the biological materials, and the experimental setup for each type of measurements. Finally, we introduced the tools used for data analysis of electrophysiological measurements.

Chapter 4

Results

In this chapter, we present the results obtained with each type of electrical analysis that was performed with our TFT platform. These electrical analyses include the use of TFT-MEAs for: recordings of electrophysiological properties of cardiomyocytes, demonstration of electrochemical measurements, and displacement of skeletal muscle cells by dielectrophoresis.

4.1 Electrophysiology

4.1.1 Extracellular Potentials of Cardiomyocytes

Culture of Cardiomyocytes on TFT-MEAs

In this study, we describe the results of *in vitro* recordings of the extracellular potential of cardiomyocyte cultures with a novel MEA using the TFT technology. Our results show the possibility to use our TFT-MEA for *in vitro* electrophysiological investigations. We successfully demonstrated that beating cardiomyocytes can be cultured on the TFT platform, and that their electrical activity can be captured. **Figure 4.1** shows a photo of cardiomyocytes cultured on a TFT-MEA and their extracellular signal recorded on one electrode.

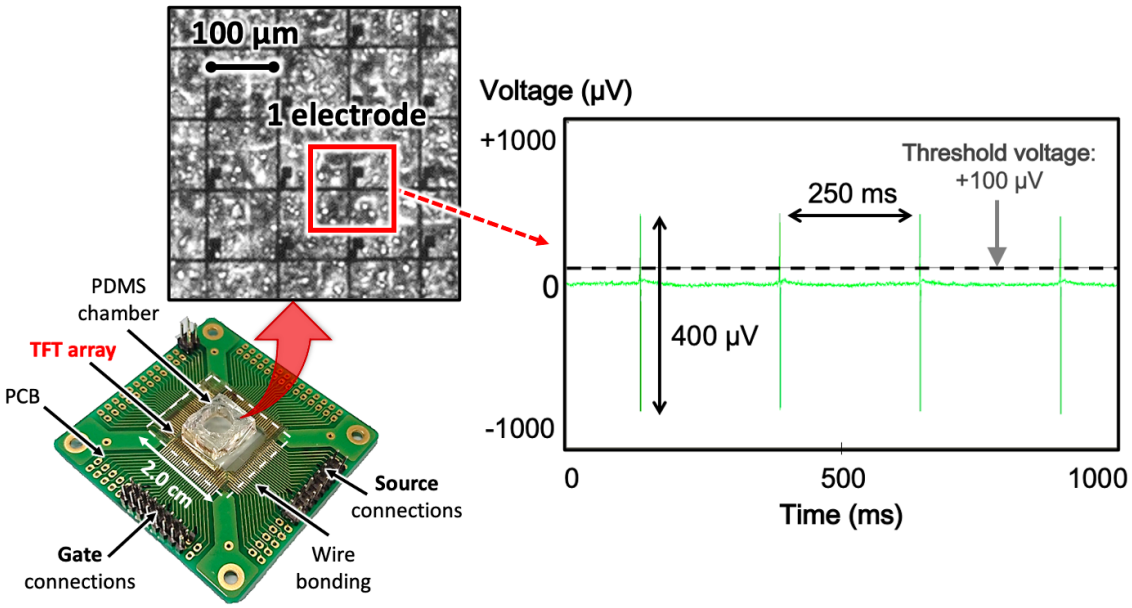

Figure 4.1: Extracellular potential of cardiomyocytes recorded on one microelectrode of a TFT-MEA

Cell contraction was observed with an inverted microscope while the extracellular potential of cells was recorded. We could observe that cardiomyocytes would form continuous layers of cells attached to the TFT substrate. Depending on the cell density, cardiomyocytes would form a monolayer or multiple layers of cells when plated at a concentration higher than $\sim 2.5 \times 10^5$ cells/30 µL/device on the targeted electrodes. Regarding the cell density, it seems that cells tend to form monolayers, but also multilayers when we increase the cell density as seen on **Figure 4.2**. Moreover, it seems that cells prefer growing on glass substrate rather than on ITO electrodes. As a result, cells were seeded directly on the targeted ITO electrodes with a droplet of 30 µL.

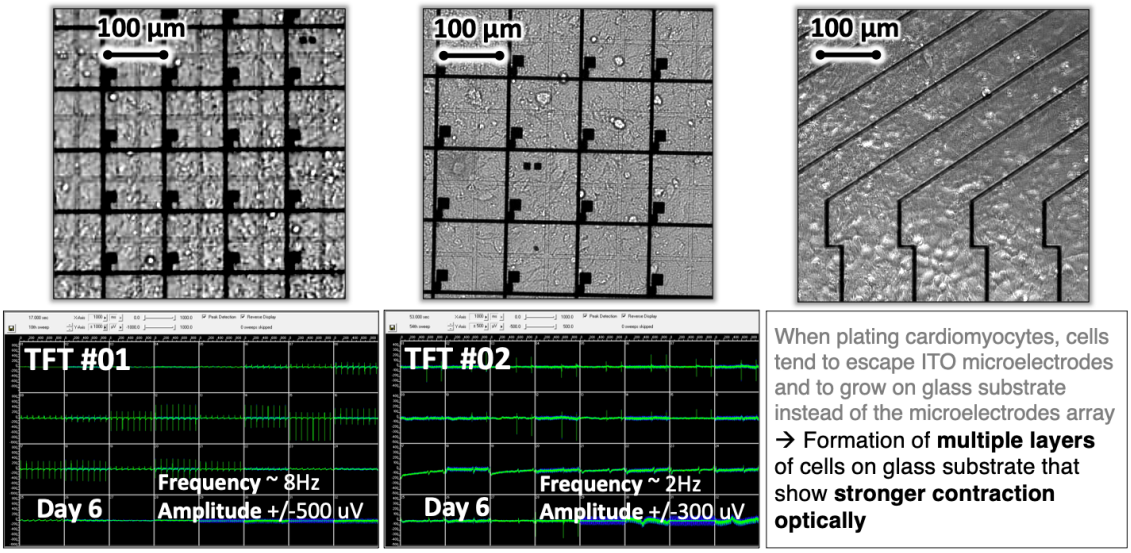

Figure 4.2: Layers of cardiomyocytes cultured on TFT-MEAs: (left) multilayers of cells when plating at $\sim 1.0 \times 10^6$ cells/30 µL (ITO electrodes), (middle) monolayer of cells when plating at $\sim 5.0 \times 10^5$ cells/30 µL (ITO electrodes), (right) multilayers of cells when plating at $\sim 2.0 \times 10^6$ cells/30 µL (glass substrate)

Detection of Extracellular Potential

As shown in **Figure 4.3**, different types of waveform have been observed in experiments, with a typical width of 3-4 ms. These waveforms are similar to the one expected by the literature when using simulated filed potentials with different values for R_j and C_{je}, and measuring field potentials of mouse cardiomyocytes with standard MEAs [120]. Results also confirm that *in vitro* recordings of the extracellular signals of excitable cells is similar in shape to signals obtained with ECG analyses. Moreover, our measurements could successfully be repeated with different cell preparations.

Extracellular recordings with TFT-MEAs show peak-to-peak (pk-pk) measurements of the depolarization and repolarization spikes of cardiomyocytes comprised between -500 µV and +200 µV. Average pk-pk amplitudes up to 1.5 mV could still be detected in some cultures of cardiomyocytes. In **Figure 4.1**, we recorded a signal period of 250 ms, which corresponds to a frequency of 4 Hz. In this study, periods of recorded signals were mainly comprised between 125 ms (8 Hz) and 1 second (1 Hz).

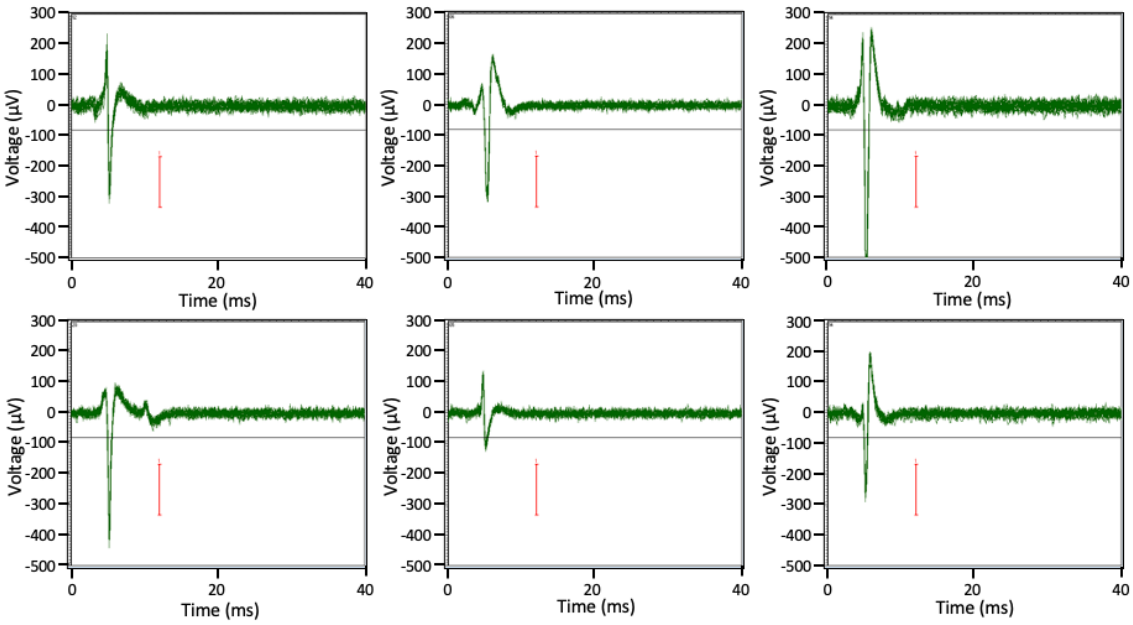

(a)

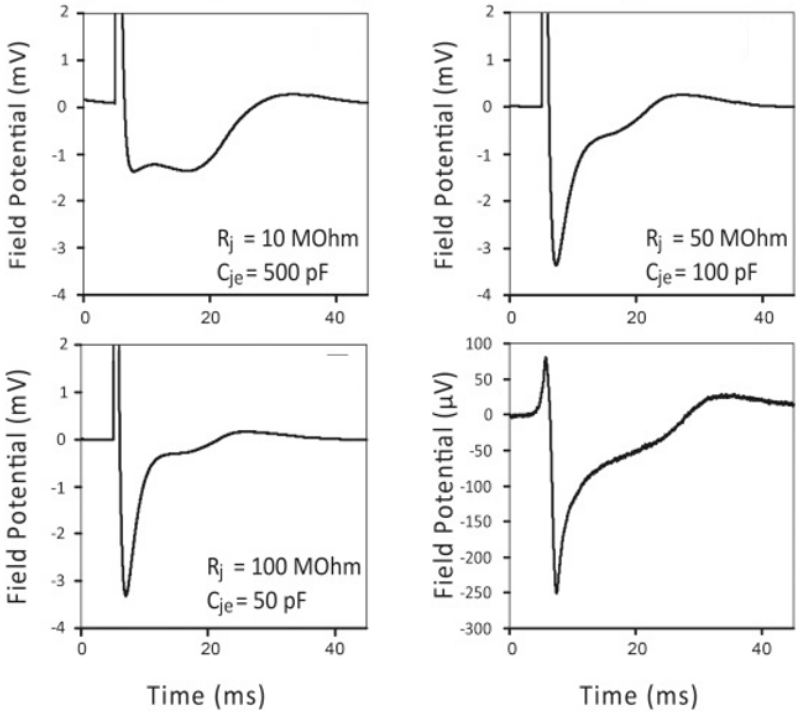

(b)

Figure 4.3: Extracellular potential of cardiomyocytes (a) recorded on TFT-MEAs, and (b) simulated and recorded on standard MEAs [120]

4.1.2 Scanning of Gate Lines

Recordings and Commutation Spikes

For electrophysiological experiments, we principally used TFT-MEAs with 28 × 28 connected electrodes. **Figure 4.4** describes the results obtained by scanning eight gate lines on on source line after filtering.

In this study, gate lines are opened for 5 seconds one after another with 1 second interval before opening the next one. In other words, for each source line, electrodes are successively ON and OFF according to the scanning of the gate lines. The difference of cell electrical activity measured on each electrode can be clearly observed in the scanning.

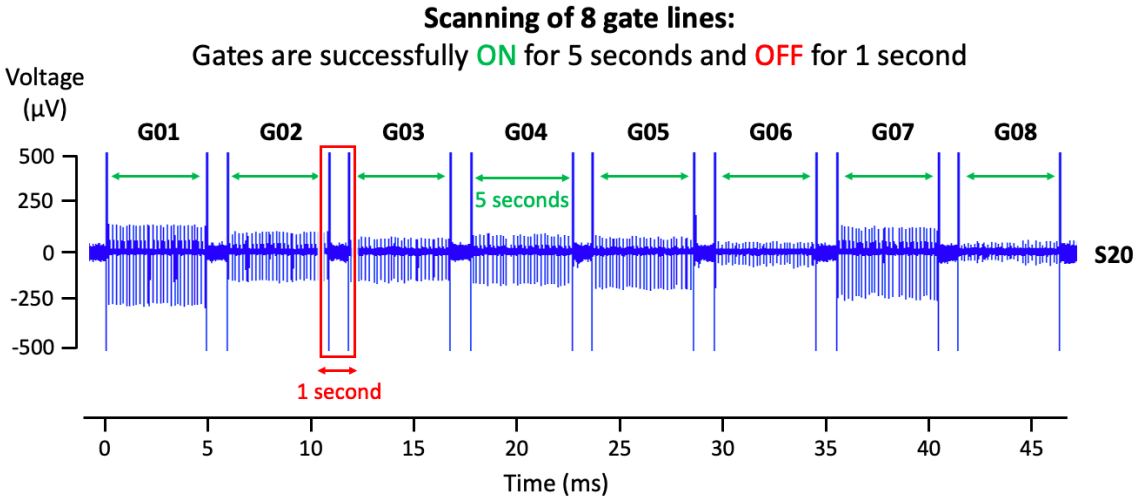

Figure 4.4: Gate scanning for extracellular recordings of cardiomyocytes with TFT-MEAs after filtering: example of a scanning of 8 gate lines; each gate line is opened for 5 seconds, with an interval of 1 second between its closing and the opening of the next gate line

We can clearly see the commutation spikes that occur when opening/closing each gate lines. With a scanning of 5 seconds ON and 1 second OFF, commutation spikes of -/+40 mV are recorded. These spikes are thus used for delimiting the gate lines and extracting the electrodes.

Synchronization and Delay of Cell Signals

By analyzing columns of electrodes, the delay between the signals measured on each electrode could be calculated. Indeed, as gate lines were scanned successfully, measurements on columns of electrodes were taken simultaneously.

We observed that cardiomyocytes were beating in synchronicity, all spikes occurring at the same time, but with a delay of a few ms depending on the distance between the electrodes. **Figure 4.5** shows the calculation of the delay between the signals recorded on columns of electrodes. In this example, we first used Excel software and calculated the delays between three signals from three electrodes. A delay of 0.6 ms between two consecutive electrodes was measured.

By doing the same type of analysis with a larger number of columns and electrodes on each column, and by using the MC Rack software analysis from Multichannel System, we could calculate the delays between the signals on every columns of electrodes from the 28×28 array of connected electrodes.

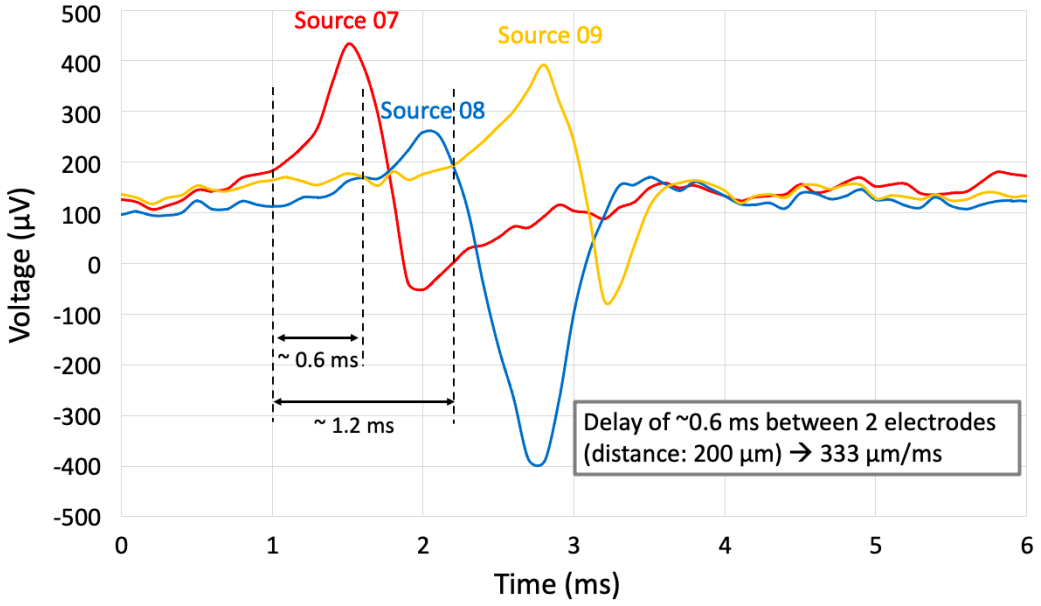

(a)

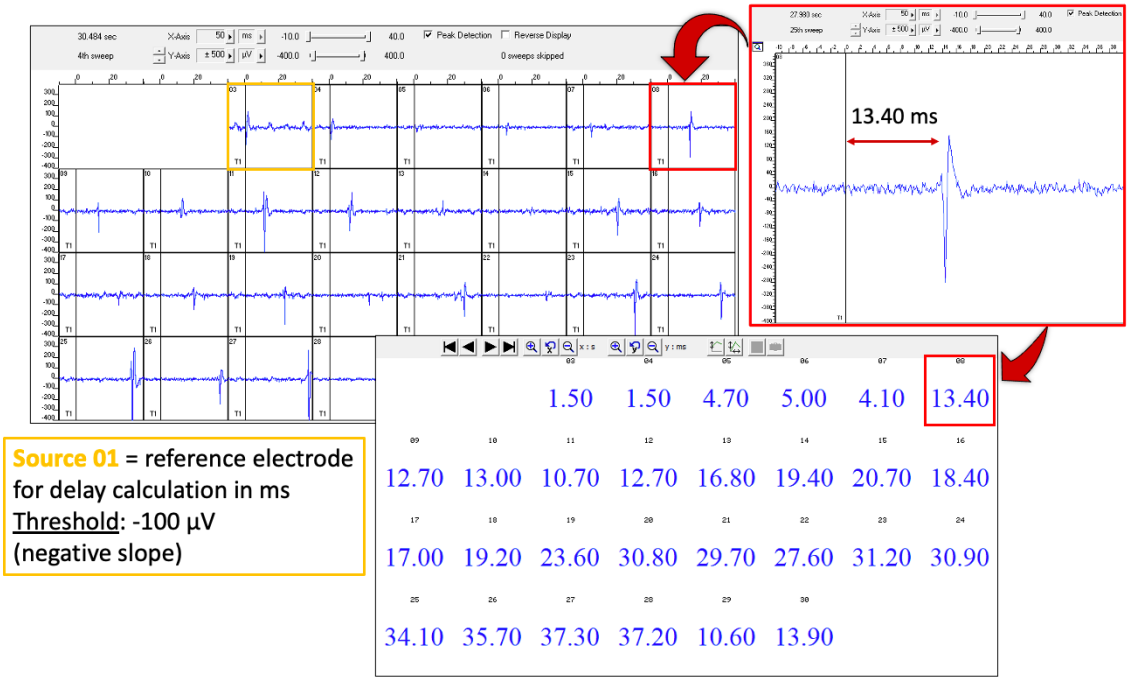

(b)

Figure 4.5: Calculation of signal velocity with (a) Excel and (b) MC Rack software analysis from Multi Channel System MCS GmbH

4.1.3 2D Mappings

Signal Amplitude with Excel

A 2D reconstruction of the average pk-pk amplitude recorded on each electrode was built after filtering and data processing with Excel calculation. The average pk-pk was calculated for each electrode over a 5 second-period. A photo of the cardiomyocyte culture and a 2D mapping of their extracellular electrical activity are shown in **Figure 4.6**.

Spike Sorting and Microscopic Observation

Our TFT-MEAs allow recordings of a large number of electrodes, which make data analysis extremely difficult and time consuming. Results were thus analyzed with the spike sorting algorithm developed by a collaborator at the University of Bordeaux for TFT-MEAs measurements. **Figure 4.7** describes the optical observation of cardiomyocytes with an inverted microscope while performing electrical recordings. It also shows the electrical recordings before filtering with equipment from Multi Channel System MCS GmbH, as well as the 2D mapping of the average pk-pk amplitude of electrical cell signals on a 28 $\times$ 28 TFT-MEA using the spike sorting algorithm. **Figure 4.8** shows additional results with the electrical and optical evolution from day 3 to day 9, as well as a 2D mapping of the period of the electrical signals measured on the same culture of cardiomyocytes as on **Figure 4.7**.

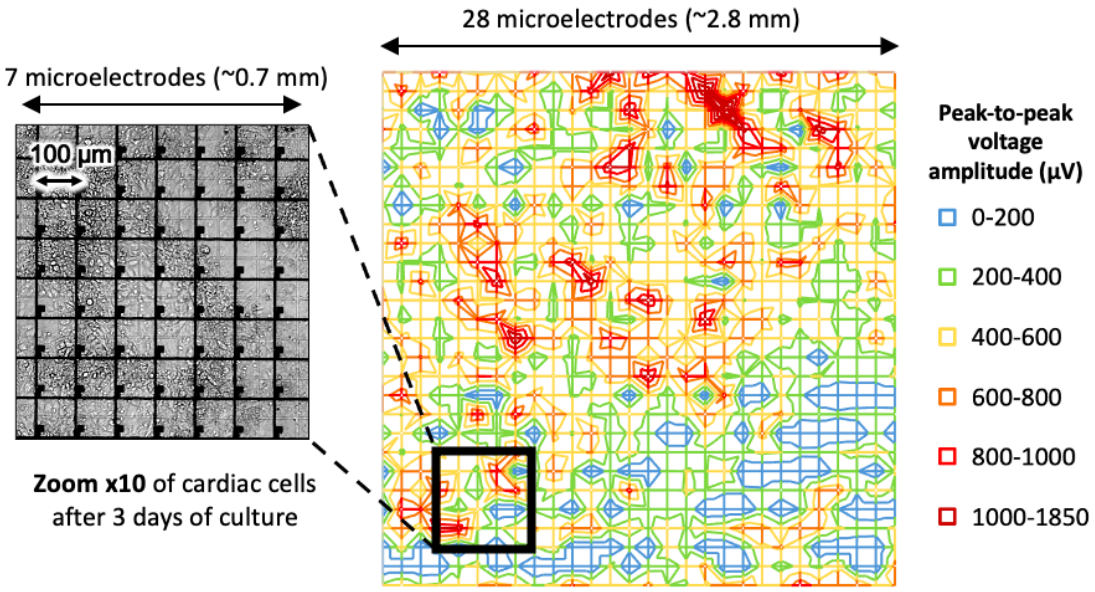

Figure 4.6: 2D mapping of cardiomyocyte electrical activity built with Excel calculation

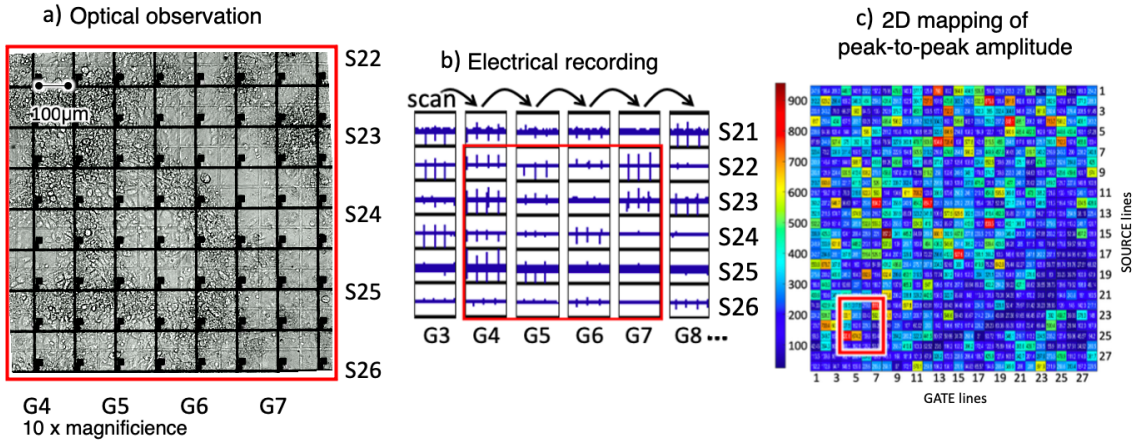

Figure 4.7: Microscopic observation of cell contraction compared with extracellular recordings of cardiomyocytes: (a) observation of cardiomyocyte culture with inverted microscope during recordings, each 100 µm × 100 µm electrode was covered by approximately ten 30 µm-diameter cells; (b) electrical recordings before filtering (successive recordings for gate lines; simultaneous recordings for source lines); (c) 2D mapping of the average pk-pk amplitude on a 28 × 28 TFT-MEA (the red square corresponds to the measurements in the red squares of (a) and (b))

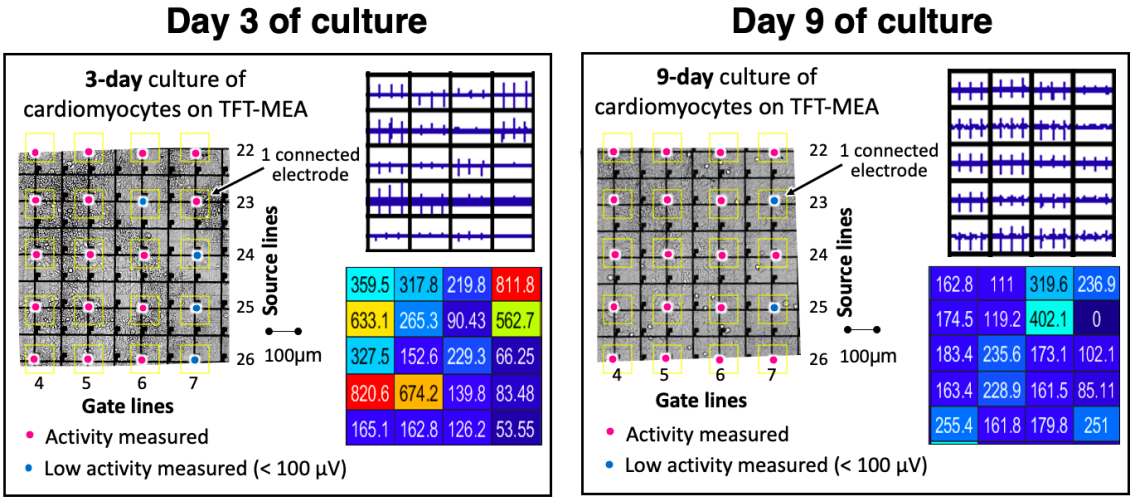

(a)

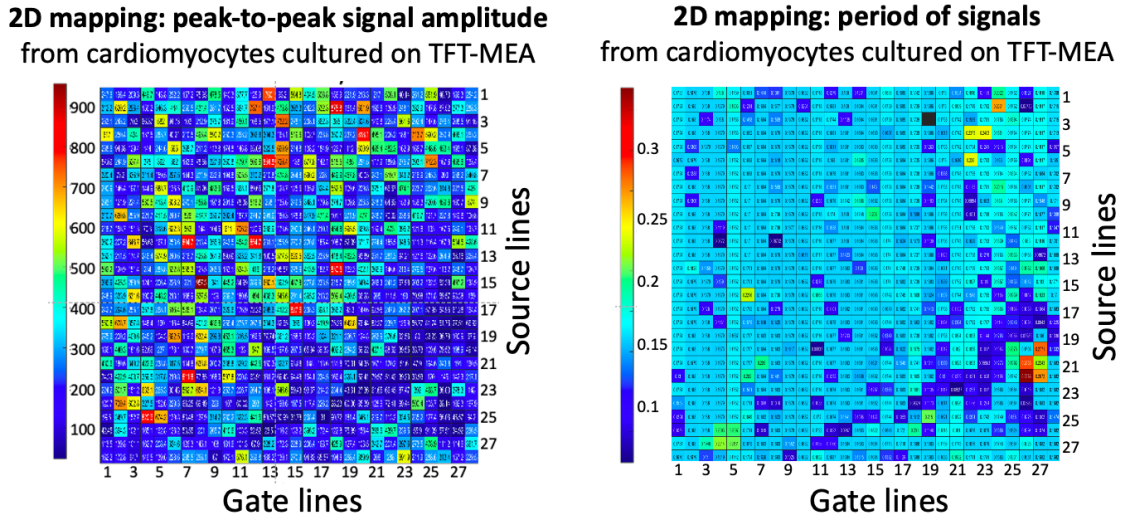

(b)

Figure 4.8: Electrical 2D mappings and optical evolution of cardiomyocytes cultured on TFT-MEAs: (a) Electrical and optical evolution of cardiomyocytes from day 3 to day 9; and (b) 2D mapping of the average pk-pk amplitude and period of the extracellular signal of cardiomyocytes cultured on a TFT-MEA

4.1.4 Signal Propagation

Calculation of the signal velocity of the cell electrical propagation within a few column of electrodes was performed. Indeed, as the gate lines were scanned for 5 seconds one after another with a delay of 1 second between each gate line, the electrical signals were recorded simultaneously only on columns of electrodes. Therefore, it is difficult to calculate the signal propagation in the whole 28 × 28 electrode array properly. Nevertheless, we first attempted to calculate the signal propagation on four columns of four electrodes each one separated by one electrode. Knowing the delay between the signals recorded on each electrode of the same column, and by supposing an average distance of 200 µm between two consecutive electrodes, we calculated a signal propagation comprised between 103 µm/ms and 500 µm/ms as shown in **Figure 4.9**.

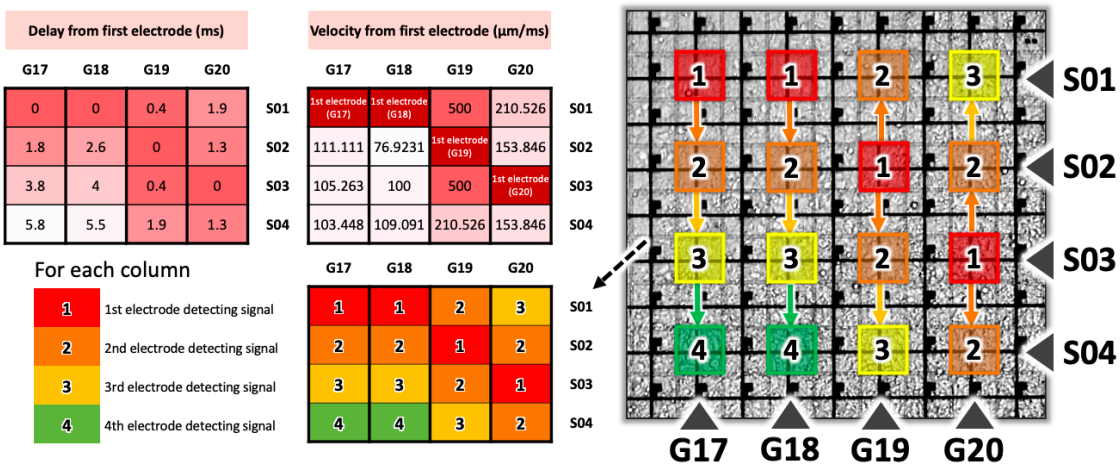

Figure 4.9: Excel calculation of delay and velocity of cell electrical signal on an array of 4 × 4 electrodes separated by one electrode from each other

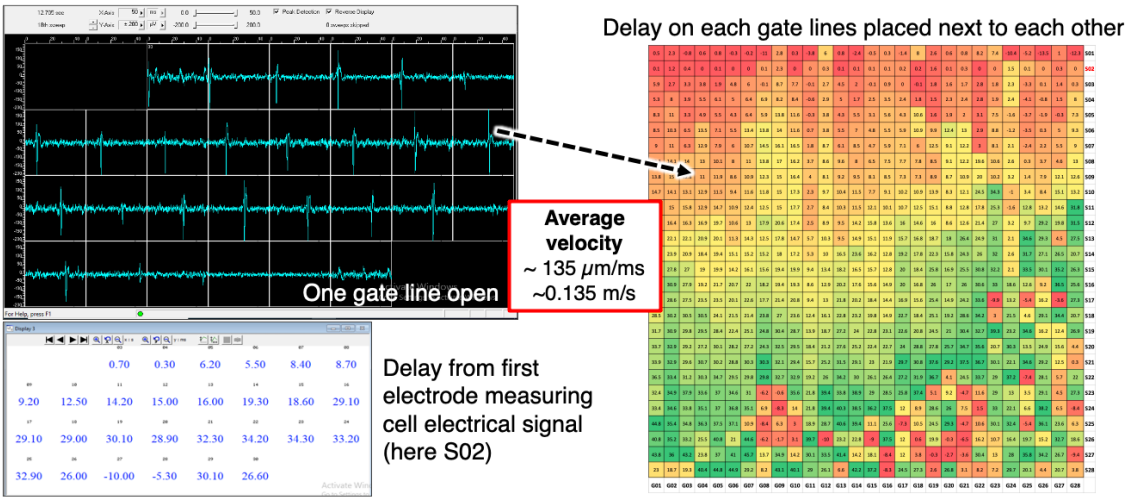

Figure 4.10: Calculation of delay and velocity of cell electrical signal on an array of 28 × 28 electrodes separated by one electrode from each other using MC Rack software analysis from Multi Channel System MCS GmbH

For each column, we classified the electrode by the delay between the detection of the cell electrical signal by using the first electrode detecting a signal as reference. Then, we placed the results for each column next to each other. A prospective wave propagation can thus be observed on the 4 × 4 electrode array analyzed with Excel.

Additionally, we also used MC Rack software from Multi Channel System MCS GmbH to do the same calculation on the whole array of 28 × 28 electrodes. Results are presented in **Figure 4.10** that shows a 28 × 28 map of the prospective signal propagation. We can observe a zone with inconsistent values corresponding to the zone with low pk-pk amplitudes, which suggests that cardiomyocytes in this region may not be well connected to rest of the cell network.

4.1.5 Regions of Active Cardiomyocytes

Culture of heart cells, cardiomyocytes and fibroblasts, was also performed as shown in **Figure 4.11**. Scanning of the cell electrical signals was done over seven rows of eight electrodes. For each row, the electrical activity was measured during 5 seconds on each electrode successively. We can see the synchronicity of the cellular signals with an average pk-pk amplitude of around 400 µV. These results show a good agreement between optical observation and electrical recordings, which indicates the efficiency of TFT technology for the development of MEAs.

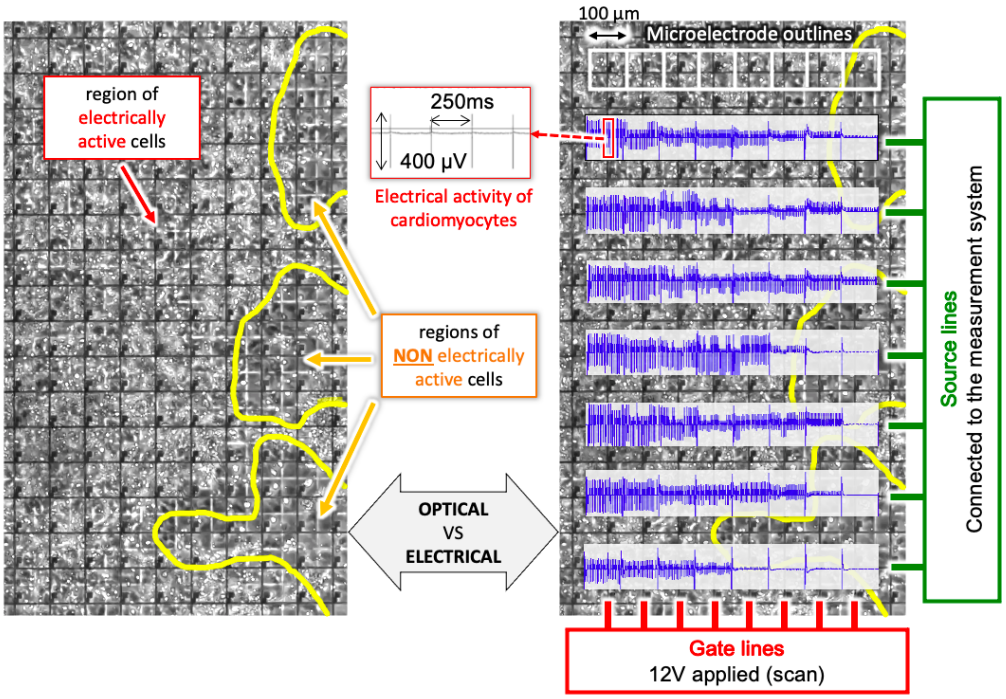

Figure 4.11: Culture of heart cells (cardiomyocytes and fibroblasts) and the corresponding electrical signals measured: scanning of the cell electrical signals performed on 7 rows of 8 electrodes; for each row, the electrical activity is measured during 5 seconds on each electrode successively

The regions of active cardiomyocytes can be distinguished from the non-active cells. Cell electrical activity of ~ 240 beats per minute (BPM) was thus successfully measured and confirmed by optical observation performed simultaneously. The positive and negative deflections of the electrical signals usually detected on ECG were clearly observed.

4.1.6 Evolution of Cell Culture

The cell culture was evaluated over several days and analyzed with our spike sorting algorithm. **Figure 4.12** shows a clear decrease of the signal amplitude and period over 4 days of culture. We can observe some regions of the cell culture that are completely black. These regions correspond to cardiomyocytes that are still alive, but that do not show any electrical activity and thus no contraction.

These 2D mapping reconstructions of the average pk-pk amplitude and periods of the cell signals suggest that the constant and periodic synchronized beating of cardiomyocytes was generated by pacemaker myocytes in the cell network. Cardiomyocytes were probably synchronized by the formation of gap junctions between them and formed different cell domains in the cell culture.

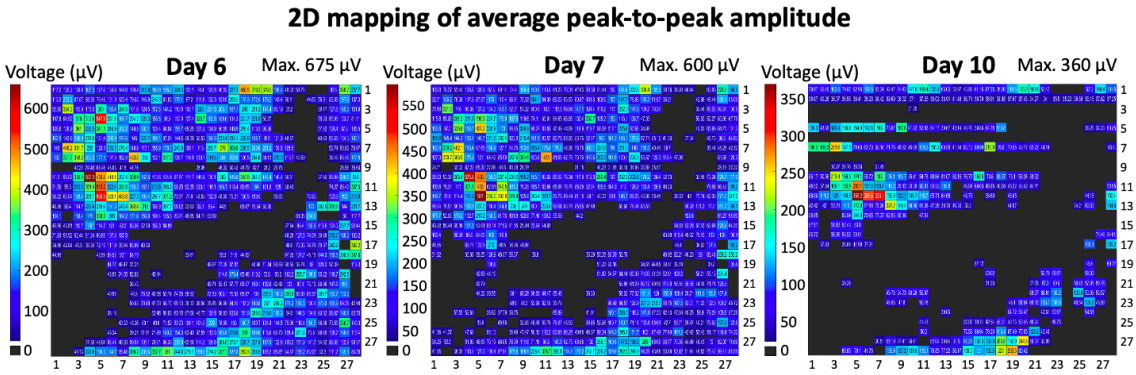

(a)

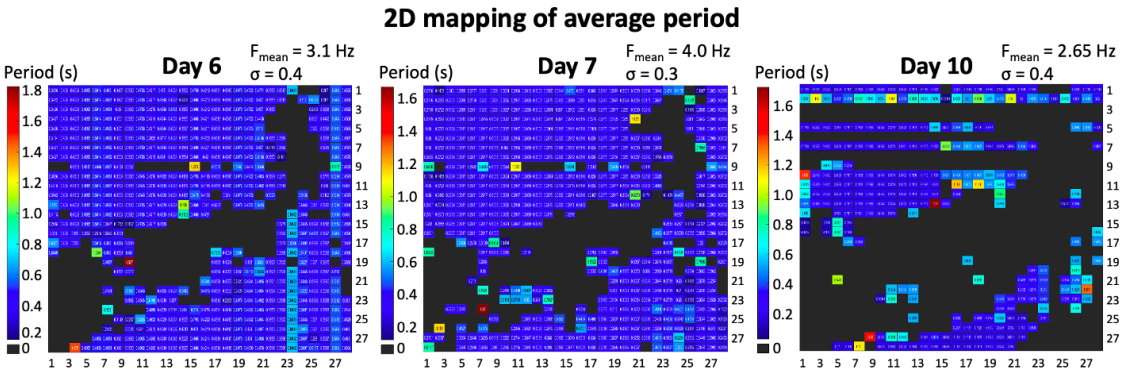

(b)

Figure 4.12: Electrical evolution of a culture of cardiomyocytes over several days: (a) 2D mappings of the average pk-pk amplitude measured on each electrode; (b) 2D mappings of the average period measured on each electrode

4.1.7 Effect of Temperature

Finally, we evaluated the effect of temperature on the electrical activity of cardiomyocytes cultured on TFT-MEAs during recordings. In **Figure 4.13**, we observe a decrease of the period of the measured signal on one electrode from 350 ms at room temperature to 250 ms at +34°C. These results show the importance and effect of the temperature of the cell culture medium during experiments. **Figure 4.14** shows 2D mappings of the average pk-pk amplitude and period at +37°C and +27°C calculated with our spike sorting algorithm. We can observe a decrease of ∼65 µV in the signal amplitude and a decrease of ∼105 ms in the period.

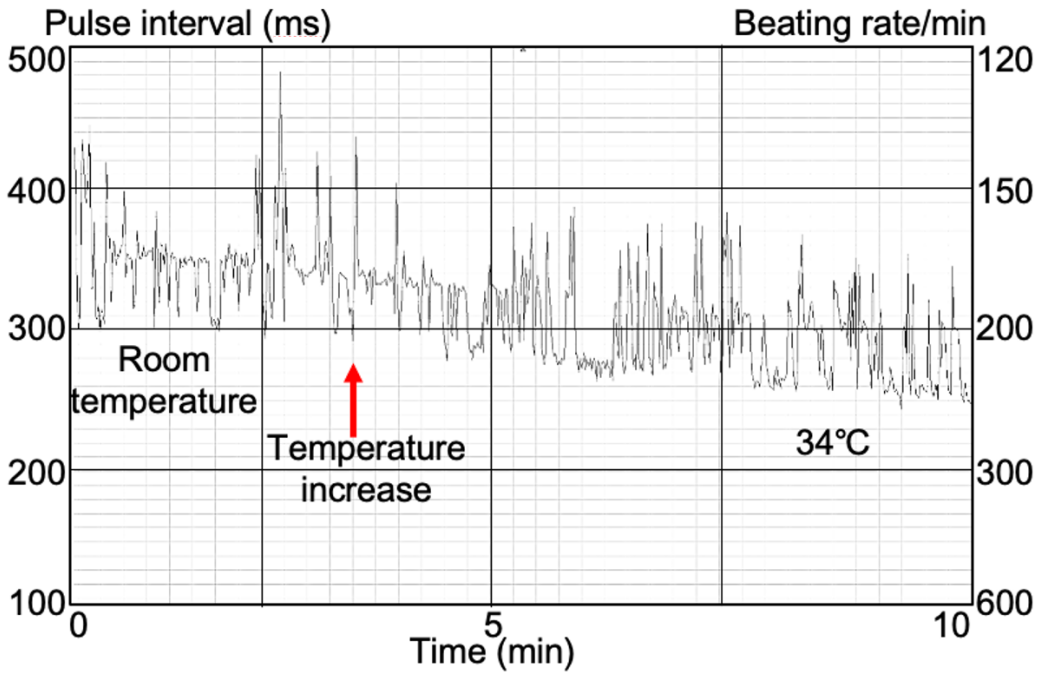

Figure 4.13: Effect of the temperature on the frequency of cardiomyocyte electrical signals

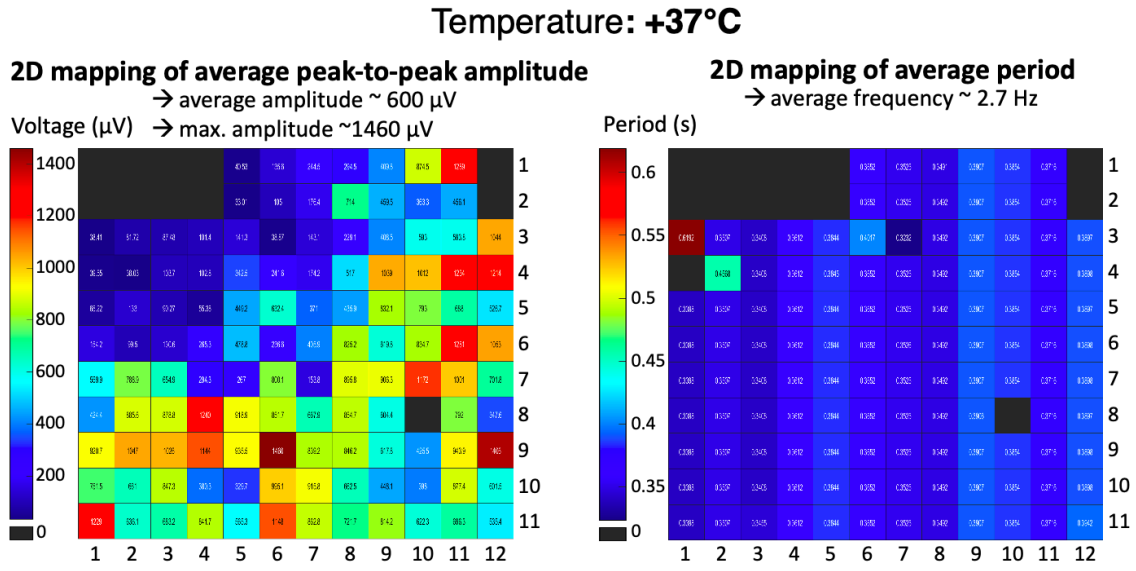

(a)

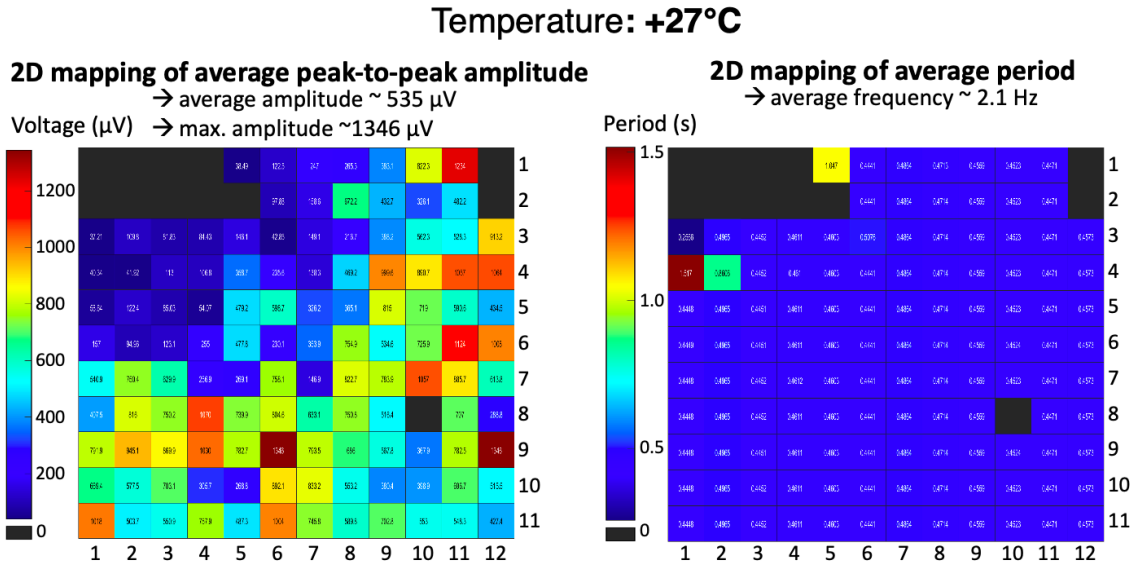

(b)

Figure 4.14: 2D mappings of the average pk-pk amplitude and period of cardiomyocyte signals at +37°C and +27°C

4.2 Electrochemistry

4.2.1 Cyclic Voltammetry

Cyclic voltammetry was performed with our TFT-MEAs. The purpose of these measurements was to investigate the effectiveness of our TFT-MEA structure. We selected 2 mM $K_3[Fe(CN)_6]$ in 1 M KCl in order to obtain large level of SNR ratio. Standard gold WE was compared with ITO WE from TFTs. **Figure 4.15** shows the potential difference between the WE and the RE scanned between -0.6 V and +0.6 V at 0.1 V/s.

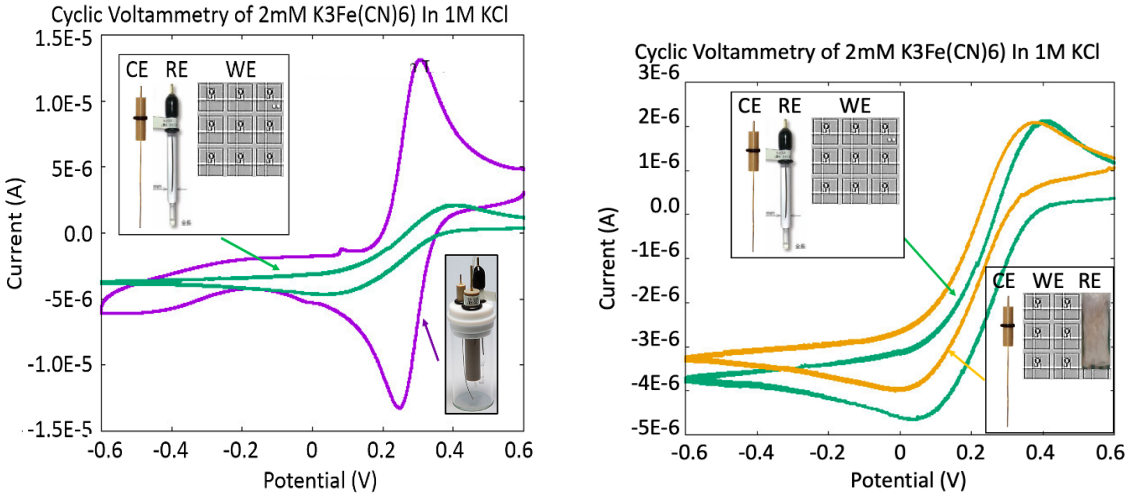

(a) (b)

Figure 4.15: Results of cyclic voltammetric experiments: (a) cyclic voltammetry of 2 mM K3Fe(CN)6 with 2 mm^2 standard gold WE (purple curve), and 0.01 mm^2 ITO WE of TFT device (green curve) (scan rate: 0.1 V/s); (b) cyclic voltammetry of 2 mM K3Fe(CN)6 with ITO WE with standard Ag/AgCl RE (green curve) or integrated Ag/AgCl RE (orange curve) (scan rate: 0.1 V/s)

The current with TFT devices is lower than with standard gold WE, which is certainly due to the difference of electrode size: 0.01 mm^2 for the ITO WE, and 2 mm^2 for the standard gold WE. However both curves show a similar shape with two redox peaks. The positions of the peaks are different probably because the WEs are made of different materials.

We also compared the standard Ag/AgCl glass RE with the integrated Ag/AgCl RE on the TFT substrate. For these measurements, both WEs are ITO electrodes. Very similar curves have been obtained. The variation in current or peak positions can be explained by the integration process of Ag/AgCl RE, which was an ink placed directly on the substrate. Indeed, this Ag/AgCl ink might not show exactly the same material property as standard Ag/AgCl RE.

Despite the necessity of some quantitative improvements, these two experiments have qualitatively demonstrated that ITO microelectrodes can be used as WE and that Ag/AgCl ink can be used as in integrated RE on the TFT platform. As a result, a complete integrated sensor can be built on the platform.

4.2.2 Amperometry

Based on these results, amperometric experiments were performed with tyramine in PBS at 10 µM, 100 µM and 1 mM.

Figure 4.16 presents the results obtained with standard gold WE and ITO WE. The RE is an Ag/AgCl standard glass electrode, and the CE is a standard Pt electrode. Curves of current density versus time were obtained with a scan rate of 0.05 V/s. Additionally, curves of current versus tyramine concentration were also plotted at t = 100 seconds with the same scan rate: 0.05 V/s.

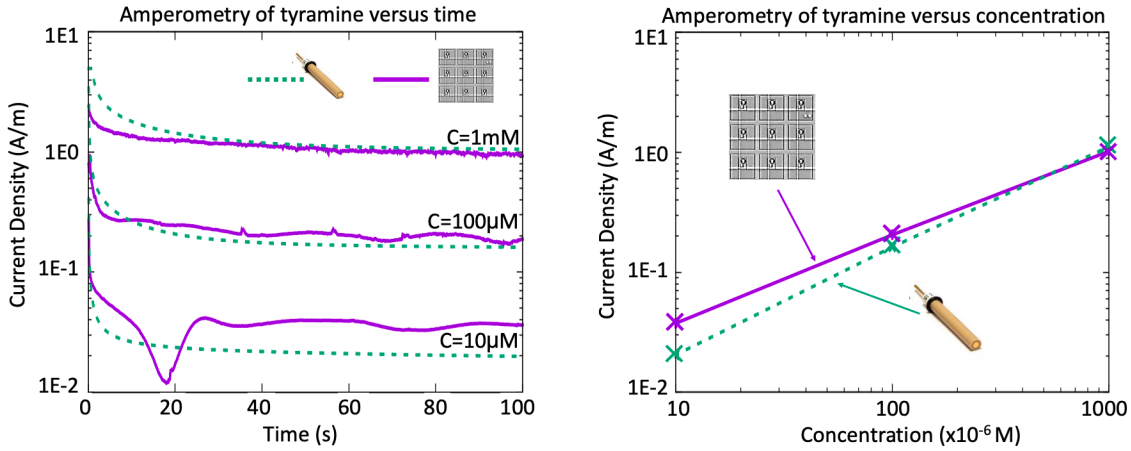

(a) (b)

Figure 4.16: Results of amperometric experiments with an Ag/AgCl standard glass electrode as WE, and a standard Pt electrode as CE: (a) amperometry of tyramine: current versus time, at 10 µM, 100 µM and 1 mM, using a standard gold WE or an ITO WE of TFT device (scan rate: 0.05 V/s); (b) amperometry of tyramine: current versus tyramine concentration at t = 100 seconds, using a standard gold WE or an ITO WE of TFT device (scan rate: 0.05 V/s)

Very similar results between both standard gold and ITO WE were obtained, which confirms that meaningful electrochemistry can be performed with ITO WE of TFT devices.

However, the measurements with ITO WE show some instability and a higher noise sensitivity compared with standard gold WE. The reason of that instability can be attributed to various factors: the usage of ITO material that is not a noble material for electrochemistry; the connection of the WE to TFT in an array that might increase the sensitivity to noise; or an instability of the TFT during electrochemical measurements.

No changes were observed on ITO electrodes for the range of potential applied during the measurements: [-0.6 V, +0.6 V]. The reason for the lower current with ITO WE can be due to the smaller dimension of the WE. A dip on the amperometry curve can also be observed at 10 µM with ITO WE, which might be due to some instability that happened during the measurement of the very low current.

4.3 Dielectrophoresis

4.3.1 Preliminary Tests

DEP was first performed with liver cells (HepG2) to explore the possibility of cell patterning and displacement on TFT-MEAs. Additionnaly, 10 µm microbeads were also added to the cell solution to evaluate the possibility to separate cells from microbeads with our TFT platform.

In order to protect the microelectrodes from high voltage, the TFT substrate was coated with a thin layer of Teflon. For our experiments, we prepared 400 nm Teflon-coated TFT-MEAs. Moreover, efficient DEP requires a low conductivity medium. Cells were thus centrifuged and culture medium was replaced with a 300 mM D-Mannitol buffer. DEP was performed a few minutes after adding the cell/microbead solution to the PDMS culture chamber to make sure that most of the cells have reached the electrode surface. An inverted microscope was used for observation of cells through the substrate. The gate voltage used was 12 V. For the source voltage, best results were obtained with a frequency of 100 kHz and voltage of 10 V pk-pk.

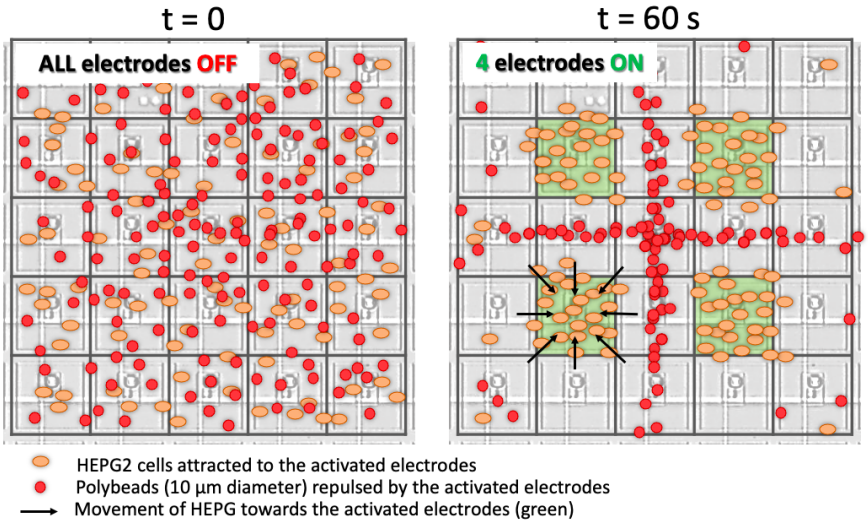

Figure 4.17: Scheme of expected DEP patterning with mammalian cells and microbeads

Figure 4.17 shows the expected results when performing DEP with a solution of cells/microbeads by switching ON four electrodes. Results obtained are shown in **Figure 4.18**. Microbeads exhibited negative DEP while HepG2 cells exhibited positive DEP as expected by the literature. This means that microbeads were repulsed from the electrodes and cells were attracted towards the electrodes. Cell displacement over three electrodes was also evaluated and results are presented in **Figure 4.19**. These results show that cell patterning and displacement is possible by performing DEP on TFT-MEAs.

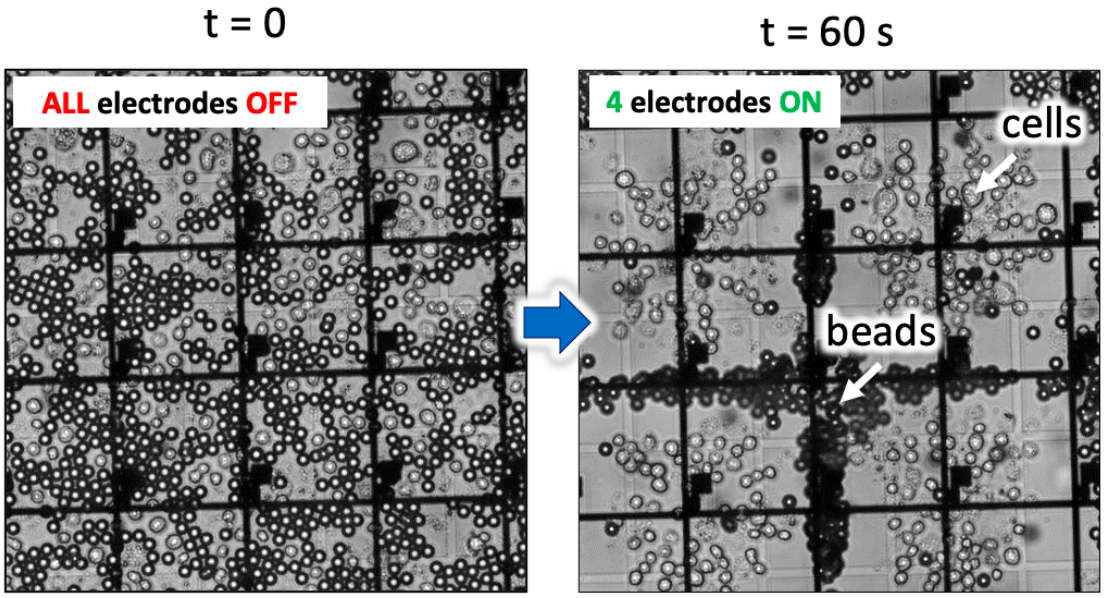

Figure 4.18: Results of DEP patterning with liver HepG2 cells and microbeads on TFT-MEA

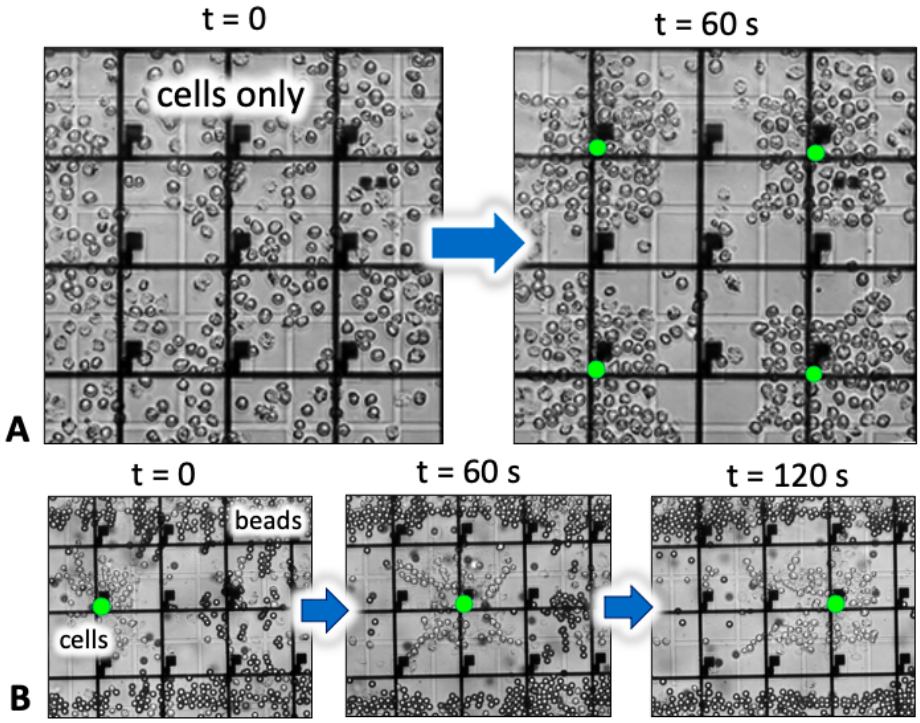

Figure 4.19: Displacement of liver HepG2 cells by DEP on TFT-MEA

4.3.2 Skeletal Muscle Cells

DEP of skeletal muscle cells (C2C12) was also tested with our TFT-MEAs. No microbeads were added to the solution for this set of experiments. C2C12 cells were also diluted in a low conductivity buffer of 300 mM D-Mannitol. Similar results to previous experiments with HepG2 cells were observed. **Figure 4.20** shows that C212 cells are clearly attracted towards the activated electrodes at a velocity of about 40 µm/s. By switching ON specific electrodes, the cells are displaced and attracted towards the activated electrodes. Best results are also observed with a source voltage of 10 V pk-pk and 100 kHz frequency. After DEP experiments with C2C12, the buffer supernatant was carefully removed and replaced with proper cell culture medium to evaluate the possibility to culture C2C12 cells after DEP experiments on our Teflon-coated TFT-MEAs. C2C12 cells could successfully be cultured on the platform post-experiments and showed similar morphology to C2C12 cells cultured on non-coated TFT-MEAs.

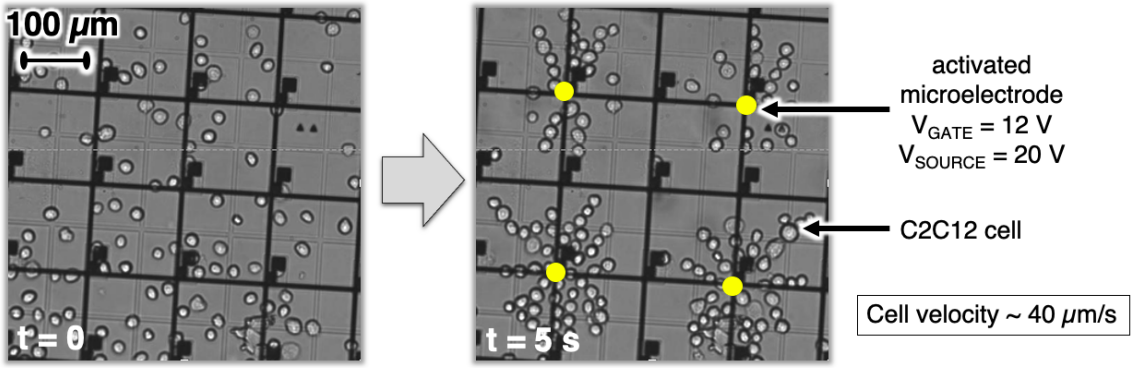

Figure 4.20: Displacement of skeletal muscle cells (C2C12) with DEP

4.4 Chapter Summary

In this chapter, we presented the results obtained with the electrical measurements performed with TFT-MEAs. This work mainly focused on the recording of the extracellular potential of cardiomyocytes cultured on TFT-MEAs. We demonstrated the measurement of the cell electrical activity and compared it with optical observation simultaneously. The evolution of the cell electrical activity was assessed over several days of culture and the effect of temperature was evaluated. Additional measurement techniques were performed such as electrochemical experiments involving cyclic voltammetry and amperometry of tyramine, as well as DEP for displacement and patterning of mammalian cells.

Chapter 5

Discussion

In this chapter, we discuss the results and issues encountered for each type of application. For electrophysiological measurements, we mainly discuss the experimental conditions, the extracellular potential recorded on TFT-MEAs and its correlation with optical observation, the evolution of the cell electrical activity, the stimulation of cells, and the scanning process of the gate lines. For electrochemical measurements, we then evaluate the possibility to perform voltammetry and amperometry with our TFT-MEA. For dielectrophoresis experiments, we discuss the patterning and displacement of mammalian cells on TFT substrates and the effect of the Teflon coating. Finally, we discus additional points, such as the cell viability, the reuse of TFT devices, and the feasibility of performing additional electrical measurements with the TFT platform from an electromagnetic point of view.

5.1 Electrophysiology

5.1.1 Analysis Conditions

Regardless of the analysis tool or method used, the importance of optimizing and standardizing of the measurement and analysis conditions cannot be overestimated. These cover both the properties of the cells to be analyzed and the external conditions before and during the experiment process.

Cardiomyocytes

Many methods are capable of analyzing cells in varying densities, but the outcome may vary greatly between single cells and cell cultures. Cell density has been shown to have an effect on several different characteristics of cardiomyocytes, including gene expression profile and electrophysiological properties [121]. In cultures of multiple heart cells where cardiac fibroblasts may also be present, the difference is likely to be even larger. In addition to the cell density, the age and maturation state of the cells is an important issue. Although there is no single correct answer to how old the cells should be and what is mature enough, these parameters must be carefully assessed and standardized to obtain comparable results. In this study, we observed that a cell culture with a high cell density ($> 2.5 \times 10^5$ cells/30 µL) and multiple layers of cells would show stronger cell contraction and electrical activity.

In this study, all cell preparations adhered tightly to the TFT substrate and contracted isometrically, avoiding the motion artifacts that might cause deterioration in the SNR. This allows recordings over many days, facilitating, for example, investigations of long-term drug effects. After 1 to 3 days in culture, the cells formed one or several confluent layers that usually exceeded the area of the electrode array. In some cases, areas of increased cell density could be observed where a few layers of cells were growing on top of each other. The cardiomyocytes showed spontaneous activity, a regular beating driven by pacemaker heart cells in the culture. *In vitro* recordings of field potentials on TFT-MEAs were performed after 3 days of culture.

Recording

In this study, we were able to make measurements of the extracellular potential of cardiomyocytes on a large surface area, and to construct a 2D mapping of the electrical characteristics of the signals. The measurement area and the number of connections can be freely chosen according to the purpose of the experiments: measurement can be performed anywhere in the cell culture, as long as the gate and source lines are connected. The high density of transparent microelectrodes on the TFT substrate provides a clear advantage over conventional MEAs.

Raw data were filtered with a bandstop resonator filter at 50 Hz and Q-factor of 10, combined with a high-pass filter with a cutoff frequency of 200 Hz. Depending on the microelectrode, these two filters provided a noise attenuation of 6 dB to 13 dB, compared to an attenuation of 0.5 dB to 2 dB for the electrophysiological signals. After filtering, the noise level stabilized everywhere between 20 µV and 30 µV. Only signals with amplitude above 100 µV were retained as signals coming from cells. Improvement can be performed to further reduce the noise level at the hardware level by improving amplification of the signal and protecting further the measurement setup from external noise, and at the software level by improving the recognition of low-level signals buried in noise. In the end, measurements could be repeated with a reasonable noise level.

Temperature

Concerns about recording conditions, such as temperature, are true for any cell assay. To illustrate the effect of temperature on the cardiomyocyte beating, we measured the cellular activity of cardiomyocytes at +34 °C and at room temperature (RT). Our results demonstrated that lowering the temperature leads to a clear decrease of -8 beats/min/°C. This observation underlines the importance of using a heating plate while performing extracellular recordings of cardiomyocytes. Moreover, this also suggests that special care should be taken to place the cells on a heating plate as soon as they are removed from the incubator.

A hypothesis would be that the interval between action potentials of the pacemaker myocytes increased as the temperature decreased. The mechanism underlying this activity depression at lower temperatures is thought to be as follows: the ATP production rate decreases, whereas the demand on ATP increases, because of the activation of ion channels and ion pumps in order to accelerate depolarization and repolarization. The decrease in the activity of ion channels and ion pumps is also caused by the decrease in the ion concentration gradient across the cell membrane, because the permeability of the membrane to ions increases at lower temperatures [122]. Thus, the temperature drop depresses the speed of ion exchange, which results in the accumulation of Ca^{2+} in the cardiomyocytes and the elongation of the contraction-relaxation cycle of sarcomeres [123].

This study showed thus that the recording conditions may greatly affect the beating characteristics of the cells, which then are reflected on the results. However, this variation of beating rate could also be due to changes in other parameters in the cell culture, such as change in pH or concentration of O_2/CO_2, since they were not standardized in our experiments. In the experimental setup for patch-clamp or other electrophysiological analysis of cardiomyocytes these issues are usually well addressed [124].

5.1.2 Properties of Extracellular Data

Cardiomyocyte Field Potential

Previous studies have already demonstrated the possibility to use our TFT-MEA for biological applications, in particular for extracellular recordings of neurons [125] and cell culture monitoring [126]. In this study, we investigated the electrical activity of cardiomyocytes. Action potentials of cardiomyocytes cultured on TFT-MEAs could be detected as fluctuations in the extracellular field potential (FP) at the adjacent recording electrode. TFT-MEAs could measure the change in FP as the action potential propagates through the cell layer relative to the recording electrode. In this respect, the recorded FP signal in the MEA assay was analogous to the recorded electrocardiogram (ECG) signal that measures changing voltage on the body surface induced by currents that flow throughout the heart. This is in contrast to the intracellular recording of action potentials with manual patch-clamp, which measures the flow of ionic currents across the membrane of cardiomyocytes.

Field Potential Parameters

The FP waveform comprises a sharp transient spike associated with Na^+ influx and membrane depolarization [127], followed by a shallower ramp during Ca^{2+} influx. The FP signal is not a measure of movement, but rather of excitability. On conventional ECG, the electrical signal is normally ending with a repolarization wave due to K^+ efflux.

However, this last wave is not properly detected with our device. This is mainly due to the external noise coming from our experimental setup, in which this small wave is dissipated. The FP duration, which is the *in vitro* analog of the QT interval, measured from the initial Na^+ spike to the maxima of the K^+ repolarization wave, could thus not be properly calculated. Additional analysis of the extracellular voltage waveform yields further descriptive parameters including spike amplitude, beat period, and beat regularity. Indeed, the recorded cardiomyocyte FP signal is information rich, providing data relating to the excitability and repolarization of the cells, as well as descriptors of beat rate and regularity [128]. Commonly reported features include:

- **Spike amplitude**: a pk-pk measure of the initial depolarizing spike. This sharp transient spike is associated with Na^+ influx and membrane depolarization. The signals recorded with our TFT-MEAs featured amplitudes between 100 µV and 1.5 mV. Although the FPs recorded from the TFT electrodes varied in amplitude, they exhibited an overall similar characteristic waveform. For most FPs the negative peak was preceded by a positive peak, which is mostly due to the fast Na^+ current contribution to potential changes, certainly indicating the contribution of neighboring previously excited tissue.

- **Beat period**: the time interval between successive Na^+ spikes. In this study, we mainly recorded signal periods between 1 Hz and 8 Hz. The regularity of the signal can be calculated as the standard deviation of the beat period.

5.1.3 Correlation between Optical and Electrical Data

The transparency of the TFT-MEA allowed the simultaneous electrical recording and optical observation of cell contraction with an inverted microscope, which is more difficult to achieve with CMOS technology. **Figure 5.1** shows the motion analysis of cardiomyocytes with a microscope, confirming the visual observation of cell contraction during electrical measurements.

We thus demonstrated that simultaneous optical and electrical sample characterization is possible by utilizing transparent ITO electrodes, which elevates the quality and quantity of acquired data. However, it could happen that cellular electrical activity was measured even though no contraction was visually observed with the microscope.

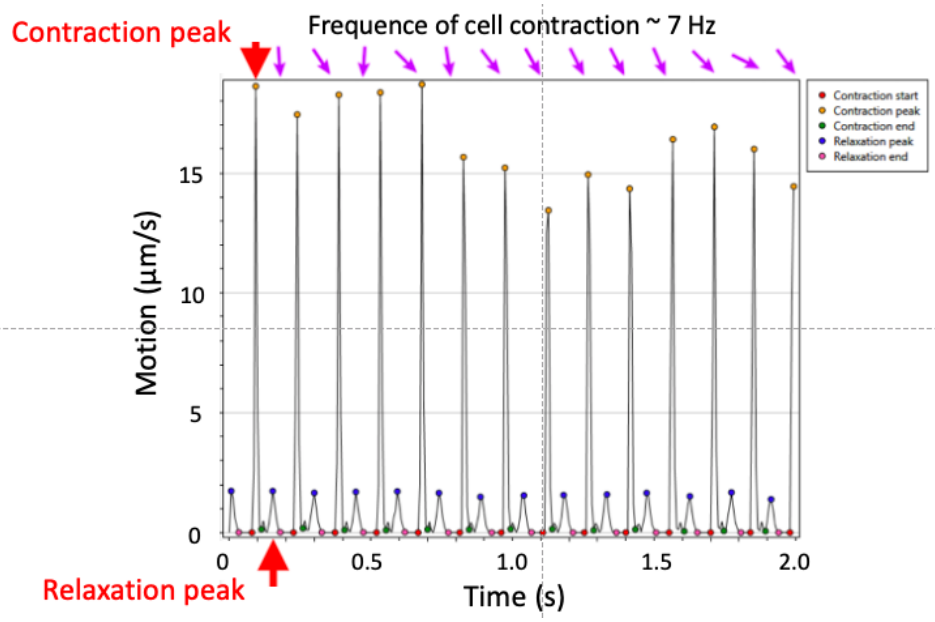

Figure 5.1: Motion analysis of neonatal heart cells with microscope

Usually, cell excitability leads to contraction. However, we suppose that there could be some instances when this can be disrupted. For example, the myosin II inhibitor, blebbistatin, may interfere with the cardiomyocyte contractile machinery but does not directly impact the cellular electrophysiology [129] [130].

We could observe that high amplitude signal would usually correlate with a high density of cells arranged in multiple layers. However, a more powerful microscope would be needed to acquire pictures and videos with a higher resolution in order to estimate the number of cells on specific areas and their morphology. Combining electrical recordings with calcium imaging could also provide more information regarding the cell physiology and characteristics of their FPs.

5.1.4 Evolution of Cell Culture

To determine if FP waveforms depended on differences between days of culture, we recorded the spontaneous electrical activity on successive days. Spontaneous electrical activity could be detected from the third day in culture. Recordings with our TFT-MEAs demonstrated a clear modification of cell activity along the day with a decrease of signal amplitude and frequency. We could observe that the signal amplitude decreased by $\sim$ 47 % from day 6 to day 10. Similarly, during the first days of cell culture, the frequency was relatively stable in the whole culture, which shows the synchronicity of the cell contraction.

However, after several days of cell culture, an irregularity in the spike frequency was usually observed. Indeed, low frequencies of cell electrical signals had an higher standard deviation. We suppose that the cell connection network might deteriorate over time, potentially through weakened gap junctions between cardiomyocytes, which would diminish ion exchanges between cells and consequently induce a decrease of their electrical activity and contraction.

5.1.5 Cell Stimulation

In this research, the electrical activity of cardiomyocytes has successfully been detected and measured with our TFT-MEAs. Cardiomyocytes spontaneously started contracting and beating after approximately 3 days of culturing. However, it happened that for some experiments, no cell contraction could be observed and no electrical activity could be measured. This was usually observed when the cell density of cardiomyocytes plated on the device was too low ($< 2.5 \times 10^5$ cells/device). In this situation, stimulation of cells can be considered in order to induce their contraction and thus electrical communication. In this section, we will discuss the possibility of two types of cell stimulation: electrical and chemical stimulation. Electrical stimulation has been attempted in this study.

Electrical Stimulation

For electrical stimulation, we connected the stimulus generator outputs (STG4000 Series) from Multi Channel Systems MCS GmbH to the selected source lines of the TFT-MEA for current and voltage driven stimulation. When performing electrical stimulation, stimulating electrodes behave as plate capacitors. The charge cannot flow back to the stimulus generator due to the high output resistance and is kept in the electrode. However, the electrode needs a quite long time to discharge itself after stimulation. As a result, stimulus artifacts interfere with the recording, and electrodes can deteriorate over time due to electrolysis. This should be avoided by choosing an appropriate stimulus method that actively discharges the electrode after the pulse.

When using voltage driven stimulation, the electrodes are discharged when the voltage level is set to zero at the end of the monophasic pulse. However, it is different in current mode. When applying a negative current pulse, the electrode is charged and needs to be actively discharged by applying an inverted pulse with a matching product of current and time. Therefore, it is better to stimulate with biphasic pulses for current driven stimulation to reduce both the stimulus artifact and to avoid an electrode damage. The easiest way is to use the same signal amplitude and the same duration with an inverse polarity. For voltage driven stimulation, monophasic pulses are appropriate.

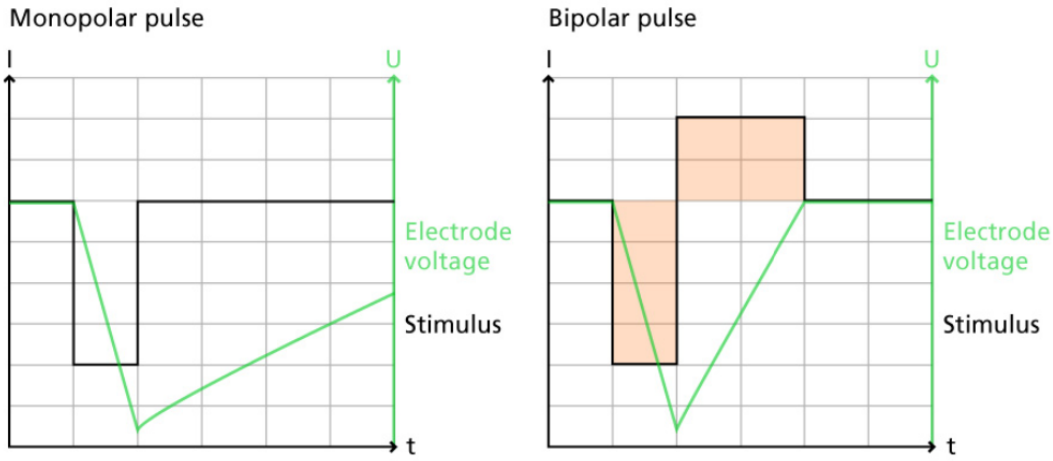

Figure 5.2: Effect of bipolar pulse on the electrode voltage [131]

Figure 5.2 shows the effect of a biphasic current pulse on the discharge of the stimulation electrode. The first monophasic pulse is followed immediately by a pulse of the opposite polarity and the same product of current and time. Theoretically, the higher the amplitude and the longer the stimulus, the higher is the impact on the electrode performance. Therefore, the amplitude and duration should be as low as possible.

As a result, we started with a low amplitude (500 mV or 1 µA) and low duration (50 µs) and then increased them slowly. Negative monophasic voltage pulses were applied to make sure that the voltage level of the stimulating electrode is zero, and thus the electrode is discharged, at the end of the pulse. When using current stimulation, biphasic stimulation was used by applying the negative phase first, to avoid a positive net charge on the electrode.

For pacing cardiomyocytes, high voltages/currents and long durations are generally required. We thus also applied voltage pulses up to 2.0 V maximum and current pulses up to 10 µA to avoid damage to the electrodes and electrolysis. Moreover, pulse durations between 100 µs to 1 ms were tested. However, no cell contraction or electrical activity could be seen or measured through electrical stimulations with our TFT-MEAs. Indeed, stimulation using planar microelectrodes is more challenging than recording.

One of the reasons is that stimulated electrodes need some time to discharge. When stimulating via MEA electrodes, an artifact can be observed on all channels during stimulation due to the high charge that is injected into the circuit. This phenomenon appears as "stimulus artifacts" that interfere with signals coming right after the stimulation. The time constant of the stimulus artifact depends on the amplifier bandwidth; if the lower cutoff frequency is quite low (e.g. 1 Hz), the stimulus artifact will be longer than with higher frequency (e.g. 10 Hz). In most cases, it is not possible to record true signals that are close to the stimulus pulse. Also, the stimulating electrode is generally not used for recording in parallel to stimulation, because the injected charge is too high, and the time constant for discharging too low. Another limitation for stimulating with MEAs is that voltage charged to planar electrodes must not go beyond 1-2 V to avoid electrolysis. This could hamper the amplitude of the current that can be delivered through the MEA [131].

As a result, electrical stimulation of mycoytes are usually not performed on MEAs. Some studies hypothesized that artificial electrical stimulation can lead to the same reactions normally produced *in vivo* in skeletal muscle tissues *in vitro*.

In a study, a model of physiological electrical stimulus has been constructed by determining electrical pulse parameters including voltage, stimulus interval, and frequency. The results demonstrated that the system was appropriate to study intracellular metabolism upon acute muscle contraction [132]. For this study, researchers used a 6-well plate containing the differentiated C2C12 myotube cells and connected to a 6-well C-dish (Ion Optix Corp., Milton, MA, USA), which functioned as the electrical stimulation apparatus. A C-Pace EP electrical pulse generator was used to generate electrical pulses (0.3 V/mm, 1.0 Hz, 4.0 ms) during a 4-day culture period [133]. The results indicate that electrical pulse stimulation produced muscle contraction, which is consistent with a previous study that reported the shortened length of skeletal muscle cells as a consequence of electrical pulse stimulation [134].

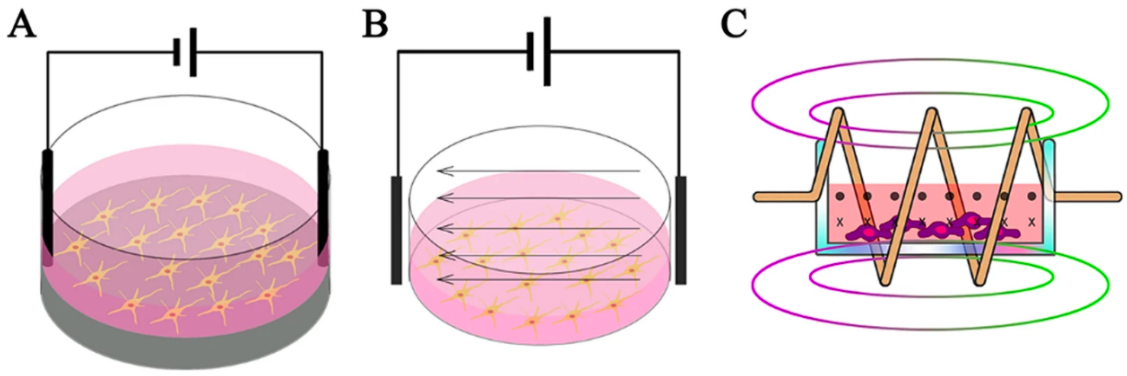

Figure 5.3: Three ways to deliver electrical stimulation to myocytes: (a) direct coupling, (b) capacitive coupling, and (c) inductive coupling [137]

As a result, in future research, we suggest to modify the method to deliver electrical stimulation. To stimulate myocytes electrically, it seems that the application of voltage pulses with an electric field parallel to the cell culture surface is more appropriate. The methods to deliver better electrical stimulation can be divided into three types: direct coupling, capacitive coupling, and inductive coupling using an electromagnetic field as shown in **Figure 5.3**.

In direct coupling, the electrodes (e.g. silver and platinum) are inserted directly into the culture medium and attached to the platform to deliver electrical stimulation. This method is most widely used because of its easy operation, but suffers from insufficient biocompatibility of the electrodes, contact with the medium lead to temperature rise, pH changes, and generation of harmful byproducts [135] [136].

In capacitive coupling, two electrodes are placed at opposite ends to provide a uniform electric field to the cells seeded on the platform, which locates between the electrodes. This system is non-invasive and thus more biologically safe compared with direct coupling. Also, it does not require a conductive platform to provide uniform electrical stimulation [138].

Finally, inductive coupling usually uses a controllable electromagnetic field generated by a conductive coil placed around the cell culture platform. This is called pulsed electromagnetic field stimulation (PEMF). The stimulus is transmitted by the pulse to mimic the natural potential transfer in the human body [137]. PEMF provides electric potential near some target cells, rather than directly apply electrical stimulation to the cells. However, PEMF treatment is taking time and resource consumption (e.g. at least 10 hour per day of stimulation) [139] [140] [141].

Chemical Stimulation

Regarding chemical stimulation of cardiomyocytes, isoproterenol (or isoprenaline) is a good candidate. Isoproterenol is a non-selective β-adrenoceptor agonist that is the isopropylamine analog of epinephrine (adrenaline). It has positive inotropic (increasing the force or speed of contraction) and chronotropic (increasing the heart rate) effects, which results in the increase of cardiac output.

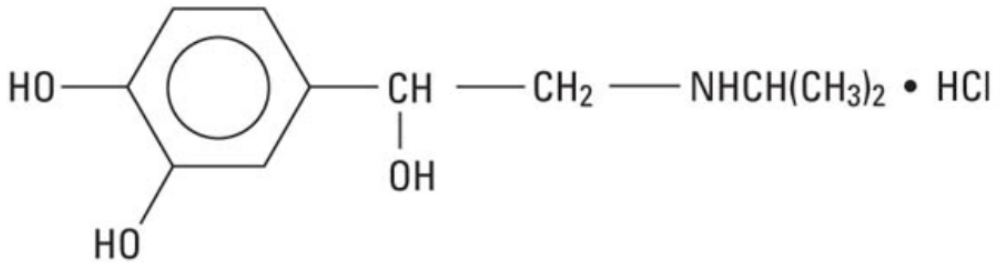

Figure 5.4: Structural formula of isoproterenol hydrochloride: it is 3,4-Dihydroxy-α-[(isopropylamino)methyl] benzyl alcohol hydrochloride, a synthetic sympathomimetic amine that is structurally related to epinephrine but acts almost exclusively on β receptors

Isoproterenol also decreases diastolic blood pressure by lowering peripheral vascular resistance. It is thus a medication (brand name: Isoprenaline Macure) used for the treatment of bradycardia (slow heart rate), heart block, and sometimes for asthma. Its molecular formula is $C_{11}H_{17}NO_3HCl$ as shown in **Figure 5.4**.

Its action is immediate once injected, with a duration of action from 10 to 15 minutes and half-life of 2.5 to 5 minutes with intravenous administration [142]. It would thus be interesting to test this compound on cardiomyocytes cultured on our TFT-MEAs to evaluate its effect on the cell contractibility and beating rate. However, we suppose that this compound should probably have an effect on cells that are already active and would increase the beating rate without changing the signal amplitude. This hypothesis still needs to be confirmed.

5.1.6 Scanning Rate

Current Methodologies for Fast Scanning

Traditional intracellular recording techniques such as patch-clamp provide a higher signal quality compared to conventional extracellular recording techniques. However, they have technical limitations regarding the number of sensing electrodes and therefore cannot provide enough information concerning the cell network function. It is thus difficult to describe the physiopathological activity of cardiomyocytes at a level where the cells start working in cooperation with other cells, providing the organized and synchronized processing of the heart.

The last decades, new approaches have been developed to increase the number of recorded cells using *in vitro* MEAs [143]. However, in order to provide an accurate description of a cell network function, simultaneous recording of all electrodes is essential. Therefore, the main technical challenge for recording through multiple electrodes has been to developed a system allowing to scan the array of electrodes to acquire data almost simultaneously. CMOS technology is one of the common technologies used for performing fast scanning and achieving almost simultaneous measurements of the extracellular potential of cells.

To accomplish this, the latest CMOS-MEAs, such as 3Brain's chips, are based on the active pixel sensor (APS) concept in order to record simultaneously thousands of extracellular electrodes and release electrical stimulation. This technology is commonly used in high-speed digital cameras. When it is adapted to MEAs, the original in-pixel circuitry is entirely redesigned to record small extracellular voltage variations resulting from cellular activity instead of detecting light changes. The pixel is used as a kind of video camera. The signal is collected as frames and each point represents the instant extracellular voltage value for each pixel (**Figure 5.5**).

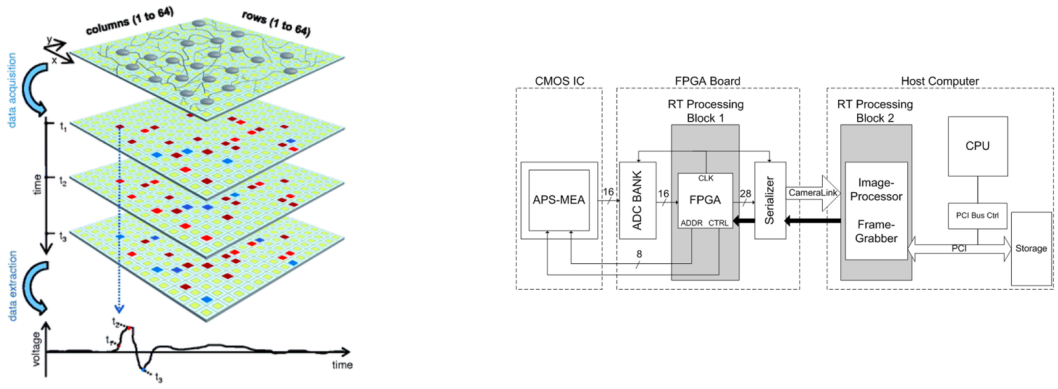

(a) (b)

Figure 5.5: Working principle of high resolution CMOS-MEA: (a) sequence of frames that encode extracellular voltage signals as pixels data for fast acquisition of extracellular electrophysiological signals [30]; (b) block diagram of the acquisition platform (white arrows = high-speed communication interfaces, black arrows = low-speed interfaces going from the host computer to the FPGA, RT = real-time processing units to be used for data preprocessing and analysis tasks [29]

A field-programmable gate array (FPGA) is used as both the control and timing device of the APS–MEA and of the bank of analog-to-digital converters (ADCs), since the addressing of the electrodes has to be synchronized with the analog-to-digital (AD) conversion [29]. Pixels can be arranged in a 64 × 64 array. They are square electrodes that can be as small as 21 µm, with a possible pitch of 21 µm. In the end, signals can be recorded at a sampling rate of 7.8 to 125 kHz for each pixel, which makes possible to reconstruct the signal into a color-coded video of the cell electrical activity by following a single pixel over time [144] [30]. To achieve this, the active electronics is acting on the recorded signals directly on the chip. Amplifiers are located below every single electrode, allowing enhancement of the signal at the source, in other words, right underneath the cells. As a result, this prevents amplification of any additional noise and signal attenuation during the propagation of the signal. This type of MEAs can thus provide a high SNR.

Scanning Speed of TFT-MEAs

The main drawback of CMOS-based MEAs is that such arrays are not transparent. Indeed the active electronics is located right below every single electrode. Therefore, a compromise has to be made between transparency and the integration of electronics for fast scanning. In this study, we developed a transparent TFT-MEA to record the extracellular potentials of cardiomyocytes.

The gate lines were opened for 5,000 ms one by one with an interval of 1,000 ms between the closing and opening of the next gate lines. With this scanning method, we could make sure that the gates were opened for a long enough time to detect the cell electrical activity. Indeed, if the cells were not strongly active (e.g. after $\sim$ 10 days of cell culture), the frequency of the electrical potential could be lower than 1 Hz. Therefore, this large switching time of 5,000 ms ON and 1,000 ms OFF could provide interesting information regarding the amplitude, period, and regularity of the signals. However, this scanning rate obviously has some limitations. As measurements are not done simultaneously on all electrodes (only column by column), this scanning method is quite limiting for some applications such as the study of the signal propagation. Nevertheless, in this research we attempted to measure the signal velocity in columns of electrodes. **Figure 5.6** shows an array of 4 $\times$ 4 electrodes and specifies when each electrode detected a signal compared to the other electrodes on the same column.

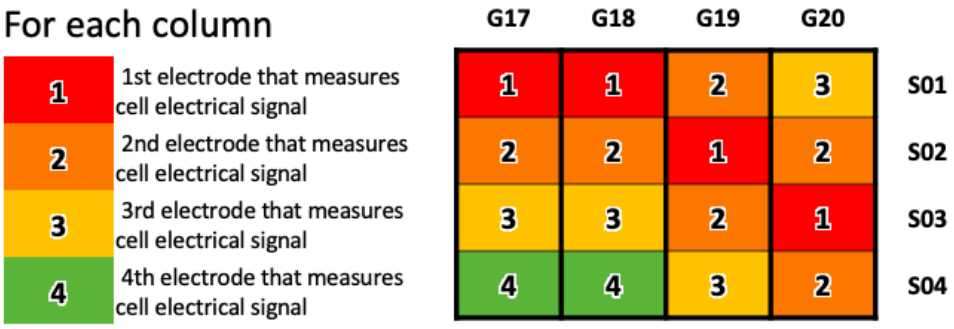

Figure 5.6: First attempt to build a mapping of signal propagation of cardiomyocyte electrical activity measured on a TFT-MEA

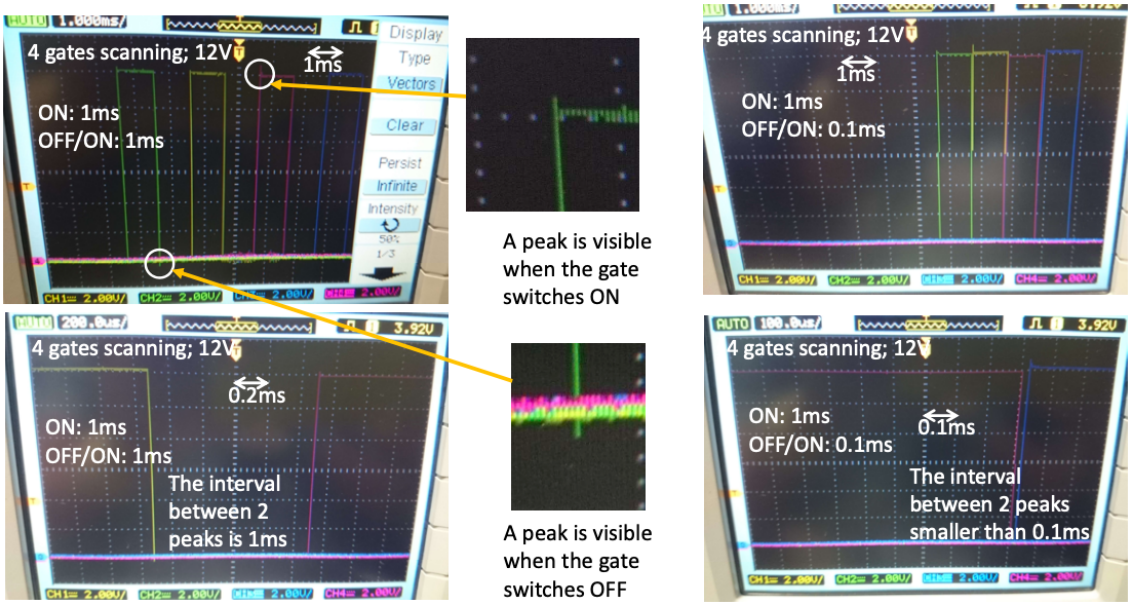

Figure 5.7: Fast scanning: measurement of the control card (JAPASTIM) output with an oscilloscope

The data were obtained from a cell culture that showed a strong and regular electrical activity within its cell network (average amplitude of 400 µV and frequency of 4 Hz). As a result, this mapping seems to show some kind of wave of signal propagation. However, in order to obtain a proper evaluation of the signal propagation in the cell culture, it is essential to measure signals almost simultaneously on each column of electrodes and thus to increase the scanning rate. The limitations of the scanning speed is mainly due to the instrumentation. Although the scanning rate of the control card can be increased, measurements are still limited by the sampling frequency of the measurement system. Fast scanning measurements were still tested with an oscilloscope and showed that it is possible to perform scanning of 1 ms ON and 1 ms OFF, as well as 1 ms ON and 0.1 ms OFF, as show in **Figure 5.7**.

However, this scanning rate would not be high enough to obtain enough points for each signal. The measurement system from Multi Channel Systems MCS GmbH can reach a sampling frequency of 20 kHz, which means that one point is measured every 50 µs. Supposing that we have a TFT-MEA of 20 × 20 microelectrodes, and that the control card can scan 20 gate lines at 1 ms ON and 0.1 ms OFF, 20 points would be obtained (1 ms of measurement) for each gate line every 20 ms. According to our observations, the duration of cardiac field potentials from cardiomyocytes can go from 1 ms to 5 ms approximately. Therefore, many spikes of their field potentials would be missed. However, it would be interesting to test this scanning speed to evaluate how much data could still be extracted with this method.

Additionally, in order to increase the accuracy of the signal, several gate lines could be opened simultaneously by overlapping them. For example, gate 1 and 2 would be opened first, then gate 2 and 3, then gate 3 and 4, and so on. Although this technique would require a lot of data analysis and the development of specific software for reconstruction of the signals, it is still an interesting opportunity to improve the scanning method with our control card.

Commutation Spikes

Another observation made during the scanning process of our TFT-MEAs is the commutation spikes that emerge when opening and closing each gate lines. These commutation spikes bring noise that is commonly referred to as "clock feedthrough noise".

Figure 5.8 shows the commutation spikes observed with 1,000 ms delay between the closing / opening of each gate line. A +40 mV positive peak and a -40 mV negative peak are observed when closing and opening the gate line, each one disturbing the signal for approximately 1.3 ms and 17 ms respectively.

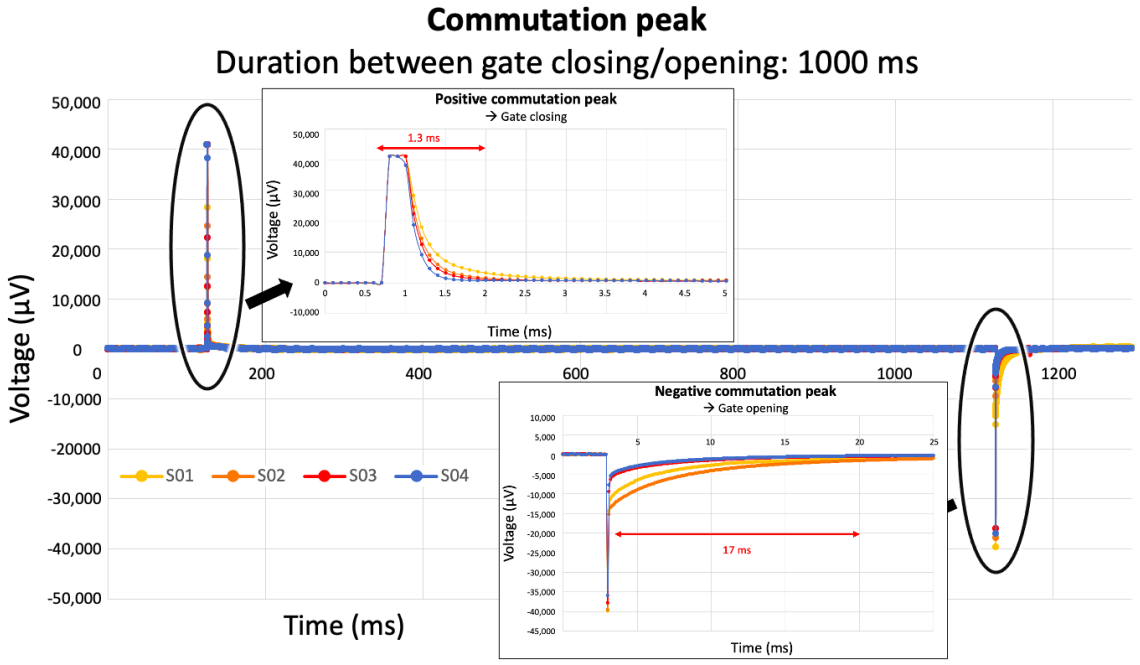

Figure 5.8: Commutation spikes when duration between opening/closing gates is 1000 ms

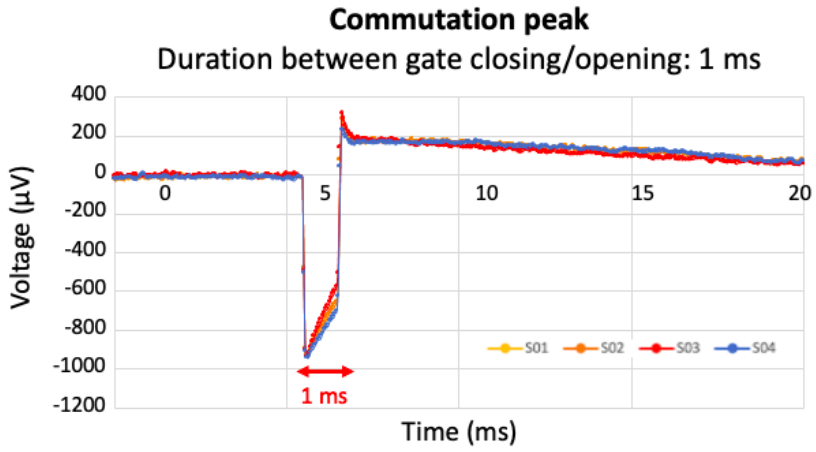

Figure 5.9: Commutation spikes when duration between opening/closing gates is 1 ms

In addition, **Figure 5.9** shows the commutation spikes observed with 1 ms delay between the closing / opening of each gate line. A -900 µV negative peak and a +300 µV positive peak are observed. In this case, the signal is not disturbed for a too long period of time, although it takes approximately 15 ms to go back to the baseline. We can notice that for a delay of 1,000 ms, positive and negative peaks are observed when closing and opening the gate lines respectively, while the opposite is observed when the delay is 1 ms; negative and positive peaks are observed when closing and opening the gate lines respectively. We suppose it happens because of the short delay of 1 ms the positive and negative spikes add up. On **Figure 5.8**, the positive peak reaches its absolute maximal value for 0.5 ms, while it is less than 0.1 ms for the negative peak which is thus much sharper. This could explain why the signal goes first negative and then a bit positive for 1 ms delay.

These commutation spikes are certainly due to some charge and discharge of the transistors when opening and closing the gate lines. Indeed, when voltage changes very fast, current goes from ON to OFF and a reverse current flows immediately for a very short moment. This could be considered to be the cause of the spike noise.

5.1.7 Drug Testing

Cardiomyocytes are responsible for heart contractions and are the main cell type in the human heart with respect to volume. Irregularities in heartbeat, due to cardiac electrical dysfunction, are one of the most frequent causes of mortality and morbidity in industrialized society. Therefore, elaborate *in vitro* models are needed for obtaining a better understanding of how potent pharmaceutical agents affect cardiac electrophysiology.

As a result, this TFT-MEA has potential applications in drug screening, such as measuring the dose-response curve of isoproterenol, a β-adrenergic agonist with a positive chronotropic effect.

5.2 Electrochemistry

5.2.1 Significance

In this research, we demonstrated that the TFT platform could also be used as an electrochemical sensor for biological compounds. Indeed, biological phenomena cannot be described only through measurements of cell electrical activity. Cell communications also involve biochemical components. Therefore a truly versatile sensing platform to monitor cell or tissue communications also requires the possibility to perform electrochemical sensing. A collaborator has already used the TFT technology to develop an albumin sensor using impedance measurement [145]. However that technique requires the use of a low conductivity medium, which is not compatible with the culture of biological cells due to the high conductivity of their culture medium.

Therefore, in this work we have fabricated an Ag/AgCl based chemical sensor by coating Ag/AgCl ink on the dedicated RE area of the TFT array. Experiments have qualitatively demonstrated that ITO microelectrodes can be used as WE and that Ag/AgCl ink can be used as an integrated RE on the TFT platform. As a result, a complete integrated sensor can be built on the platform.

5.2.2 ITO Working Electrode

Optical observation of TFT substrates after electrochemical experiments showed that ITO electrodes and vias, which connect the surface electrode to the drain of the transistor, were changing color and thus probably damaged. This phenomenon happened especially on ITO electrodes that are not connected (gate and source lines not connected) during electrochemical measurements.

A possible explanation would be that when the TFT device is connected to an electrical device (such as the control card), some electrical charges enter the TFTs and might get stuck inside. All these charges cannot escape and might trigger the random opening of TFTs. This could lead to exchanges of charges and electrons and thus redox reactions of ITO microelectrodes. This theory could also explain another issue that was encountered during some electrophysiological experiments. Indeed, it could happen that electrical signals from cardiomyocytes were measured even though all connected TFTs were closed (no voltage was applied to the connected gate lines). A solution to that problem would be to connect and control all gate lines by grounding the gate lines where no electrochemical measurements would be performed.

Additionally, ITO-based electrode is not a noble metal and thus not an ideal electrode material for electrochemical sensing. However, the main reason for using ITO in this study was to test the possibility of performing electroanalysis with our ITO-based TFT platform that was already developed for electrophysiology, with the perspective to combine both techniques in the future. ITO electrodes might also produce a high electrochemical signal, and low background noise towards signaling species, i.e. a high SNR [146]. In case the use of ITO material limits some target applications, post-processing of gold patterns can be performed following the same post-process as described in [111]. The drawback is that the electrodes with gold pattern will lose their transparency. In that case, it could be decided that electrochemical measurements will be performed only on some dedicated sites in the microelectrode array.

The size of ITO electrodes should also be taken into consideration to make sure there is no overlap of diffusion layers. In electrochemistry, the diffusion layer can be defined as the region in the vicinity of an electrode where the concentrations are different from their value in the solution. This concentration approaches asymptotically the value in the bulk solution. Therefore, the thickness of the diffusion layer is arbitrary.

The diffusion layer thus depends on the diffusion coefficient (D) of the analyte, the voltage scan rate (ν) in V/s, and the potential difference (Δ E) between the onset of electrolysis and the potential at which steady-state current is obtained. It is usually considered that the diffusion layer should be:

$$d > 2\sqrt{2D\frac{\Delta E}{\nu}}$$

According to our amperometric results, it seems that the limited current response is not totally obtained with our TFT-MEA. This indicates that there might be an overlap of diffusion layers. However, longer measurements (a least 200 seconds) should be performed for confirmation. In case of overlaps of diffusion layers, a structure with auxiliary electrode could be considered to suppress the expansion on the TFT-MEA [147].

5.2.3 Integrated Reference Electrode

Figure 5.10 presents the integrated RE that was placed in the TFT substrate for our electrochemical experiments. Our results showed that proper electrochemistry can be performed by placing Ag/AgCl ink on the RE area of our TFT-MEA. However, this RE is not stable and oxides with time on both dry substrate and in culture medium. To avoid oxidation of the RE, a possible solution would be to protect and cover it with a porous polymer for example.

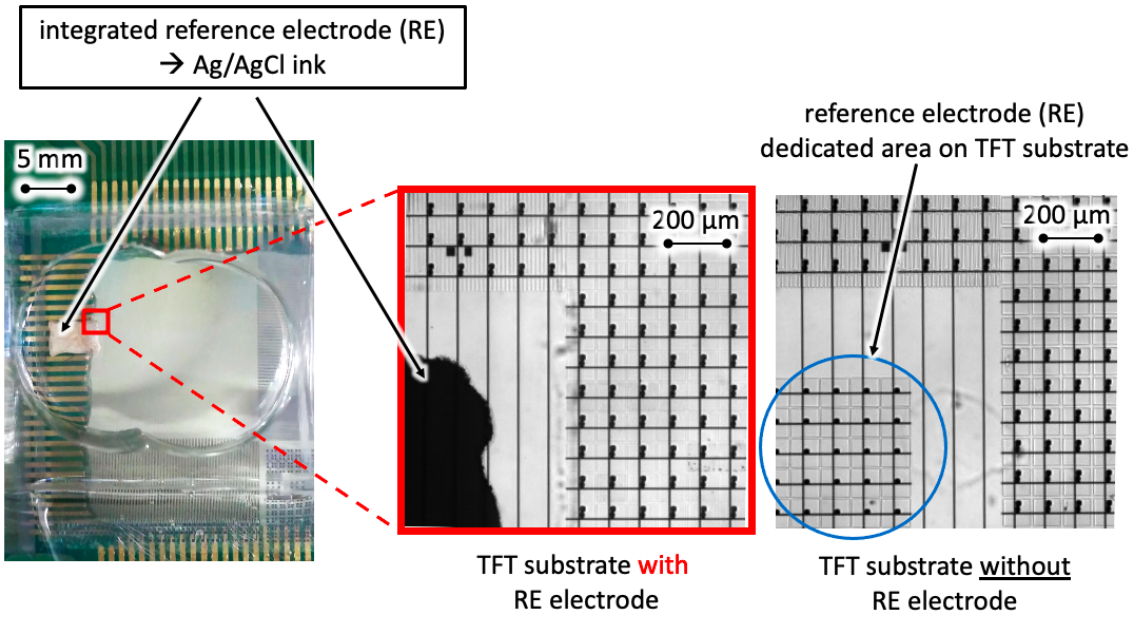

Figure 5.10: Integrated reference electrode on TFT substrate

5.2.4 Electrode Polarization

The influence of the electrode polarization on the cellular electrophysiology activity during electrochemical measurements should also be considered. Indeed, some mechanical side-effects of the electrochemical process may develop isolating barriers at the interface between electrodes and analytes. These side-effects can then influence the reaction mechanisms on the electrode. In our case, the application of voltage during electrochemical measurement and the apparition of current, due to electrochemical reaction, might affect the electrical activity of the cells. In case the electrode polarization is shown to have an influence on the cellular electrophysiological activity, investigations to determine to what extent it affects the activity, and whether the effect is reversible, should be investigated.

5.2.5 Conductive Lines

Finally, some damages on the TFT substrates were observed after electrochemical experiments. Observation with a confocal microscope showed that conductive lines of TFTs "vanished" post-experiments. A possible reason of this phenomenon might come from the electrochemical current that could be too high and thus burns the TFTs and their conductive lines during experiments. To solve this problem, a possible solution would be to perform measurements with lower concentrations of analytes. As current is proportional to the analyte concentration, a decrease of the amount of analytes could help with this issue. Also, concentrations in µM range are closer to the concentration of analytes usually measured in biological experiments.

5.2.6 Unspecific and Specific Detection

Mechanism of Tyramine

Tyramine is a vasoactive amine that has the capacity to increase both the mean arterial blood pressure and heart rate [148]. The cardiac organ and brain do not produce tyramine. This molecule is acquired through alimentation and is metabolized in our digestive system. The prevention of tyramine metabolism in the small intestine, liver and endothelium by irreversible monoamine oxidase A (MAOA), monoamine oxidase B (MAOB) or MAOA inhibitors can lead to its presence in the circulation [149] [150].

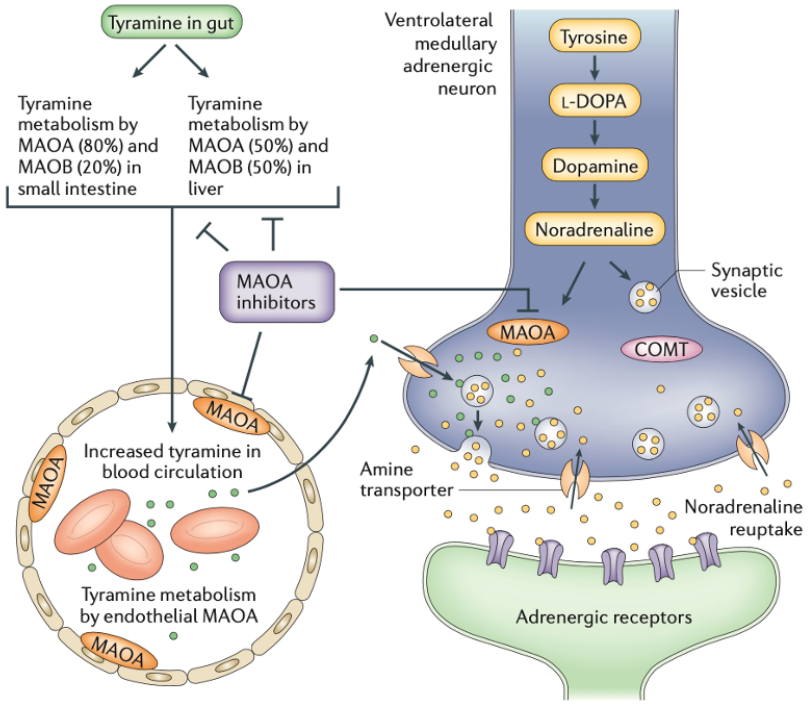

Figure 5.11: Cardiovascular effects of tyramine [151]

As a result, the uptake of tyramine by adrenergic neurons in the ventrolateral medulla, in which MAOA is also inhibited, initiates the release of noradrenaline into the synaptic cleft. This leads to the stimulation of cardiovascular sympathetic nervous system activity (**Figure 5.11**) [151]. The SNS releases hormones, such as catecholamines, epinephrine and norepinephrine through sympathetic nerves. Cardiac sympathetic innervation includes innervation of the sinoatrial (SA) node, which allows sympathetic nerves to increase heart rate by increasing the slope of diastolic depolarization during the spontaneous SA node action potential. Sympathetic nerves also innervate the myocardium. Increases in sympathetic activity increase myocardial contractility and, therefore, increase stroke volume and thus blood pressure [152].

Tyramine was chosen for our electrochemical experiments of amperometry, because this molecule was directly availabe in our laboratory. However, the development of a tyramine sensor for cultures of cardiomyocytes would not be valuable as tyramine does not interact with cardiomyocytes directly. However, tyramine is also considered as a neuromodulator. Threfore, if co-cultures of neurons and cardiomycoytes can be performed on our TFT-MEA, a tyramine sensor might be interesting to develop.

Integration of Specific Sensor

Amperometric experiments performed with tyramine showed the future possibility to integrate a tyrosinase-based biosensor on the TFT platform. The limitations of the present study naturally includes the non specificity of the sensor. Indeed, no treatment was performed on ITO microelectrodes beforehand.

In the future, a voltammetric tyrosinase-based biosensor for the determination of tyramine could be developped. Tyrosinase catalyzes oxidation of tyramine to corresponding o-quinone. Therefore, by binding tyrosinase to the microelectrode arrays, the reduction of tyrosinase by tyramine can generates current correlated to the tyramine concentration that can be measured [153].

However, as explained in the previous section, the development of a different type of sensor would be wiser for understanding the fundamental parameters of cardiomyocyte metabolism, i.e. the extracellular acidification rates (ECARs) (determined from measured pH) and oxygen consumption rates (OCRs) (determined from measured O_2 level). The ECARs are often used as a measure of glycolytic metabolism, while the OCRs are used as a measure of oxidative phosphorylation [154]. These types of sensors could be fabricated by modifying the ITO microelectrode surface with an iridium oxide (IrOx) or ruthenium oxide (RuOx) sheet sputtered on the surface.

5.3 Dielectrophoresis

5.3.1 Cell Mobility and Patterning

The results demonstrate that efficient DEP with TFT devices can be performed on myocytes. However, due to the 100 kHz limitation of the signal in frequency because of the characteristics of the TFTs, DEP can be performed only with lower frequencies. As a consequence, it is not possible to reach the crossover frequency: DEP can be only negative (repulsive) for 10 µm polystyrene microbeads and only positive (attractive) for cells. According to the Bode diagram that was built in order to determine the range of frequencies that can be used for our experiments, we observed -10 dB attenuation at 10 kHz and -20 dB attenuation at 1 MHz.

As a result, DEP can be performed with signals of 100 kHz, maximum. Therefore, the crossover frequency between positive and negative DEP cannot be reached, and it is expected to observe only one sort of DEP effect with our TFT-MEAs. Here, polystyrene microbeads show opposite DEP behavior compared to mammalian cells.

We also showed that cells could attached and be cultured on Teflon-coated TFT-MEAs after DEP experiments. This opens the possibility to perform long-term DEP experiments on cell cultures. For example, voltage could be applied to some targeted regions on cell cultures to manage the cell orientation. This would be especially interesting for culturing skeletal muscle cells on TFT-MEAs and orienting the cell configuration similar to the one we can see in muscle tissues. Then, electrical stimulation could be applied to observe the effect of that cell patterning on cell contraction.

5.3.2 Insulation layer

The Teflon layer allowed the application of high voltage to the source lines of the transistors (e.g. +/-10 V). **Figure 5.12** shows a row of damaged electrodes after DEP experiments on a TFT substrate without Teflon treatment. No damage of the electrodes was observed during experiments with Teflon-coated TFT substrates.The Teflon layer protected the electrodes from the cell culture medium and electrolysis.

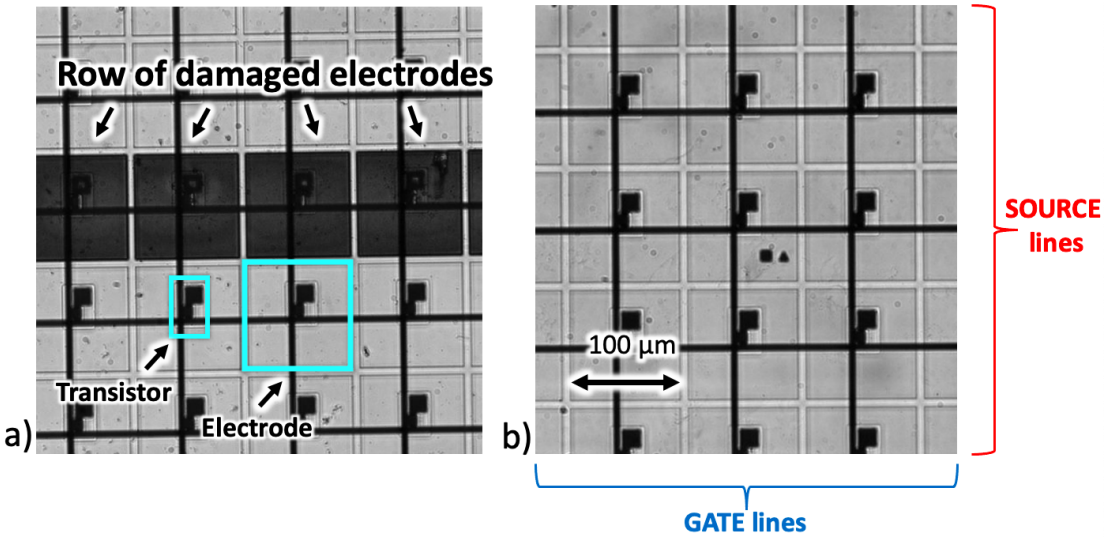

Figure 5.12: Damaged vs undamaged TFT array substrate after DEP experiments: (a) damaged TFT array substrate without Teflon-coating treatment; (b) undamaged TFT array substrate with Teflon-coating treatment

However, we could argue that it would not be possible to perform voltage sensing on a Teflon-coated TFT-MEA as the Teflon layer works as an insulator. Consequently, it would be difficult to combine this technique with recordings of the electrical activity of excitable cells, such as cardiomyocytes.

Another type of material that would allow voltage sensing on TFT substrates should thus be used and tested for DEP. Another possibility would be to pattern the layer of Teflon (e.g. on every two lines), so that some microelectrodes without Teflon coating would be dedicated to electrophysiological recordings.

5.4 Cell Viability and Activity

5.4.1 Cell Viability

In order to perform electrical measurements on cell cultures for long-term analyses, it is critical for the TFT devices to be biocompatible and support the growth of biological cells. The non-toxicity of the TFT substrate itself is thus fundamental. Proliferation of C2C12 cells has been evaluated on different substrates: glass, ITO, and flat-bottomed 96-well plate (made from polystyrene). Cells were seeded and cultured for 48 hours (after full confluence) in the incubator at +37 °C at 95 % humidity. The cells were then detached with trypsin and counted to compare the proliferation rate on each type of substrate. **Table 5.1** shows the results obtained in this experiment.

Substrate	Number of cells/mL t = 0	Number of cells/mL t = 48 h	Living Rate	Growth Percentage
96-well plate (polystyrene)	7.00×10^4	1.75×10^5	100 %	+ 150 %
glass	7.00×10^4	1.42×10^5	98 %	+ 103 %
indium tin oxide (ITO)	7.00×10^4	1.28×10^5	100 %	+ 83 %

Conventional substrate = **96-well plate** ELISA plate (e.g. polystyrene)
TFT surface = **glass** substrate + **ITO** electrodes

Table 5.1: Proliferation of C2C12 cells on different substrates: glass, indium tin oxide (ITO), and flat-bottomed 96-well plate (made from polystyrene)

We observe an increase of +150%, +103%, and +83% of cells on the 96-well plate, glass substrate, and ITO substrate respectively. Culture plates are fabricated for optimal cell culture to perform cell-based research. Therefore, the proliferation rate is unsurprisingly higher for cells cultured on the 96-well plate. Moreover, the proliferation rate is a bit higher for cells cultured on glass substrate than for cells cultured on ITO substrate. These results confirm what has been observed during experiments when cardiomyocytes were cultured on our TFT-MEAs. Indeed, cells tend to escape the ITO electrodes to grow on the regions free from electrodes (glass substrate). However, the living rate is close to 100 % for each type of substrate. Thus, it seems that the surface material might have an effect on the cell proliferation rate, but not on the cell viability.

Regarding DEP experiments, we observed that around 30% of C2C12 cells would die after 30 minutes of DEP experiment in 300 mM Mannitol buffer. However, we also demonstrated that C2C12 cells could be cultured on the TFT substrate after changing the buffer medium to the appropriate cell culture medium. Nevertheless, additional tests should be performed to measure the proliferation rate of C2C12 cells on our Teflon-coated devices after DEP experiments in order to bring quantitative results on this observation.

5.4.2 Cell Electrical Activity

Another point to take into consideration when performing electrical measurements of cells cultured on our TFT-MEAs, is the potential effect that switching ON/OFF of TFTs might have on the cell viability and electrical activity during and after experiments. Indeed, when opening and closing the gates, commutation spikes of +/- 40 mV could be observed and measured through the source lines. We should not ignore the possibility that this voltage might have an effect on the viability and electrical activity of cells. However, no effect was observed optically during and after electrical measurements for electrophysiological studies of cardiomyocytes. This means that optical observations did not show any deterioration of the cells due to the opening/closing of gate lines using our TFT-MEAs. Similarly, no decrease of the cell contraction activity was observed optically during and after electrophysiological measurements.

Regarding electrical recordings of the cell culture activity, electrical measurements would be performed as soon as cell contraction could be optically observed (usually on day 3). All connected gate lines would be scanned every day for 2 weeks. During experiments, it could happen that cardiomyocytes showed a high electrical activity (signal amplitude and frequency) at the beginning, a decrease of activity for a few days, and a new increase of activity later even though measurements were performed every day.

Therefore, qualitative results show that the activation of TFTs for scanning of the cell culture surface may not have an impact on the cell culture viability and activity. However, quantitative experiments should be performed to confirm these observations. A possibility would be to culture cells on TFT-MEAs and perform electrophysiological measurements on some devices only. Cells would then be detached and counted on all devices. In this way, we could compare the number of cells that were still alive on each device, and look at a possible effect of electrical measurements on the cell viability.

Meanwhile, experiments showed that the cell density seems to be the major factor that would predict the level of cell electrical activity. Indeed, we observed that the chance of observing cell contraction and measuring their electrical signal was low if the density of cardiomyocytes was lower than 2.0×10^5 cells/device. The activity of cells was much stronger if the cell density was between 2.5×10^5 and 1.0×10^6 cells/device so that cardiomyocytes could easily and quickly form a strong cell network. Moreover, we observed the cell activity was more intense when exchanging the cell culture medium before performing electrophysiological measurements, which means that the nutrients and certainly the pH of the cell culture medium are fundamental for appropriate electrical exchanges within the cell network. Similarly, we have also showed that the temperature of the cell culture medium is also an essential factor in the electrical activity of cardiomyocytes.

As a result, even though the activation of TFTs may have an impact on the cell viability and activity, it seems that external factors such as the temperature, the culture medium, the cell density, are more critical to obtain a strong electrical activity of cardiomyocyte cultures.

5.5 Cleaning and Reuse of Device

According to the MEA manual from Multi Channel Systems MCS GmbH, long-time experiments with cell cultures and rigid cleaning methods shorten their MEA lifetime. However, their MEAs can still be reused about 30 times, depending on the coating, cell culture, and cleaning procedure. The surface of their MEAs is made from titanium nitride (TiN), which is a very stable material that, for example, is also widely used for coating heavy equipment [131].

In our case, microelectrodes are made from ITO material, which is also interesting for cell culture thanks to its optical transparency, stability under warm and humid conditions, non-toxicity, and excellent electrical conductivity [155]. Different types of cells have already been cultured on ITO-coated surfaces without observing any disadvantages or detrimental consequences [156].

In this research, some TFT-MEAs could be reused several times for electrophysiological measurements if handled with care. In some cases, TFT-MEAs were used at least 7 times for electrophysiological measurements.

However, the experimenter has to be very careful not to touch and damage the TFT substrate while using the pipette when cleaning the surface or seeding the cells for example. Indeed, touching the TFT substrates with the tip of the pipette can make scratches on the surface and thus damage it. Additionally, after several use of the same TFT-MEA, we could observe that some gate or source lines would stop working properly and only noise would be measured on the connected electrodes. One reason for these damages could be the deterioration of the bonding wires. Even though they are protected with PDMS, soaking the TFT device in 70 % ethanol several times for cleaning could be deleterious for the bonding wires. Although less frequent, we could also observe the malfunction of some TFTs themselves after reusing the same device several times. This could come from a default in fabrication, or an external chock on the TFT substrate. However, the reason why some transistors would stop functioning is still unclear and must be investigated.

Regarding the cleaning methodology, we used trypsin and ethanol. Trypsin is commonly used for cutting through enzymes and proteins. We used it to cleave the bonding proteins and extracellular matrix of cells cultured on our TFT-MEAs. As a result, cells could be detached and easily removed. Once these bulk contaminants have been removed we used ethanol to eradicate the remnant contaminants. Ethanol is indeed useful for removing organic compounds on the device.

If needed in the future, an ultrasonic bath could also be used for more efficient cleaning. This bath would operate by pulsing high frequency ultrasound into the device, which would induce vibrations and enhance the cleavage by the ethanol.

5.6 Electromagnetic Point of View

The relevance of external electric field for healthcare in terms of nerve regeneration, bone fracture, and wound healing is well established [157]. Depending on the applied stimulus parameters, a biological cell can be affected in a number of ways in the presence of the external stimulus [158]. A large number of studies have shown that electric field can be a versatile tool in influencing cellular behavior and cell fate processes.

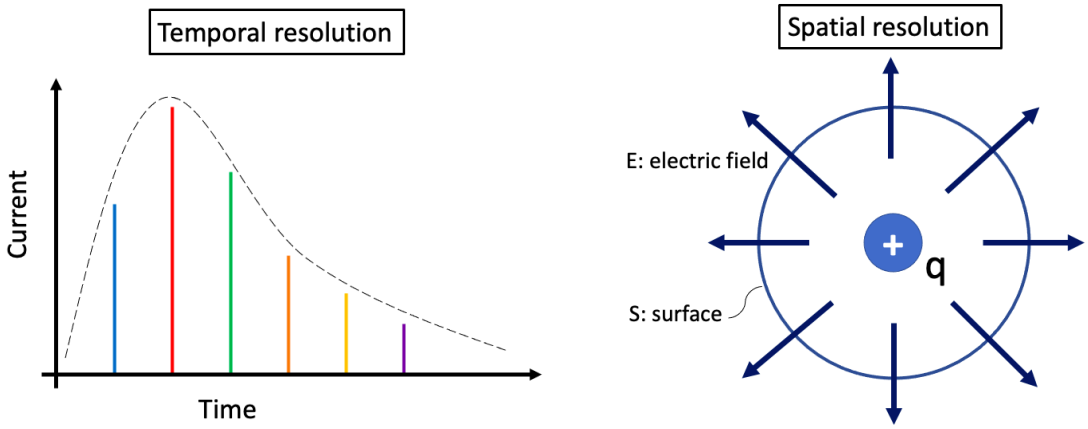

(a) (b)

Figure 5.13: Temporal and spatial resolution with differential measurements on TFT-MEAs: (a) plot of current in function of time for temporal resolution; (b) evaluation of electric field for spatial resolution

Measurements of the cell electric field could also provide more information to describe the electrophysiology and pathological activity of culture of cardiomyocytes. Moreover, by combining impedance measurements with electrophysiology, we can measure the capacitance of cells and assess their attachment quality to the substrate, which is fundamental for optimal measurements with MEAs. Therefore, it would be interesting to use our TFT-MEAs to build a map of the electro-distribution flux of cells. To achieve this, we should thus evaluate the temporal and spatial resolution of measurements (**Figure 5.13**). The temporal resolution would obviously depend on the scanning method of the TFT platform for measurements of cell signal currents. In ideal conditions, we could achieve a scanning speed in the range of µs. We thus need to evaluate how we could efficiently improve the scanning process of our TFT platform.

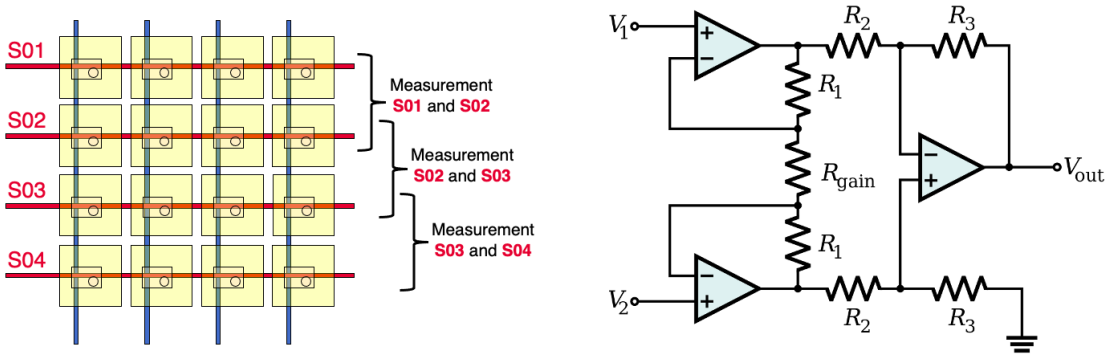

(a) (b)

Figure 5.14: Interconnection pairs for enhanced SNR: (a) source lines measured in pairs with the immediate neighbor line so that it could be connected to an instrumentation amplifier for a higher CMRR; (b) schematic of typical instrumentation amplifier

An overlap scanning (e.g. measuring through source 1 and 2, then source 2 and 3, then source 3 and 4, etc) would provide better SNR and more valuable data. In other words, source lines would be measured in pairs with the immediate neighbor line so that it could be connected to an instrumentation amplifier for a higher common mode rejection ratio (CMRR), which is the indicator of the differential amplifier to suppress signals common to the two inputs as shown in **Figure 5.14**. Current value could be measured via impedance sensing on consecutive electrodes and then be plotted in function of time in order to obtain a temporal evolution of the current distribution.

Regarding the spatial resolution, measurements of the electric field on consecutive electrodes would bring more information to speculate the flow of charges inside the cells and the direction of their propagation. Eventually, this could make possible to determine the origin of electrical communication within a network of cells. The distribution of electric charge to the resulting electric field can be described by Gauss's law. In its integral form, it states that the flux of the electric field out of an arbitrary closed surface is proportional to the electric charge enclosed by the surface, irrespective of how that charge is distributed [159]. The equation introduces the electric field (E), the total electric charge density (total charge per unit volume) (ρ) and the permittivity of free space (ε_0). Ω is any fixed volume with closed boundary surface $\partial\Omega$. The integral form of the equation can be written as following:

$$\oiint_{\partial\Omega} \mathbf{E} \cdot \mathrm{d}\mathbf{S} = \frac{1}{\varepsilon_0} \iiint_{\Omega} \rho \, \mathrm{d}V$$

Even though the law alone is insufficient to determine the electric field across a surface enclosing any charge distribution, this may be possible in cases where symmetry mandates uniformity of the field. Where no such symmetry exists, Gauss's law can be used in its differential form, which states that the divergence of the electric field is proportional to the local density of charge. The differential form of Gauss's law is:

$$\nabla \cdot \mathbf{E} = \frac{\rho}{\varepsilon_0}$$

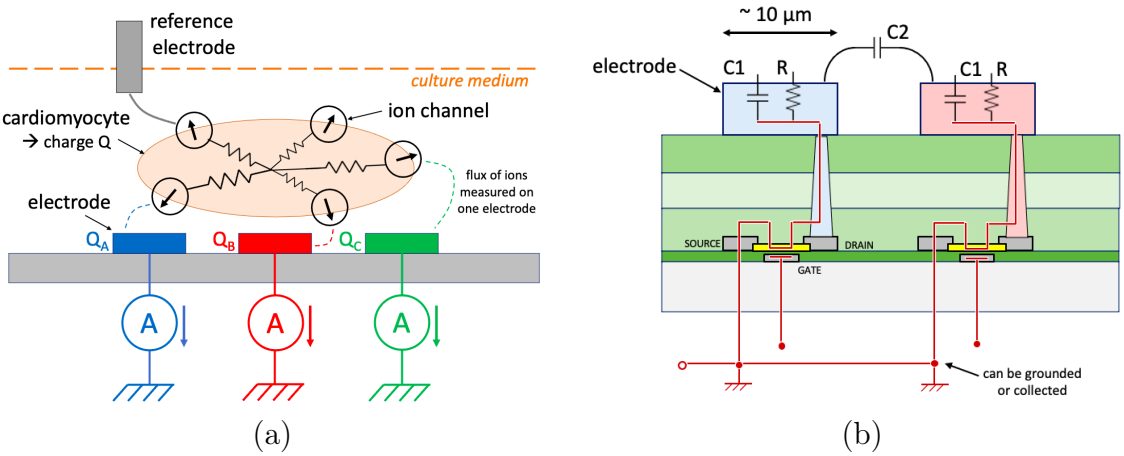

(a) (b)

Figure 5.15: Illustration of TFT-MEA for differential measurements: (a) cardiomyocyte cultured on a TFT-MEA and the exchanges of charges through the cell membrane measured on 3 electrodes; (b) schematic view of TFTs and electrode parameters C_1, C_2, and R

Moreover, the capacitive current I_{cap}, the capacitance C, the voltage V, and the charge q can be described as following:

$$I_{cap} = C\frac{\mathrm{d}V}{\mathrm{d}t}$$

$$q = CV$$

As a result, differential measurements on consecutive electrodes could allow the determination of the total charge Q in a cell and could provide more information about its position on the substrate. To accomplish this, we need to know several parameters: the electrical resistance (R) and capacitance (C_1) of electrodes, as well as the coupling capacitance (C_2) between two electrodes as shown in in **Figure 5.15**.

The capacitance needs to be very small for adequate measurements. According to these values, the size of electrodes can then be decided. However, it would be interesting to test several sizes of electrodes; similar to the cell dimension (30 µm) or larger (100 µm). As a result, this new measurement technique could bring more information about the flow of charges inside the cell network and the direction of their propagation.

5.7 Chapter Summary

In this chapter, we discussed the results obtained with the electrical measurements performed with our TFT-MEAs. We demonstrated the value of this novel platform for studying excitable cells with multiple measurement techniques; electrophysiology, electrochemistry, and DEP. We also discussed the problems met during experiments and the potential solutions to overcome them. Finally, we presented additional research that could be done for improvement of our TFT platform.

Chapter 6

Conclusion

This chapter concludes the entirety of this dissertation. We start with a summary that includes all the important points of each chapter. Afterwards, we proceed with the conclusion of this work and a discussion about the key contributions made to the development of TFT microelectrode arrays for biological applications. Finally, we consider future possible projects using this platform and the longer term impacts of this work.

6.1 Research Summary

Chapter 1: Introduction

In the introduction, we described the purpose of this thesis, which is the study of the extracellular potential of cardiomyocytes, and the assessment of other electrical measurements for biological analyses. This type of studies is primordial when it comes to better a understanding of the mechanism of heart diseases and find potential treatments. Indeed, some heart diseases are closely related to a malfunction of the cardiac conduction system leading to an irregularity in the coordination of heartbeats. This regulation depends on the electrical properties of ion movements between cardiomyocytes. These cells are electrically excitable cells and have widely been studied with *in vitro* techniques such as microelectrode arrays (MEAs).

Various devices have been used for bioanalysis of excitable cells. However, none of these techniques combine the essential requirements for optimal measurements; transparency, large number and high density of µm-size electrodes on a wide sensor array. In this study, we thus focus on the development of a device possessing these valuable characteristics for a more accurate and sensitive recording of the extracellular potential of excitable cells. The possibility to perform additional electrical techniques with the same device was also evaluated as it can provide additional biological information and control of the cell culture.

In order to complete this research, it was of interest to focus on three main electrical techniques: (1) electrophysiology, (2) electrochemistry, (3) dielectrophoresis. Several features and properties, such as the transparency of the substrate, the addressability of the targeted electrodes, and the spatial and temporal resolution have to be carefully considered. The main challenge was thus to build a high resolution microsystem for *in vitro* study of the bioelectrochemical properties and characteristics of cardiomyocytes.

This work uses the TFT technology for the development of novel MEMS for bioelectrochemical applications with an array of a 22,500 transparent square-shaped ITO microelectrodes of 100 µm that cover more than 90 % of the substrate. As a result, this study demonstrates for the first time the use of 2D TFT-MEAs for simultaneous optical and electrical analysis of cardiomyocyte cultures with high repeatability and reproducibility.

Chapter 2: Theory

In this chapter, we discussed the theory and principles behind the electrical analysis of cell cultures. The human heart contains approximately 2–3 billion cardiomyocytes, which form about 75 % of the total volume of the muscular tissue of the heart. In order to pump the blood throughout the cardiovascular system, rapid, involuntary contraction and relaxation of the cardiac muscle is vital. To accomplish this, the structure of cardiomyocytes has specific features that allow them to contract in a coordinated fashion and resist fatigue. Neighboring cardiomyocytes are joined together at their ends by intercalated disks to create a syncytium of cardiac muscle cells. Because of these junctions and bridges the heart muscle is able to act as a single coordinated unit.

Cardiomyocytes are electrically excitable cells, like neurons, which thus exhibit some unique properties. Among these properties is their ability to be electrically excited resulting in the generation of action potentials. Cardiomyocytes can initiate an electrical potential at a fixed rate that spreads rapidly from cell to cell to trigger the contractile mechanism of the heart. This property is known as autorhythmicity. Cardiomyocytes can thus be modeled as an electrical circuit that can be used for theoretical study of their intrinsic electrical properties.

Several techniques have been developed to study the conduction system of the heart. ECG is one of them and has been an essential part of the initial evaluation for patients presenting with cardiac complaints. Electrocardiography has played a fundamental role in our understanding of heart disease, and together with electrophysiology, they remain the standard technique for evaluating of the nature of rhythm disturbances. Then, there is optical imaging such as fluorescence microscopy. This technique uses calcium indicators that are fluorescent molecules which respond to the binding of Ca^{2+} ions by changing their fluorescence properties, which is useful for studies of calcium signalling in excitable cells.

Among *in vitro* electrical techniques, we can find the patch-clamp technique and MEAs for the recordings of the intracellular and extracellular potentials of excitable cells respectively. Both techniques present specific advantages. However, cell culture analyses are not possible with patch-clamp method. Nowadays, state of the art MEAs use the CMOS technology to achieve a high density of microelectrodes with active switch matrices.

Electrochemistry is also an important technique for fundamental studies of single-cell communication, exchange of chemical messenger molecules, as well as small-scale electroporation applications. Among electrochemical techniques, amperometric detection is commonly applied to the detection of electroactive analytes with high selectivity and sensitivity. Then, electrical impedance measurements can also be used for quantifying the resistance of a material to an injected electrical stimulus. Impedance-based devices are thus commonly used for the characterization of cells and tissues, and for monitoring changes in shape, growth, proliferation, or differentiation. DEP is another interesting technique that uses the dielectric properties of cells to perform patterning, separation, mixing or displacement of cells on the substrate.

In this study, we aim at developing a novel MEAs using the TFT technology for *in vitro* study of excitable cells. The basic structure of a TFT can be classified by two factors: the planarity of the semiconducting channel and the gate position in the semiconductor. Multiple types of TFTs have already been developed using different materials for the semiconducting channel. However, by combining transparent semiconductors, such as IGZO, with transparent electrodes, TFT substrates can be made transparent.

Chapter 3: Methodology

Based on the theory of this research, we described the methodology we developed to perform our experiments. We first described the TFT-MEAs used in this study. A TFT-MEA is made of a large, dense array of 150 × 150 transparent square-shaped ITO microelectrodes of 100 µm on a 25 mm x 27 mm substrate. The transistor is a three terminal component (gate, source, and drain) on a bottom-gate configuration. The surface electrode is connected to the drain terminal trough-via. A sandwich insulating layer of SiN, structural polymer, and SiN/SiO is placed between the surface electrode and the gate/source lines to prevent interference. The gate, source, and drain terminals are made of metal, while the N-type conducting channel is made of IGZO.

Each electrode is independently connected to an integrated TFT, which is used for switching ON/OFF the corresponding electrode. By applying an electric potential to a gate line (column), all TFTs connected to that line are switched ON. With a measurement system, or signal generator connected to a source line (row), the electrodes at the gate/source lines intersection can be used for sensing or for applying an electrical signal respectively.

The TFT substrate is mounted on a PCB with a hole made beforehand, so that optical transparency of the whole device remains possible. Connections between the pads of the TFT substrate and the pads of the PCB are done by wire bonding. Finally, a PDMS chamber is placed on the TFT substrate for cell culture and PDMS is added around the culture chamber for fixing it to the TFT substrate and protecting the bonding wires from potential damages. Characterization of the TFT device has been performed and justified the choice of 12 V applied to the gate lines during experiments for reaching the saturation region and switching ON all the transistors.

For electrophysiological measurements, the extracellular potentials of cardiomyocytes is recorded with our TFT-MEA. Cells are isolated from neonatal mouse hearts and cultured on a sterilized device for at least 3 days. The device is place on a petri dish and stored in an incubator at +37°C. During measurements, the TFT-MEA is placed in a small incubator under an inverted microscope. Extracellular potentials of cardiomyocytes are recorded through the source lines of our TFT-MEA with an acquisition system from Multi Channel System MCS GmbH. A control card developed in our laboratory is used for scanning the gate lines of the TFT-MEA. However, the large number of electrodes on TFT-MEAs provide a huge set of data difficult to analyze without proper software. An algorithm for electrophysiological data bioanalysis was thus developed in collaboration with the University of Bordeaux.

For electrochemistry, an Ag/AgCl reference electrode is integrated directly on the TFT substrate. Gate lines are controlled by the control card and source lines are connected to an ALS electrochemical analyzer. Cyclic voltammetry is performed to investigate the possibility to use the ITO electrodes of TFT-MEAs as working electrodes. Amperometric experiments are also realized with tyramine, which is a vasoactive amine derived from tyrosine, at different concentrations.

For DEP experiments, a 400 nm Teflon layer is coated on the TFT substrate to protect the electrodes from potential damage when applying a voltage higher than 3 V. HepG2 and C2C12 cells are used for DEP experiments. They are prepared in a low conductivity medium of 300 mM D-Mannitol and place in the PDMS culture chamber. Gate and source lines are controlled via the control card by applying DC and AC signals respectively.

Chapter 4: Results

Here, we provide some experimental evaluation of the new technique. First, we described the results of *in vitro* measurements of cardiomyocyte extracellular potential with our TFT-MEA. Our results demonstrate that beating cardiomyocytes can be cultured and their electrical activity captured with our TFT platform. Different types of waveform were observed in all experiments with a typical width of 3 to 4 ms and a general shape similar to the one expected by the literature. The measurements could be repeated several times with different cell culture preparations.

Cell contraction was observed with an inverted microscope while the extracellular potential of cardiomyocytes was recorded. A 2D reconstruction of the average pk-pk amplitude recorded on each electrode was realized after filtering and data processing with an algorithm developed in our laboratory. The results show a good agreement between optical observation and electrical recordings, which indicates the efficacity of TFT technology for the development of microelectrode arrays. Additionally, cell cultures were evaluated over several days showing a clear decrease of the signal amplitude and period through the days. We also showed the effect of temperature on the electrical activity of cultures of cardiomyocytes.

Additional measurements were performed with our TFT-MEAs, such as cyclic voltammetry. Standard gold WE was compared with ITO WE from TFTs and showed a similar shape with two redox peaks. We also compared the standard Ag/AgCl glass RE with the integrated Ag/AgCl RE on the TFT device with ITO electrodes as WEs. Very similar curves have been obtained. These experiments have qualitatively demonstrated that ITO electrodes can be used as WE and that Ag/AgCl ink can be used as in integrated RE on the TFT platform. Based on these results, amperometric experiments were performed with tyramine. Standard gold electrode and ITO electrode as WEs were compared. Very similar results were obtained, which confirms that meaningful electrochemistry can be performed with the ITO electrodes of TFT devices.

Finally, DEP of HepG2 and C2C12 cells was performed on TFT-MEAs for evaluating the possibility of cell patterning and displacement on TFT substrates. For these experiments, Teflon-coated TFT-MEAs were used in order to protect the electrodes when applying a high voltage. A low conductivity buffer was also used for preparing the cell solutions. Microbeads were repulsed and cells were attracted towards the activated electrodes. As a result, patterning and displacement of HepG2 and C2C12 cells is possible on Teflon-coated TFT-MEAs without damaging the electrodes. Moreover, cells could be successfully cultured on the devices after DEP experiments.

Chapter 5: Discussion

This section discusses the main findings of the work. In this study, we were able to make measurements of the extracellular potential of cardiomyocytes on a large surface area, and to construct a 2D mapping of the electrical characteristics of the signals. The measurement area and the number of connections can be freely chosen according to the purpose of the experiments: measurement can be performed anywhere in the cell culture, as long as the gate and source lines are connected. The high density of electrodes on the TFT substrate provides a clear advantage over conventional MEAs. Moreover, the transparency of the TFT array allowed the simultaneous observation of cell contraction with inverted microscope, which is more difficult with CMOS technology.

Cardiomyocytes grown on our TFT platform adhere tightly to the substrate and contract isometrically, avoiding the motion artifacts that might cause deterioration in the SNR. This allows recordings over many days, facilitating, for example, investigations of long-term drug effects. However, improvement can be performed to further reduce the noise level at the hardware level by improving amplification of the signal and protecting further the measurement setup from external noise, and at the software level by improving the recognition of low-level signals buried in noise. Additionally, the scanning speed of the gate lines is still not fast enough for recording the electrical potential through all electrodes at once.

Nonetheless, we believe that this problem can be overcome by adding improvements to the control card for switching ON/OFF the gate lines at a rate higher than the frequency of the extracellular signal of cardiomyocytes.

For electrochemical measurements, we demonstrated that the TFT platform can also be used as an electrochemical sensor for biological compounds. Experiments have qualitatively demonstrated that ITO electrodes can be used as WE and that Ag/AgCl ink can be used as an integrated RE on the TFT platform. As a result, a complete integrated sensor can be built on the platform. Amperometric experiments performed with tyramine, vasoactive amine, showed the future possibility to integrate a tyrosinase-based biosensor on the TFT platform. However, this sensor is still not specific to a specific biochemical compound.

In the future, a voltammetric tyrosinase-based biosensor for the determination of tyramine could be developped. Additionally, ITO-based electrode is not a noble metal and it is thus not an ideal electrode material for electrochemical sensing. However, the principle reason for using ITO in this study was to test the possibility of performing electroanalysis with our ITO-based TFT-MEAs. To solve this, it could be decided that electrochemical measurements will be performed only on some dedicated sites with gold pattern in the TFT-MEA substrate.

Finally, the influence of the electrode polarization on the cellular electrophysiology activity during electrochemical measurements should also be considered. In case the electrode polarization is shown to have an influence on the cellular electrophysiological activity, investigations to determine to what extent it affects the activity, and whether the effect is reversible, should be investigated.

Lastly, DEP results demonstrate that efficient DEP with TFT devices can be performed on myocytes with low frequencies for patterning and displacement of cells. We also showed that cells could attached and be cultured on Teflon-coated TFT-MEAs after DEP experiments, which opens the possibility to perform long-term DEP experiments on cell cultures. The Teflon layer allowed the application of high voltage to the source lines of the transistors (20 V). No damage of the electrodes was observed during experiments. The Teflon layer protected the electrodes from the medium and electrolysis. This insulating layer prevents experiments voltage sensing on the same platform. Therefore, the use of another type of material that would allow combination of both techniques on TFT substrates should thus be investigated.

Finally, we discused additional points, such as the cell viability, the reuse of TFT devices, and the feasibility of performing additional electrical measurements with the TFT platform from an electromagnetic point of view.

Chapter 6: Conclusion

On this basis, this work demonstrated the development of a locally-addressable 2D array of ITO microelectrode platform with integrated TFTs. This novel device has been applied to *in vitro* applications, such as electrophysiological measurements by recording the extracellular potential of culture of cardiomyocytes. Additional measurement techniques have been assessed, such as electrochemical measurements of chemical compounds and dielectrophoresis of skeletal muscle cells.

This work gives the opportunity to deepen the study of the electrical properties of specific tissues by developing a real-time lab-on-chip system for brain-heart interactions using a biomimetic system between a spiking neuronal network implemented on digital platform and an *in vitro* biological heart-brain culture on TFT-MEAs. Such a system could be used for investigation of the heart-brain communication network and specific disorders using spatial and temporal adaptive stimulation on neural and cardiac cells or tissues. The use of induced pluripotent stem (iPS) cells in combination with this system could give a promising opportunity to use TFT-MEAs for the development of novel lab on a chip systems for personalized medicine.

6.2 Conclusion of this Work

The regulation of ion exchange through the phospholipid membrane of biological cells plays a crucial role in signal transmission between cells and is also essential for all vital functions of our organs. Ion currents are mediated via ion channels in cell membranes and are now important therapeutic targets. The effect of new drug candidates on the electrical activity of ion channels can be directly investigated by the patch-clamp technique. This technique is limited to the investigation of a small set or even single ion channels. In order to study the electrical flow of ions in a cell culture, MEAs are widely adopted. Although these *in vitro* arrays provide high spatial resolution, they do not combine transparency, large number and high density of small microelectrodes on a wide sensor array. These characteristics are all met by adapting the TFT technology to the development of MEAs.

On this basis, we have shown for the first time in the world that ITO microelectrodes of the TFT platform can be used not only for electrophysiological measurements of cultures of cardiomyocytes, but also for electrochemical measurements and DEP through appropriate functionalization.

By culturing cardiomyocytes on TFT-MEAs, we demonstrated the recordings of their extracellular potentials on a 28 × 28 array with high repeatability and reproducibility, while observing the cell contraction with an inverted microscope. Some analyses could thus be performed such as calculation of the signal velocity, evaluation of the effect of temperature and day of culture, and 2D mapping construction of the cultured cells according to their signal amplitude and period.

Voltammetric and amperometric measurements were also conducted in this study. Our experiments have qualitatively demonstrated that ITO electrodes can be used as WE and that Ag/AgCl ink can be used as in integrated RE on the TFT platform. As a result, a complete integrated sensor can be built on the platform. Amperometry experiments performed with tyramine, vasoactive amine, showed the future possibility to integrate a tyrosinase-based biosensor on the TFT platform.

Finally, DEP was performed with skeletal muscle cells on Teflon-coated TFT-MEAs. Results showed it is possible to pattern and move cells over several electrodes on our TFT-MEAs. Cells survived the low conductivity buffer required for DEP experiments. Moreover, after replacing the buffer by proper cell culture medium, cells could attach to the Teflon-coated TFT substrate and be cultured on the device. This technique could be useful for cell patterning of myocytes and recording of their extracellular potentials on the same TFT-MEA.

Many heart diseases, like cardiac ischemic and stroke, are related to problems of communication between heart cells, and at a larger scale, between cardiovascular and nervous systems. Thanks to its unique and valuable features, we believe that the TFT platform can provide more insights and information for the understanding of the key communication between heart cells and tissues. To conclude, the TFT technology is at the interface between the patch-clamp technique and optical measurements, with a promising future in the development of novel lab on a chip devices.

6.3 Future Research Outlook

This work can be the initiation of a potential development of new lab on a chip (LOC) system for preclinical and clinical studies to study pharmacological effects on dissociated cell cultures in a more simple, controlled environment. Indeed, this work can be seen as a precursor for the development of a real-time LOC system of brain-heart interactions using a biomimetic system between a spiking neuronal network (SNN) implemented on digital platform and an *in vitro* biological heart-brain culture on a bio-hybrid platform of MEAs. By combining a biomimetic system to this bio-hybrid platform, it would be possible to investigate the real-time communication and information transfer from a hardware SNN implemented on an FPGA board and on an *in vitro* biological heart-brain network, by real-time encoding dynamics of a SNN.

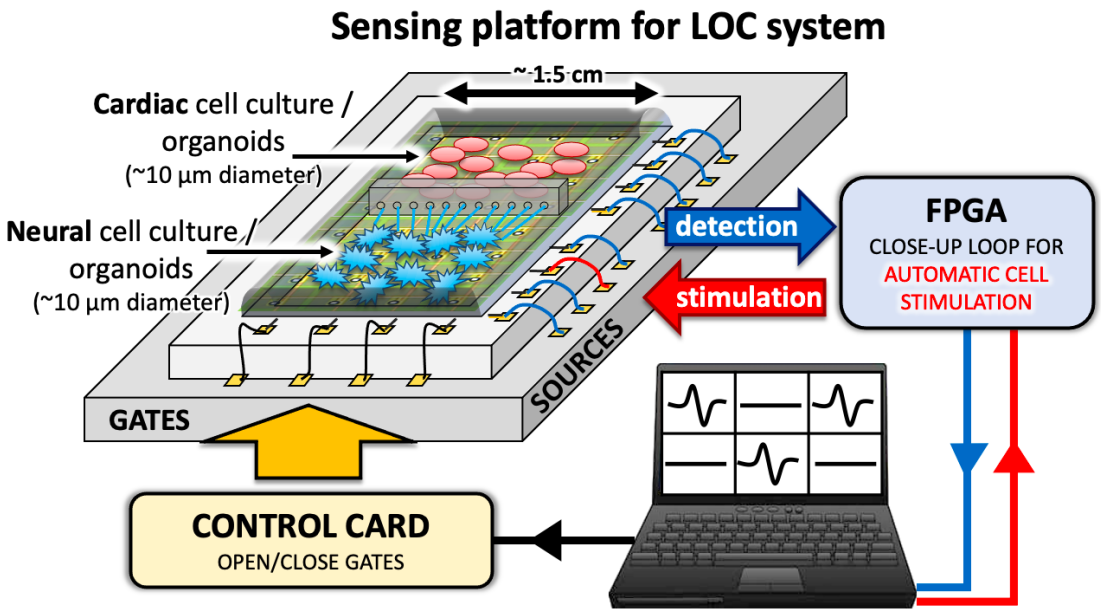

Figure 6.1: Prospective lab on chip biohybrid system for investigation of brain-heart cell co-cultures/organoids

Figure 6.1 shows an illustration of the prospective LOC biohybrid system for investigation of brain-heart cell co-cultures. To achieve this goal, neural and cardiac cells or organoids could be co-cultured on TFT-MEAs. After improvement of the TFT-MEAs by integration of microfluidics and microfabrication, scanning speed of the TFT-MEAs can be revised, so that the signal propagation of the cell electrical activity could be easily calculated within the whole cell culture.

It would also be interesting to developed a specific analytical program for extraction of all characteristics of the cell electrical signals and for a better understanding of the correlation between specific signal characteristics and the biological condition of the cells and organoids.

This brain-heart LOC system includes an FPGA used as a neuro-biomimetic system to create a closed-loop for automatic cell stimulation with real-time analysis. The cell electrical signals from neural cells can be detected by the system and sent it back to the cardiac cells for automatic stimulation without direct biological connections between the neural cells and cardiac cells. Such a system could be used to investigate the heart-brain communication network and specific disorders using spatial and temporal adaptive stimulation on neural and cardiac cells.

As a result, this LOC system can lead to the development and manufacture of an accurate and real-time automated testing equipment (ATE) for various biomedical applications in therapeutic development, via drug testing, drug screening, or disease modeling. Such microsystem is fitted to the size of the cells and organoids allowing to gather much higher information on a larger number of samples with concomitant reduction in sample consumption and time duration of preclinical and clinical studies. New drugs and medicines could be developed much faster, which is a crucial advantage in case of the raise of global diseases.

Finally, this research project can also provide new information about the mechanism of brain-heart interaction vial electrical impulses. The use of iPS cells may also provide an opportunity to develop novel LOC systems by using TFT-MEAs with applications in personalized medicine. The development of a real-time LOC system of brain-heart interactions using a biomimetic system would thus offer a tremendous advantage over the standard manufactured devices.

Bibliography

[1] S. S. Virani *et al.*, "Heart disease and stroke statistics-2020 update: A report from the american heart association," *Circulation*, vol. 141, no. 9, pp. e139–e596, 2020.

[2] S. L. Murphy, J. Xu, K. D. Kochanek, and E. Arias, "Mortality in the united states, 2017," *NCHS Data Brief*, no. 328, pp. 1–8, 2018.

[3] D. G. Fu, "Cardiac arrhythmias: Diagnosis, symptoms, and treatments," *Cell Biochem Biophys*, vol. 73, no. 2, pp. 291–296, 2017.

[4] R. J. Myerburg, K. M. Kessler, L. Zaman, C. A. Conde, and A. Castellanos, "Survivors of prehospital cardiac arrest," *JAMA*, vol. 247, no. 10, pp. 1485–90, 1982.

[5] J. S. Ploem, "The use of a vertical illuminator with interchangeable dichroic mirrors for fluorescence microscopy with incidental light," *Z Wiss Mikrosk*, vol. 68, no. 3, pp. 129–42, 1967.

[6] M. E. Spira and A. Hai, "Multi-electrode array technologies for neuroscience and cardiology," *Nature Nanotechnology*, vol. 8, no. 2, pp. 83–94, 2013.

[7] M. E. J. Obien, K. Deligkaris, T. Bullmann, D. J. Bakkum, and U. Frey, "Revealing neuronal function through microelectrode array recordings," *Frontiers in Neuroscience*, vol. 8, p. 423, 2015.

[8] T. Meyer, U. Kraushaar, and E. Guenther, *Microelectrode Array (MEA) high resolution electrophysiological mapping of cardiac cell, tissue and organ preparations*, vol. 25, pp. 112–115. 2010.

[9] D. Terutsuki, H. Mitsuno, Y. Okamoto, T. Sakurai, A. Tixier-Mita, H. Toshiyoshi, Y. Mita, and R. Kanzaki, "Odor-sensitive field effect transistor (OSFET) based on insect cells expressing insect odorant receptors," in *2017 IEEE 30th International Conference on Micro Electro Mechanical Systems (MEMS)*, pp. 394–397, 2017.

[10] Y. Xu, X. Xie, Y. Duan, L. Wang, Z. Cheng, and J. Cheng, "Review of impedance measurements of whole cells," *Biosensors & bioelectronics*, vol. 77, pp. 824–836, 2015.

[11] I. K'Owino and O. Sadik, "Impedance spectroscopy: A powerful tool for rapid biomolecular screening and cell culture monitoring," *Electroanalysis*, vol. 17, no. 23, pp. 2101–2113, 2005.

[12] K. Cheung, S. Gawad, and P. Renaud, "Impedance spectroscopy flow cytometry: On-chip label-free cell differentiation," *Cytometry.*

Part A : the journal of the International Society for Analytical Cytology, vol. 65, pp. 124–32, 2005.

[13] F. J. Gruhl, "Cell biology and microsystems - What a combination," *2010 2nd Circuits and Systems for Medical and Environmental Applications Workshop, CASME 2010*, 2010.

[14] L. Yobas, "Microsystems for cell-based electrophysiology," *Journal of Micromechanics and Microengineering*, vol. 23, p. 083002, 2013.

[15] F. R. Simões and M. G. Xavier, "Electrochemical sensors," *Nanoscience and its Applications*, pp. 155–178, 2017.

[16] J. Seymour, F. Wu, K. Wise, and E. Yoon, "State-of-the-art MEMS and microsystem tools for brain research," *Microsystems & Nanoengineering*, vol. 3, p. 16066, 2017.

[17] M. A. Mansor and M. R. Ahmad, "Single cell electrical characterization techniques," *International Journal of Molecular Sciences*, vol. 16, no. 6, pp. 12686–12712, 2015.

[18] J. Abbott, T. Ye, L. Qin, M. Jorgolli, R. S. Gertner, D. Ham, and H. Park, "CMOS nanoelectrode array for all-electrical intracellular electrophysiological imaging," *Nature Nanotechnology*, vol. 12, no. 5, p. 460—466, 2017.

[19] A. Tixier-Mita, S. Ihida, G. A. Cathcart, F. A. Shaik, and T. H, "More than moore applications with thin-film-transistors array sub-

strates from liquid cristal display: New devices for biological cells analyses," *ECS Transactions*, vol. 72, no. 3, pp. 39–46, 2016.

[20] A. Tixier-Mita, S. Ihida, B.-D. Ségard, G. A. Cathcart, T. Takahashi, H. Fujita, and H. Toshiyoshi, "Electronic device from TFT display for applications on biological cells," *2015 International Conference on Solid State Devices and Materials (SSDM)*, 2015.

[21] C. A. Thomas, P. A. Springer, G. E. Loeb, Y. Berwald-Netter, and L. M. Okun, "A miniature microelectrode array to monitor the bioelectric activity of cultured cells," *Experimental cell research*, vol. 74, no. 1, p. 61—66, 1972.

[22] G. Gross, E. Rieske, G. Kreutzberg, and A. Meyer, "A new fixed-array multi-microelectrode system designed for long-term monitoring of extracellular single unit neuronal activity in vitro," *Neuroscience letters*, vol. 6, pp. 101–5, 1977.

[23] J. Pine, "Recording action potentials from cultured neurons with extracellular microcircuit electrodes," *Journal of Neuroscience Methods*, vol. 2, no. 1, pp. 19–31, 1980.

[24] J. Pine, "A history of MEA development," *Taketani M., Baudry M. (eds) Advances in Network Electrophysiology*, vol. 2, no. 1, pp. 3–23, 2006.

[25] J. Whitson, D. Kubota, K. Shimono, Y. Jia, and M. Taketani, "Multi-electrode arrays: Enhancing traditional methods and en-

abling network physiology," *Taketani M., Baudry M. (eds) Advances in Network Electrophysiology*, pp. 38–68, 2006.

[26] A. Natarajan, M. Stancescu, V. Dhir, C. Armstrong, F. Sommerhage, J. J. Hickman, and P. Molnar, "Patterned cardiomyocytes on microelectrode arrays as a functional, high information content drug screening platform," *Biomaterials*, vol. 32, no. 18, p. 4267—4274, 2011.

[27] L. Berdondini, T. Overstolz, N. de Rooij, M. Koudelka-Hep, M. Wany, and P. Seitz, "High-density microelectrode arrays for electrophysiological activity imaging of neuronal networks," in *ICECS 2001: 8th IEEE International Conference on Electronics, Circuits and Systems*, vol. 3, pp. 1239–1242, 2001.

[28] K. Imfeld, S. Neukom, A. Maccione, Y. Bornat, S. Martinoia, P. A. Farine, M. Koudelka-Hep, and L. Berdondini, "Large-scale, high-resolution data acquisition system for extracellular recording of electrophysiological activity," *IEEE transactions on bio-medical engineering*, vol. 55, no. 8, pp. 2064–2073, 2008.

[29] L. Berdondini, K. Imfeld, A. Maccione, M. Tedesco, S. Neukom, M. Koudelka-Hep, and S. Martinoia, "Active pixel sensor array for high spatio-temporal resolution electrophysiological recordings from single cell to large scale neuronal networks," *Lab on a chip*, vol. 9, pp. 2644–2651, 2009.

[30] J. Müller, M. Ballini, P. Livi, Y. Chen, M. Radivojevic, A. Shadmani, V. Viswam, I. L. Jones, M. Fiscella, R. Diggelmann, A. Stettler, U. Frey, D. J. Bakkum, and A. Hierlemann, "High-resolution CMOS MEA platform to study neurons at subcellular, cellular, and network levels," *Lab on a chip*, vol. 15, no. 13, p. 2767—2780, 2015.

[31] N. Kimizuka and S. Yamazaki, *CAAC-IGZO Field-Effect Transistor*, ch. 4, pp. 216–284. John Wiley & Sons, Ltd, 2016.

[32] A. Tixier-Mita, S. Ihida, B.-D. Ségard, G. A. Cathcart, T. Takahashi, H. Fujita, and H. Toshiyoshi, "Review on thin-film transistor technology, its applications, and possible new applications to biological cells," *Japanese Journal of Applied Physics*, vol. 55, no. 4S, 2016.

[33] I. Banerjee, J. W. Fuseler, R. L. Price, T. K. Borg, and T. A. Baudino, "Determination of cell types and numbers during cardiac development in the neonatal and adult rat and mouse," *American Journal of Physiology-Heart and Circulatory Physiology*, vol. 293, no. 3, pp. H1883–H1891, 2007.

[34] A. Nag, "Study of non-muscle cells of the adult mammalian heart: a fine structural analysis and distribution," *Cytobios*, vol. 28, no. 109, p. 41—61, 1980.

[35] M. B. Knight, "In vitro tools for quantifying structure–function relationships in cardiac myocyte cells and tissues," master thesis,

UC Irvine, 2015.

[36] D. Bers, *Excitation-Contraction Coupling and Cardiac Contractile Force*, vol. 237 of *Developments in Cardiovascular Medicine*. Springer Netherlands, 2nd ed., 2001.

[37] S. Göktepe, O. J. Abilez, K. K. Parker, and E. Kuhl, "A multiscale model for eccentric and concentric cardiac growth through sarcomerogenesis," *Journal of theoretical biology*, vol. 265, no. 3, p. 433—442, 2010.

[38] G. Olivetti, E. Cigola, R. Maestri, D. Corradi, C. Lagrasta, S. Gambert, and P. Anversa, "Aging, cardiac hypertrophy and ischemic cardiomyopathy do not affect the proportion of mononucleated and multinucleated myocytes in the human heart," *Journal of molecular and cellular cardiology*, vol. 28, no. 7, p. 1463—1477, 1996.

[39] G. G. Matthews, "Cellular physiology of nerve and muscle," ch. Cellular Physiology of Muscle Cells, Wiley-Blackwell, 4th ed., 2013.

[40] L. Sallé and F. Brette, "T-tubules: a key structure of cardiac function and dysfunction," *Archives des maladies du coeur et des vaisseaux*, vol. 100, no. 3, p. 225—230, 2007.

[41] R. Zak, "Development and proliferative capacity of cardiac muscle cells," *Circulation research*, vol. 35, pp. 17–26, 1974.

[42] K. E. Porter and N. A. Turner, "Cardiac fibroblasts: at the heart of myocardial remodeling," *Pharmacology & Therapeutics*, vol. 123, no. 2, p. 255—278, 2009.

[43] M. L. Martin and B. C. Blaxall, "Cardiac intercellular communication: are myocytes and fibroblasts fair-weather friends?," *Journal of cardiovascular translational research*, vol. 5, no. 6, p. 768–782, 2012.

[44] J. J. Tomasek, G. Gabbiani, B. Hinz, C. Chaponnier, and R. A. Brown, "Myofibroblasts and mechano-regulation of connective tissue remodelling," *Nature reviews. Molecular cell biology*, vol. 3, no. 5, p. 349–363, 2002.

[45] T. Martins-Marques, D. J. Hausenloy, J. P. G. Sluijter, L. Leybaert, and H. Girao, "Intercellular communication in the heart: Therapeutic opportunities for cardiac ischemia," *Trends in Molecular Medicine*, vol. 27, no. 3, pp. 248–262, 2021.

[46] L. M. Biga, S. Dawson, A. Harwell, R. Hopkins, J. Kaufmann, M. LeMaster, P. Matern, K. Morrison-Graham, D. Quick, and J. Runyeon, *Anatomy & Physiology*. OpenStax/Oregon State University, 2019.

[47] A. Saxton, M. A. Tariq, and B. Bordoni, "Anatomy, thorax, cardiac muscle." StatPearls [Internet]. Treasure Island (FL): StatPearls Publishing, 2021. available from: https://www.ncbi.nlm.nih.gov/books/NBK535355/.

[48] B. Alberts, A. D. Johnson, J. Lewis, D. Morgan, M. Raff, K. Roberts, and P. Walter, *Molecular Biology of the Cell.* W. W. Norton & Company, 6th ed., 2014.

[49] S. H. Wright, "Generation of resting membrane potential," *Advances in Physiology Education*, vol. 28, no. 4, pp. 139–142, 2004.

[50] P. Enyedi and G. Czirják, "Molecular background of leak K+ currents: Two-pore domain potassium channels," *Physiological Reviews*, vol. 90, no. 2, pp. 559–605, 2010.

[51] R. E. Klabunde, "Cardiac electrophysiology: normal and ischemic ionic currents and the ECG," *Advances in Physiology Education*, vol. 41, no. 1, pp. 29–37, 2017.

[52] J. T. Koivumäki, T. Korhonen, and P. Tavi, "Impact of sarcoplasmic reticulum calcium release on calcium dynamics and action potential morphology in human atrial myocytes: A computational study," *PLOS Computational Biology*, vol. 7, no. 1, pp. 1–14, 2011.

[53] D. E. Becker, "Fundamentals of Electrocardiography Interpretation," *Anesthesia Progress*, vol. 53, no. 2, pp. 53–64, 2006.

[54] W. F. Boron and E. L. Boulpaep, *Medical Physiology.* Elsevier, 3rd ed., 2016.

[55] E. Goldberger, "A simple, indifferent, electrocardiographic electrode of zero potential and a technique of obtaining augmented,

unipolar, extremity leads," *American Heart Journal*, vol. 23, no. 4, pp. 483–492, 1942.

[56] W. B. Fye, "A history of the origin, evolution, and impact of electrocardiography," *The American Journal of Cardiology*, vol. 73, no. 13, pp. 937–949, 1994.

[57] M. AlGhatrif and J. Lindsay, "A brief review: history to understand fundamentals of electrocardiography," *Journal of community hospital internal medicine perspectives*, vol. 2, 2012.

[58] P. Kligfield, *Heart Disease: A textbook of Cardiovascular Medicine*, vol. 21. W. B. Saunders, Philadelphia, 5th ed., 1997.

[59] L. S. Lilly, *Pathophysiology of Heart Disease: A Collaborative Project of Medical Students and Faculty*. Lippincott Williams & Wilkins, 6th ed., 2015.

[60] S. Zhang, A. Doyle, and A. Noheria, "Irregular wide complex tachycardia-mediated cardiomyopathy," *Circulation*, vol. 139, no. 14, pp. 1750–1752, 2019.

[61] A. Ahola, R. P. Pölönen, K. Aalto-Setälä, and J. Hyttinen, "Simultaneous measurement of contraction and calcium transients in stem cell derived cardiomyocytes," *Annals of biomedical engineering*, vol. 46, no. 1, p. 148–158, 2018.

[62] M. B. Cannell, J. R. Berlin, and W. J. Lederer, "Intracellular calcium in cardiac myocytes: calcium transients measured using fluorescence imaging," *Society of General Physiologists series*, vol. 42, p. 201—214, 1987.

[63] R. Jaimes, R. D. Walton, P. Pasdois, O. Bernus, I. R. Efimov, and M. W. Kay, "A technical review of optical mapping of intracellular calcium within myocardial tissue," *American Journal of Physiology-Heart and Circulatory Physiology*, vol. 310, no. 11, p. H1388–H1401, 2016.

[64] S. Bedut, C. Seminatore-Nole, V. Lamamy, S. Caignard, J. A. Boutin, O. Nosjean, J.-P. Stephan, and F. Coge, "High-throughput drug profiling with voltage- and calcium-sensitive fluorescent probes in human iPSC-derived cardiomyocytes," *American Journal of Physiology-Heart and Circulatory Physiology*, vol. 311, no. 1, pp. H44–H53, 2016.

[65] K. Penttinen, H. Siirtola, J. Àvalos Salguero, T. Vainio, M. Juhola, and K. Aalto-Setälä, "Novel analysis software for detecting and classifying Ca2+ transient abnormalities in stem cell-derived cardiomyocytes," *PLoS ONE*, vol. 10, no. 8, p. e0135806, 2015.

[66] E. Neher and B. Sakmann, "Single-channel currents recorded from membrane of denervated frog muscle fibres," *Nature*, vol. 260, p. 799—802, 1976.

[67] B. Sakmann and E. Neher, *Single-Channel Recording*. Springer US, 2nd ed., 1995.

[68] E. Neher, "Ion channels for communication between and within cells," vol. 12, pp. 1–14, 03 1992.

[69] B. Sakmann, "Elementary steps in synaptic transmission revealed by currents through single ion channels," *Neuron*, vol. 8, no. 4, pp. 613–629, 1992.

[70] F. Sigworth and E. Neher, "Single Na+ channel currents observed in cultured rat muscle cells," *Nature*, vol. 287, no. 5781, pp. 447–449, 1980.

[71] T. Akita, M. Ohara, and Y. Okada, *Patch-Clamp Techniques*, ch. Patch-Clamp Techniques: General Remarks, pp. 21–41. Springer Protocols Handbooks, 2012.

[72] M. Fejtl, A. Stett, W. Nisch, K.-H. Boven, and A. Möller, *Advances in Network Electrophysiology Using Multi-Electrode Arrays*, ch. On Micro-Electrode Array Revival: Its Development, Sophistication of Recording, and Stimulation, p. 24–37. Springer, 2006.

[73] A. Offenhäusser and W. Knoll, "Cell-transistor hybrid systems and their potential applications," *Trends in biotechnology*, vol. 19, no. 2, p. 62—66, 2001.

[74] K. Banach, M. D. Halbach, P. Hu, J. Hescheler, and U. Egert, "Development of electrical activity in cardiac myocyte aggregates derived from mouse embryonic stem cells," *American Journal of Physiology-Heart and Circulatory Physiology*, vol. 284, no. 6, pp. H2114–H2123, 2003.

[75] Y. Feld, M. Melamed-Frank, I. Kehat, D. Tal, S. Marom, and L. Gepstein, "Electrophysiological modulation of cardiomyocytic tissue by transfected fibroblasts expressing potassium channels," *Circulation*, vol. 105, no. 4, pp. 522–529, 2002.

[76] I. Kehat, A. Gepstein, A. Spira, J. Itskovitz-Eldor, and L. Gepstein, "High-resolution electrophysiological assessment of human embryonic stem cell-derived cardiomyocytes," *Circulation Research*, vol. 91, no. 8, pp. 659–661, 2002.

[77] R. Adams, "Probing brain chemistry with electroanalytical techniques," *Analytical chemistry*, vol. 48, no. 14, pp. 1126A–1138A, 1976.

[78] M. Wightman, J. A. Jankowski, R. T. Kennedy, K. Kawagoe, T. J. Schroeder, D. Leszczyszyn, J. Near, E. Diliberto, and O. H. Viveros, "Temporally resolved catecholamine spikes correspond to single vesicle release from individual chromaffin cells," *Proceedings of the National Academy of Sciences of the United States of America*, vol. 88, pp. 10754–10758, 1992.

[79] C. Spegel, A. Heiskanen, L. Skjolding, and J. Emnéus, "Chip based electroanalytical systems for cell analysis," *Electroanalysis*, vol. 20, no. 6, pp. 680–702, 2008.

[80] J. Wang. John Wiley & Sons, Inc: Hoboken, New Jersey, 3rd ed., 2006.

[81] W. Wei-Song, K. Wei-Ting, H.-Y. Huang, and L. Ching-Hsing, "Wide dynamic range CMOS potentiostat for amperometric chemical sensor," *Sensors*, vol. 10, 2010.

[82] K. L. Adams, M. Puchades, and A. G. Ewing, "In vitro electrochemistry of biological systems," *Annual Review of Analytical Chemistry*, vol. 1, no. 1, pp. 329–355, 2008.

[83] P.-D. N, "Live cell analysis: when electric detection interfaces microfluidics," *Journal of biochips and tissue chips*, vol. 88, p. S1:001, 2011.

[84] M. Schwarz, M. Jendrusch, and I. Constantinou, "Spatially resolved electrical impedance methods for cell and particle characterization," *Electrophoresis*, vol. 41, no. 1-2, pp. 65–80, 2020.

[85] J. Fleming, "Electronic interfacing with living cells," *Advances in biochemical engineering/biotechnology*, vol. 117, pp. 155–78, 2009.

[86] R. Szulcek, H. Bogaard, and G. P. van Nieuw Amerongen, "Electric cell-substrate impedance sensing for the quantification of endothelial

proliferation, barrier function, and motility," *Journal of Visualized Experiments*, 2014.

[87] D. Das, K. Shiladitya, K. Biswas, P. Dutta, A. Parekh, M. Mandal, and S. Das, "Wavelet-based multiscale analysis of bioimpedance data measured by electric cell-substrate impedance sensing for classification of cancerous and normal cells," *Physical Review E*, vol. 92, 2015.

[88] A. H. Kramer, J. Joos-Vandewalle, A. L. Edkins, C. L. Frost, and E. Prinsloo, "Real-time monitoring of 3T3-L1 preadipocyte differentiation using a commercially available electric cell-substrate impedance sensor system," *Biochemical and biophysical research communications*, vol. 443, no. 4, pp. 1245–1250, 2014.

[89] R. C. Nordberg, J. Zhang, E. H. Griffith, M. W. Frank, B. Starly, and E. G. Loboa, "Electrical cell-substrate impedance spectroscopy can monitor age-grouped human adipose stem cell variability during osteogenic differentiation," *STEM CELLS Translational Medicine*, vol. 6, no. 2, pp. 502–511, 2017.

[90] I. Giaever and C. R. Keese, "A morphological biosensor for mammalian cells," *Nature*, vol. 366, no. 6455, p. 591—592, 1993.

[91] H. T. Ngoc Le, J. Kim, J. Park, and S. Cho, "A review of electrical impedance characterization of cells for label-free and real-time assays," *BioChip Journal*, vol. 13, 2019.

[92] J.-W. Choi, A. Pu, and D. Psaltis, "Optical detection of asymmetric bacteria utilizing electro orientation," *Opt. Express*, vol. 14, no. 21, pp. 9780–9785, 2006.

[93] M. Z. Rashed and S. J. Williams, "Advances and applications of isomotive dielectrophoresis for cell analysis," *Analytical and Bioanalytical Chemistry*, vol. 412, p. 3813–3833, 2020.

[94] S. Afshar, E. Salimi, K. Braasch, M. Butler, D. J. Thomson, and G. E. Bridges, "Multi-frequency DEP cytometer employing a microwave sensor for dielectric analysis of single cells," *IEEE Transactions on Microwave Theory and Techniques*, vol. 64, no. 3, pp. 991–998, 2016.

[95] Y. Ojima and S. Miyata, "Discrimination methodology of living-cells and microbeads using dielectrophoresis and fluid-induced shear force," *Journal of Biorheology*, vol. 29, pp. 42–50, 2015.

[96] H. A. Pohl and I. Hawk, "Separation of living and dead cells by dielectrophoresis," *Science*, vol. 152, no. 3722, p. 647—649, 1966.

[97] M. Tellez-Gabriel, C. Charrier, B. Brounais-Le Royer, M. Mullard, H. K. Brown, F. Verrecchia, and D. Heymann, "Analysis of gap junctional intercellular communications using a dielectrophoresis-based microchip," *European journal of cell biology*, vol. 96, no. 2, p. 110–118, 2017.

[98] F. Vidor, T. Meyers, and U. Hilleringmann, "Flexible electronics: Integration processes for organic and inorganic semiconductor-based thin-film transistors," *Electronics*, vol. 4, pp. 480–506, 2015.

[99] K. Jerzy, *Amorphous and Microcrystalline Semiconductor Devices. Volume II: Materials and Device Physics.* Artech House, 1992.

[100] M. J. Powell, "The physics of amorphous-silicon thin-film transistors," *IEEE Transactions on Electron Devices*, vol. 36, no. 12, pp. 2753–2763, 1989.

[101] B. Stannowski, "Silicon-based thin-film transistors with a high stability," 2002.

[102] M. Stewart, R. S. Howell, L. Pires, and M. K. Hatalis, "Polysilicon TFT technology for active matrix OLED displays," *IEEE Transactions on Electron Devices*, vol. 48, no. 5, pp. 845–851, 2001.

[103] D. Kumaki and S. Tokito, "Newly developed silver nanoparticle ink for organic tft circuits fabricated with high resolution printing system," in *2017 International Conference on Electronics Packaging (ICEP)*, pp. 441–442, 2017.

[104] A. F. Paterson, S. Singh, K. J. Fallon, T. Hodsden, Y. Han, B. C. Schroeder, H. Bronstein, M. Heeney, I. McCulloch, and T. D. Anthopoulos, "Recent progress in high-mobility organic transistors: A reality check," *Advanced Materials*, vol. 30, no. 36, p. 1801079, 2018.

[105] Y. Yamauchi, Y. Kamakura, Y. Isagi, T. Matsuoka, and S. Malotaux, "Study of novel floating-gate oxide semiconductor memory using indium–gallium–zinc oxide for low-power system-on-panel applications," *Japanese Journal of Applied Physics*, vol. 52, p. 094101, 2013.

[106] T. P. Brody, "The thin film transistor - a late flowering bloom," *IEEE Transactions on Electron Devices*, vol. 31, no. 11, pp. 1614–1628, 1984.

[107] P. Görrn, P. Hölzer, T. Riedl, W. Kowalsky, J. Wang, T. Weimann, P. Hinze, and S. Kipp, "Stability of transparent zinc tin oxide transistors under bias stress," *Applied Physics Letters*, vol. 90, no. 6, p. 063502, 2007.

[108] E. M. C. Fortunato, P. M. C. Barquinha, A. C. M. B. G. Pimentel, A. M. F. Goncalves, A. J. S. Marques, L. M. N. Pereira, and R. F. P. Martins, "Fully transparent ZnO thin-film transistor produced at room temperature," *Advanced Materials*, vol. 17, no. 5, pp. 590–594, 2005.

[109] K. Nomura, H. Ohta, A. Takagi, T. Kamiya, M. Hirano, and H. Hosono, "Room-temperature fabrication of transparent flexible thin-film transistors using amorphous oxide semiconductors," *Nature*, vol. 432, pp. 488–492, 2004.

[110] T. Rudenko, V. Kilchytska, M. K. M. Arshad, J.-P. Raskin, A. Nazarov, and D. Flandre, "On the mosfet threshold voltage extraction by transconductance and transconductance-to-current ratio change methods: Part i—effect of gate-voltage-dependent mobility," *IEEE Transactions on Electron Devices*, vol. 58, no. 12, pp. 4172–4179, 2011.

[111] A. Tixier-Mita, S. Ihida, G. Cathcart, F. A. Shaik, H. Fujita, Y. Mita, and H. Toshiyoshi, "A test structure to characterize transparent electrode array platform with TFTs for bio-chemical applications," in *International Conference of Microelectronic Test Structure*, 2017.

[112] U. Egert and T. Meyer, "Heart on a chip — extracellular multielectrode recordings from cardiac myocytes in vitro," *Practical Methods in Cardiovascular Research*, 2005.

[113] R. Khwanchuea, M. Mulvany, and C. Jansakul, "Cardiovascular effects of tyramine: Adrenergic and cholinergic interactions," *European journal of pharmacology*, vol. 579, pp. 308–17, 2008.

[114] M. Z. H. Khan, X. Liu, J. Zhu, F. Ma, W. Hu, and X. Liu, "Electrochemical detection of tyramine with ITO/APTES/ErGO electrode and its application in real sample analysis," *Biosensors & Bioelectronics*, vol. 108, pp. 76–81, 2018.

[115] A. Tixier-Mita, B.-D. Segard, Y.-J. Kim, Y. Matsunaga, H. Fujita, and H. Toshiyoshi, "TFT display panel technology as a base for biological cells electrical manipulation - application to dielectrophoresis," vol. 2015, pp. 354–357, 2015.

[116] G. Ihrke, E. B. Neufeld, T. Meads, M. R. Shanks, D. Cassio, M. Laurent, T. A. Schroer, R. E. Pagano, and A. L. Hubbard, "WIF-B cells: an in vitro model for studies of hepatocyte polarity," *The Journal of cell biology*, vol. 123, no. 6, p. 1761—1775, 1993.

[117] D. K. McMahon, P. A. Anderson, R. Nassar, J. B. Bunting, Z. Saba, A. E. Oakeley, and N. N. Malouf, "C2C12 cells: biophysical, biochemical, and immunocytochemical properties," *The American journal of physiology*, vol. 266, no. 6, pp. C1795–C17802, 1994.

[118] H. Lecoeur, "Nuclear apoptosis detection by flow cytometry: influence of endogenous endonucleases," *Experimental cell research*, vol. 277, no. 1, pp. 1–14, 2002.

[119] P. K. Wong, T. H. Wang, J. H. Deval, and C. M. Ho, "Electrokinetics in micro devices for biotechnology applications," *IEEE/ASME Transactions on Mechatronics*, vol. 9, no. 2, pp. 366–376, 2004.

[120] T. L. G. J, B. S. R, v. B. J, P. R, and M. C. L, "Interpretation of field potentials measured on a multi electrode array in pharmacological toxicity screening on primary and human pluripotent stem

cell-derived cardiomyocytes," *Biochemical and Biophysical Research Communications*, vol. 497, no. 4, pp. 1135–1141, 2018.

[121] M. Uesugi, A. Ojima, T. Taniguchi, N. Miyamoto, and K. Sawada, "Low-density plating is sufficient to induce cardiac hypertrophy and electrical remodeling in highly purified human iPS cell-derived cardiomyocytes," *Journal of pharmacological and toxicological methods*, vol. 69, 2013.

[122] M. Miragoli, N. Salvarani, and S. Rohr, "Myofibroblasts induce ectopic activity in cardiac tissue.," *Circulation research*, vol. 101, no. 8, p. 755–758, 2007.

[123] T. Uchida, R. Kitora, and K. Gohara, "Temperature dependence of synchronized beating of cultured neonatal rat heart-cell networks with increasing age measured by multi-electrode arrays," *Trends in Medicine*, vol. 18, 2018.

[124] E. Laurila, A. Ahola, J. Hyttinen, and K. Aalto-Setälä, "Methods for in vitro functional analysis of iPSC derived cardiomyocytes - special focus on analyzing the mechanical beating behavior," *Biochimica et Biophysica Acta (BBA) - Molecular Cell Research*, vol. 1863, no. 7, Part B, pp. 1864–1872, 2016.

[125] F. A. Shaik, G. A. Cathcart, S. Ihida, Y. Ikeuchi, A. Tixier-Mita, and H. Toshiyoshi, "Electrical stimulation, recording and impedance-based real-time position detection of cultured neurons using thin-

film-transistor array," *Journal of Microelectromechanical Systems*, vol. 27, no. 3, pp. 424–433, 2018.

[126] G. A. Cathcart, A. Tixier-Mita, A.-C. Ihida, Satoshi Eiler, and H. Toshiyoshi, "Non-mutative cell viability measurement on an IGZO transparent thin film transistor electrode array," *The transactions of the Institute of Electrical Engineers of Japan*, vol. 140, no. 8, pp. 193–200, 2020.

[127] M. Halbach, U. Egert, J. Hescheler, and K. Banach, "Estimation of action potential changes from field potential recordings in multicellular mouse cardiac myocyte cultures. cellular physiology and biochemistry," *International journal of experimental cellular physiology, biochemistry, and pharmacology*, vol. 13, no. 5, p. 271–284, 2003.

[128] M. Clements, "Multielectrode array (MEA) assay for profiling electrophysiological drug effects in human stem cell-derived cardiomyocytes," *Current protocols in toxicology*, vol. 68, 2016.

[129] X.-B. Abassi, Y. A., N. Li, W. Ouyang, A. Seiler, M. Watzele, R. Kettenhofen, H. Bohlen, A. Ehlich, E. Kolossov, X. Wang, and X. Xu, "Dynamic monitoring of beating periodicity of stem cell-derived cardiomyocytes as a predictive tool for preclinical safety assessment," *British journal of pharmacology,*, vol. 165, no. 5, p. 1424–1441, 2012.

[130] L. Doerr, U. Thomas, D. R. Guinot, C. T. Bot, S. Stoelzle-Feix, M. Beckler, M. George, and N. Fertig, "New easy-to-use hybrid system for extracellular potential and impedance recordings," *Journal of Laboratory Automation*, vol. 20, no. 2, pp. 175–188, 2015.

[131] Multi Channel Systems MCS GmbH, *Microelectrode Array (MEA) Manual*, March 2021.

[132] A. Ito, Y. Yamamoto, M. Sato, K. Ikeda, M. Yamamoto, H. Fujita, E. Nagamori, Y. Kawabe, and M. Kamihira, "Induction of functional tissue-engineered skeletal muscle constructs by defined electrical stimulation," *Scientific reports*, vol. 4, p. 4781., 2014.

[133] I. H. Lee, Y. J. Lee, H. Seo, Y. S. Kim, J. O. Nam, B. D. Jeon, and T. D. Kwon, "Study of muscle contraction induced by electrical pulse stimulation and nitric oxide in C2C12 myotube cells," *Journal of exercise nutrition & biochemistry*, vol. 22, no. 1, p. 22–28, 2018.

[134] Y. Manabe, S. Miyatake, M. Takagi, M. Nakamura, A. Okeda, T. Nakano, M. F. Hirshman, L. J. Goodyear, and N. L. Fujii, "Characterization of an acute muscle contraction model using cultured C2C12 myotubes," *PLOS ONE*, vol. 7, no. 12, pp. 1–10, 2013.

[135] H. Samadian, S. S. Zakariaee, M. Adabi, H. Mobasheri, M. Azami, and R. Faridi-Majidi, "Effective parameters on conductivity of mineralized carbon nanofibers: an investigation using artificial neural networks," *RSC Adv.*, vol. 6, pp. 111908–111918, 2016.

[136] M. P. Prabhakaran, L. Ghasemi-Mobarakeh, G. Jin, and S. Ramakrishna, "Electrospun conducting polymer nanofibers and electrical stimulation of nerve stem cells," *Journal of bioscience and bioengineering*, vol. 112, no. 5, pp. 501–507, 2011.

[137] R. Balint, N. J. Cassidy, and S. H. Cartmell, "Electrical stimulation: A novel tool for tissue engineering," *Tissue Engineering Part B: Reviews*, vol. 19, no. 1, pp. 48–57, 2013.

[138] J. Vaca, J. Guevara, F. Vega, and D. Garzón-Alvarado, "An in vitro chondrocyte electrical stimulation framework: A methodology to calculate electric fields and modulate proliferation, cell death and glycosaminoglycan synthesis," *Cellular and Molecular Bioengineering*, vol. 9, 2015.

[139] Y.-C. Fu, C.-C. Lin, J.-K. Chang, C.-H. Chen, I.-C. Tai, G.-J. Wang, and M.-L. Ho, "A novel single pulsed electromagnetic field stimulates osteogenesis of bone marrow mesenchymal stem cells and bone repair," *PloS one*, vol. 9, p. e91581, 2014.

[140] R. Hess, A. Jaeschke, H. Neubert, V. Hintze, S. Moeller, M. Schnabelrauch, H.-P. Wiesmann, D. A. Hart, and D. Scharnweber, "Synergistic effect of defined artificial extracellular matrices and pulsed electric fields on osteogenic differentiation of human MSCs," *Biomaterials*, vol. 33, no. 35, pp. 8975–8985, 2012.

[141] C. Chen, X. Bai, Y. Ding, and I.-S. Lee, "Electrical stimulation as a novel tool for regulating cell behavior in tissue engineering," *Biomaterials Research*, vol. 23, 2019.

[142] NIH DailyMed, *Label: Isoproterenol hydrochloride injection, solution*, 2018.

[143] A. Maccione, M. Gandolfo, S. Zordan, H. Amin, S. Di Marco, T. Nieus, G. N. Angotzi, and L. Berdondini, "Microelectronics, bioinformatics and neurocomputation for massive neuronal recordings in brain circuits with large scale multielectrode array probes," *Brain Research Bulletin*, vol. 119, pp. 118–126, 2015.

[144] E. Ferrea, A. Maccione, L. Medrihan, T. Nieus, D. Ghezzi, P. Baldelli, F. Benfenati, and L. Berdondini, "Large-scale, high-resolution electrophysiological imaging of field potentials in brain slices with microelectronic multielectrode arrays," *Frontiers in Neural Circuits*, vol. 6, p. 80, 2012.

[145] D. Zhu, M. Ono, G. Cathcart, S. Ihida, A. Tixier-Mita, Y. Sakai, and K. Komori, "Development of thin film transistor-based biosensors toward label-free multiple immunoasssays," in *18th Asian Pacific Confederation of Chemical Engineering Congress (APPChE'2019)*, vol. 3, (Sapporo, Japan), p. PL243, 2019.

[146] M. R. Akanda, A. Osman, M. Nazal, and M. Aziz, "Review - recent advancements in the utilization of indium tin oxide (ITO) in

electroanalysis without surface modification," *Journal of The Electrochemical Society*, vol. 167, p. 037534, 2020.

[147] T. Kuno, K. Niitsu, and K. Nakazato, "Amperometric electrochemical sensor array for on-chip simultaneous imaging," *Japanese Journal of Applied Physics*, vol. 53, p. 04EL01, jan 2014.

[148] J. P. Finberg and G. K, "Selective inhibitors of monoamine oxidase type b and the "cheese effect"," *International Review of Neurobiology*, vol. 100, pp. 169–190, 2011.

[149] M. Youdim and M. Weinstock, "Therapeutic applications of selective and non-selective inhibitors of monoamine oxidase a and b that do not cause significant tyramine potentiation," *Neurotoxicology*, vol. 25, pp. 243–250, 2004.

[150] F. Hasan, J. M. McCrodden, N. P. Kennedy, and K. F. Tipton, "The involvement of intestinal monoamine oxidase in the transport and metabolism of tyramine," *Journal of neural transmission. Supplementum*, vol. 26, pp. 1–9, 1988.

[151] M. B. H. Youdim, D. Edmondson, and K. F. Tipton, "The therapeutic potential of monoamine oxidase inhibitors," *Nature reviews. Neuroscience*, vol. 7, no. 4, pp. 295–309, 2006.

[152] E. C. J. Hart and N. Charkoudian, "Sympathetic neural regulation of blood pressure: Influences of sex and aging," *Physiology*, vol. 29, no. 1, pp. 8–15, 2014.

[153] J. Kochana, K. Wapiennik, P. Knihnicki, A. Pollap, P. Janus, M. Oszajca, and P. Kuśtrowski, "Mesoporous carbon-containing voltammetric biosensor for determination of tyramine in food products," *Analytical and bioanalytical chemistry,*, vol. 408, no. 19, p. 5199–5210, 2016.

[154] E. Tanumihardja, R. H. Slaats, A. D. van der Meer, R. Passier, W. Olthuis, and A. van den Berg, "Measuring both pH and O2 with a single on-chip sensor in cultures of human pluripotent stem cell-derived cardiomyocytes to track induced changes in cellular metabolism," *ACS Sensors*, vol. 6, pp. 267–274, 2021.

[155] H. Kim, C. M. Gilmore, A. Piqué, J. S. Horwitz, H. Mattoussi, H. Murata, Z. H. Kafafi, and D. B. Chrisey, "Electrical, optical, and structural properties of indium–tin–oxide thin films for organic light-emitting devices," *Journal of Applied Physics*, vol. 86, no. 11, pp. 6451–6461, 1999.

[156] S.-H. Moon, Y.-W. Cho, H.-E. Shim, J.-H. Choi, C.-H. Jung, I.-T. Hwang, and S.-W. Kang, "Electrically stimulable indium tin oxide plate for long-term in vitro cardiomyocyte culture," *Biomaterials Research*, vol. 24, 2020.

[157] C. P. Huang, X. M. Chen, and Z. Q. Chen, "Osteocyte: the impresario in the electrical stimulation for bone fracture healing," *Medical hypotheses*, vol. 70, no. 2, pp. 287–290, 2008.

[158] S. Beebe, P. Fox, L. Rec, K. Somers, R. Stark, and K. Schoenbach, "Nanosecond pulsed electric field (nsPEF) effects on cells and tissues: apoptosis induction and tumor growth inhibition," *IEEE Transactions on Plasma Science*, vol. 30, no. 1, pp. 286–292, 2002.

[159] K. Ravikumar, B. Basu, and A. Dubey, "Analysis of electrical analogue of a biological cell and its response to external electric field," *Regenerative Engineering and Translational Medicine*, vol. 5, pp. 10–21, 2019.

Publications

Scientific journals

1. Anne-Claire Eiler, Pierre-Marie Faure, Junichi Sugita, Satoshi Ihida, Dongchen. Zhu, Yasuyuki Sakai, Katsuhito Fujiu, Kikuo Komori, Hiroshi Toshiyoshi, and Agnès Tixier-Mita, "Application of a Thin-Film Transistor Array for Cellular-Resolution Electrophysiology and Electrochemistry," *IEEE Transactions on Electron Devices*, 2021, pp.1-8 (invited paper)

2. Grant A. Cathcart, Agnès Tixier-Mita, Satoshi Ihida, Anne-Claire Eiler, Hiroshi Toshiyoshi, "Non-Mutative Cell Viability Measurement on an IGZO Transparent Thin Film Transistor Electrode Array," *The transactions of the Institute of Electrical Engineers of Japan*, 2020, Vol. 140 (8), pp. 193-200

3. Anne-Claire Eiler, Junichu Sugita, Satoshi Ihida, Hiroshi Toshiyoshi, Katsuhito Fujiu, Timothée Lévi, and Agnès Tixier-Mita, "Spike Sorting Tool for Analysis of Extracellular Cardiac Signals recorded by Thin-Film-Transistor Sensor Arrays," *Journal*

of Robotics, Networking and Artificial Life, 2020, Volume 7, Issue 1, pp. 48 – 51

4. Agnès Tixier-Mita, Satoshi Ihida, Damien Blanchard, Marie Shinohara, Anne-Claire Eiler, Grant Alexander Cathcart, Pierre- Marie Faure, Takahashi Kohno, Yasuyuki Sakai, Timothée Lévi, Hiroshi Toshiyoshi, "2D Dielectrophoresis Using an Active Matrix Array made by Thin-Film-Transistor Technology," *The Institute of Electrical Engineers of Japan*, 2019, Volume 14: 1280 – 1288

5. Stephany Mai Nishikawa, Farad Khoyratee, Anne-Claire Eiler, Soo Hyeon Kim, Satoshi Ihida, Hiroshi Toshiyoshi, Agnès Tixier-Mita, Yoshiho Ikeuchi, Takashi Kohno, Kazuyuki Aihara, Teruo Fujii, Timothée Lévi, "Neuro-hybrid systems: the future for biomedical applications," *Seisan Kenkyu*, 2019, Volume 71: 787-790

International Conferences

6. Anne-Claire Eiler, Junichi Sugita, Satoshi Ihida, Hiroshi Toshiyoshi, Katsuhito Fujiu, and Agnès Tixier-Mita,"A thin-film-transistor active matrix array for 2D real space electrical imaging of heart cell cultures," *The 30th Anniversary World Congress on Biosensors*, 27-29 July 2021 – poster, peer-reviewed (online)

7. Anne-Claire Eiler, Pierre-Marie Faure, Junichi Sugita, Satoshi Ihida, Dongchen Zhu, Yasuyuki Sakai, Katsuhito Fujiu, Kikuo

Komori, Hiroshi Toshiyoshi, and Agnès Tixier-Mita, "Thin-Film-Transistor Platform for Electrophysiological and Electrochemical Characterization of Cells," *IEEE 66th International Electron Devices Meeting (IEDM 2020)*, 2-16 December 2020, San Francisco, US – oral, peer-reviewed (online, IEEE EDS Japan Joint Chapter Student Award)

8. Anne-Claire Eiler, Junichu Sugita, Satoshi Ihida, Hiroshi Toshiyoshi, Katsuhito Fujiu,Timothée Lévi, and Agnès Tixier-Mita, "Bioelectrical Signal Analysis of Mouse Cardiomyocyte Culture recorded on Thin-Film-Transistor Sensor Arrays," *The 2020 International Conference on Artificial Life and Robotics*, 13-16 January 2020, Beppu, Oita, Japan, OS6-4 – oral, peer-reviewed

9. Anne-Claire Eiler, Khoyratee Farad, Satoshi Ihida, Hiroshi Toshiyoshi, Timothée Lévi, and Agnès Tixier-Mita, "A Bio-Hybrid Platform Using Thin-Film-Transistor Arrays And A Biomimetic Neural Network," *The 11th International Symposium on Microchemistry and Microsystems*, 17-20 May 2019, Yangling, Shaanxi, China, O-43 – oral, peer-reviewed

Domestic Conferences

10. Pierre-Marie Faure, Anne-Claire Eiler, Satoshi Ihida, Junichi Sugita, Katsuhito Fujiu, Hiroshi Toshiyoshi, Agnès Tixier-Mita,"A Matlab Spiking Sorting Algorithm for Data Processing of In-Vitro

Cardiomyocyte Electrophysiology with a Thin-Film-Transistor Platform," *The 37th Sensor Symposium*, 26-28 October 2020, 27P3-SSL-64 – poster, peer-reviewed (online)

11. Anne-Claire Eiler, Satoshi Ihida, Damien Blanchard, Timothée Lévi, Hiroshi Toshiyoshi, and Agnès Tixier-Mita, "Insulation layer improvement for efficient mammalian cell dielectrophoresis on Thin-Film-Transistor device"," *The 36th Sensor Symposium*, 19-21 November 2019, Hamamatsu, Shizuoka, Japan, 20pm3-LN2-100 – poster, peer-reviewed

Additional Presentations

12. Anne-Claire Eiler, Pierre-Marie Faure, Junichi Sugita, Satoshi Ihida, Dongchen Zhu, Yasuyuki Sakai, Katsuhito Fujiu, Kikuo Komori, Hiroshi Toshiyoshi, Agnès Tixier-Mita,"A Thin-Film Transistor Platform for Bioelectrochemical Measurements," *IIS PhD Student Live 2020*, The University of Tokyo, 4 March 2021 – 1-minute oral presentation and poster

13. Anne-Claire Eiler, Pierre-Marie Faure, Junichi Sugita, Satoshi Ihida, Dongchen Zhu,Yasuyuki Sakai, Katsuhito Fujiu, Kikuo Komori, Hiroshi Toshiyoshi, Agnès Tixier-Mita, Workshop, "A Thin-Film Transistor Array for Recording of the Electrical Properties of Biological Cells," 第 *11* 回集積化 *MEMS* 技術研究ワー

クショッフ, 28 January 2021 – poster

14. Anne-Claire Eiler, Pierre-Marie Faure, Satoshi Ihida, Hiroshi Toshiyoshi, et Agnès Tixier-Mita, "Mesures électro-physiologiques de cellules cardiaques utilisant une nouvelle matrice de microélectrodes," *J·FR 2020: French Research Day 2020*, December 2020 – 5-minute Flash Talk

15. Anne-Claire Eiler, Satoshi Ihida, Hiroshi Toshiyoshi, and Agnès Tixier-Mita, "Nouveau Microsystème pour Analyse de Cultures Cellulaires," *J·FR 2019: French Research Day 2019*, October 2019 – poster

16. Anne-Claire Eiler, "Rediscovering our body through recordings of biolectrical signals," *Three Minute (3MT) Thesis*, The University of Tokyo, Japan, 23 May 2020– oral presentation (online)

Award

"第19回 2020年IEEE EDS Japan Chapter Student Award (IEDM)" for the presentation given at the *2020 IEEE International Electron Devices Meeting (IEDM)* that was held online on 12-18 December 2020 [6] (awarded on February 10, 2021).